Beyond the Synchrotron: The Dawn of Laser-Compton X-ray and Gamma-ray Science

Norman Rostoker Distinguished Lecture
University of California, Irvine

Dr. C. P. J. Barty
Chief Technology Officer
National Ignition Facility & Photon Science Directorate
Lawrence Livermore National Laboratory
Livermore, California
April 10, 2014

This work performed under the auspices of the U.S. Department of Energy by Lawrence Livermore National Laboratory under Contract DE-AC52-07NA27344

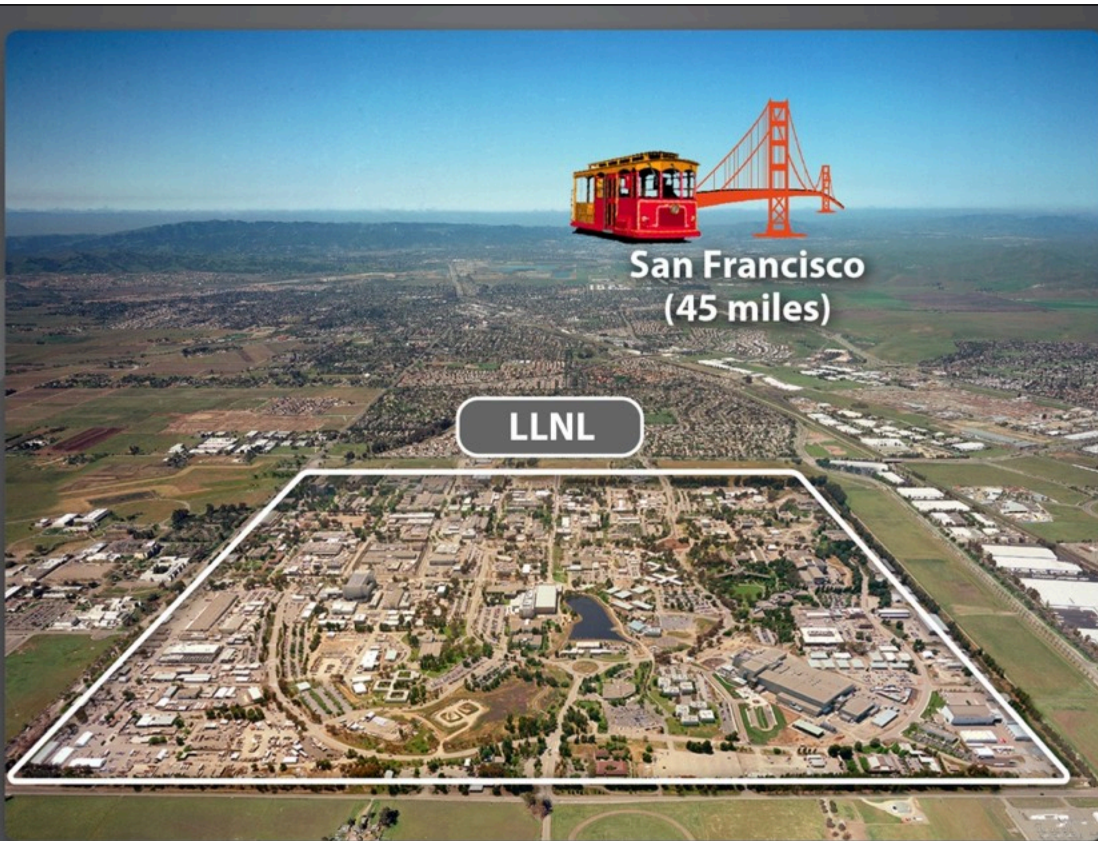


San Francisco
(45 miles)
Lasers, Lasers Nothing but Lasers

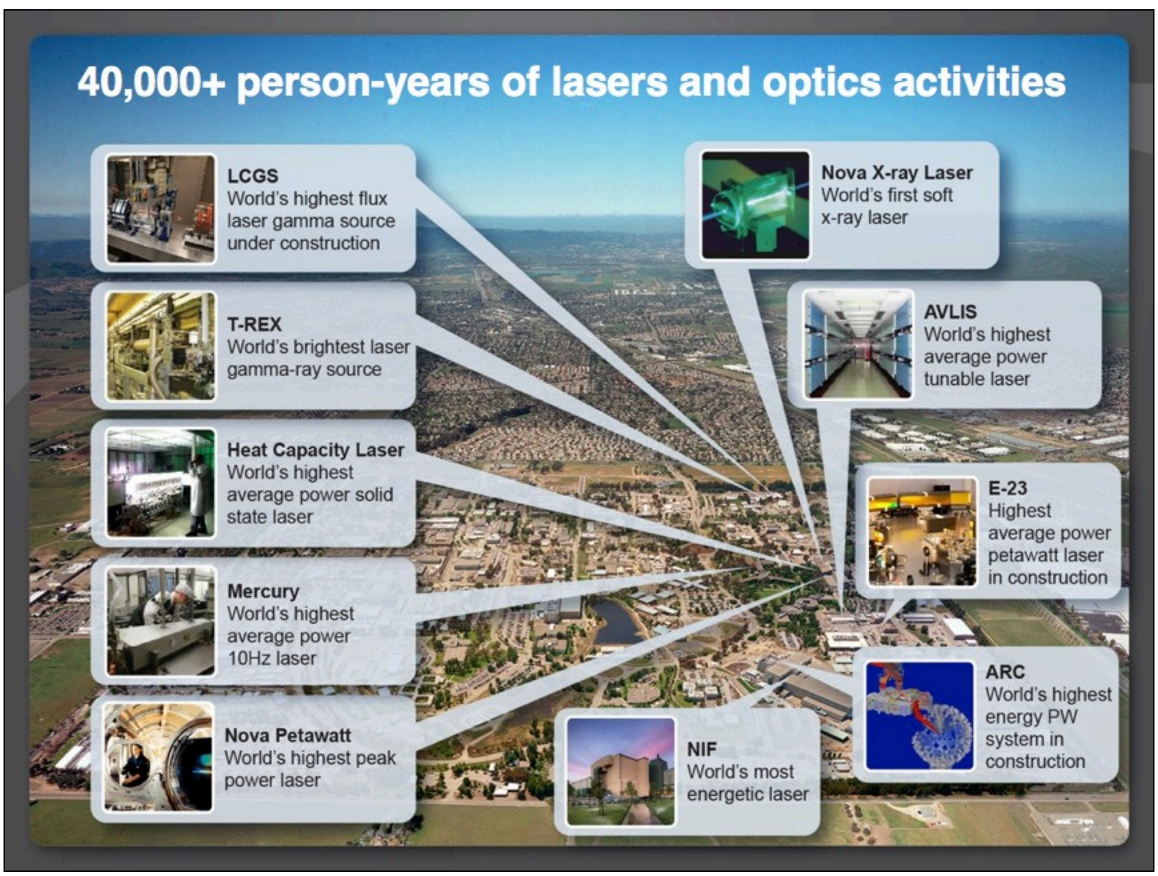
40,000+ person-years of lasers and optics activities
LCGS
World's highest flux laser gamma source under construction
T-REX
World's brightest laser gamma-ray source
Heat Capacity Laser
World's highest average power solid state laser
Mercury
World's highest average power 10Hz laser
Nova Petawatt
World's highest peak power laser
NIF
World's most energetic laser
Nova X-ray Laser
World's first soft x-ray laser
AVLIS
World's highest average power tunable laser
E-23
Highest average power petawatt laser in construction
ARC
World's highest energy PW system in construction

40,000+ person-years of lasers and optics activities

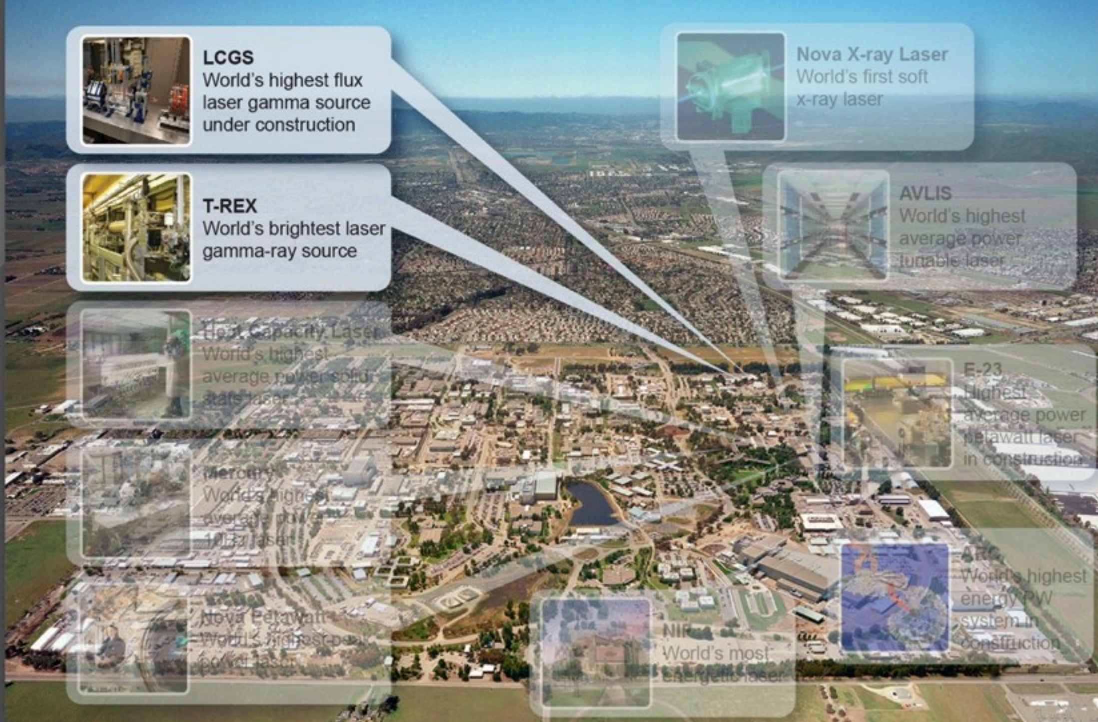

Laser Compton back scattering off of high energy electrons can produce tunable, high energy photons

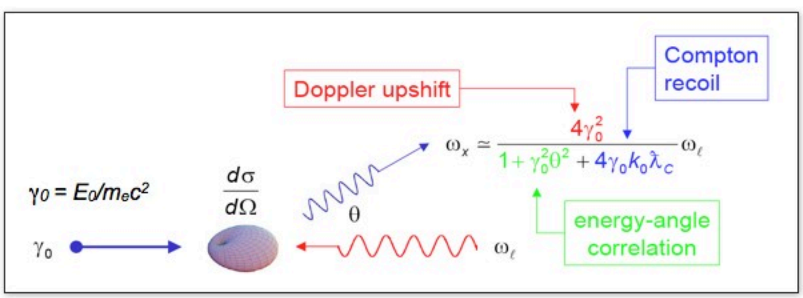

Energy-momentum conservation yields ~$4\gamma^2$ Doppler upshift

1965 First Light: 8 photons

PHYSICAL REVIEW VOLUME 138, NUMBER 6B 21 JUNE 1965

High-Energy Photons from Compton Scattering of Light on 6.0-GeV Electrons*

CARLO BEMPORAD†, RICHARD H. MILBURN, AND NOBUYUKI TANAKA
Department of Physics, Tufts University, Medford, Massachusetts

AND

MIRCEA FOTINO
Cambridge Electron Accelerator, Harvard University, Cambridge, Massachusetts

(Received 28 January 1965; revised manuscript received 1 March 1965)

Compton scattering of optical photons on 6.0-GeV electrons has been observed at the Cambridge Electron Accelerator. A giant-pulsed ruby-laser burst of 0.2 J, impinging upon a 2-mA circulating electron current, was observed to yield about 8 scattered photons per pulse. These photons acquire, through a twofold Doppler shift, energies of hundred of MeV, and are expected to retain to a high degree the polarization of the laser beam. The observed yield is compatible with predictions based upon the theory of Compton scattering.

FIG. 6. Čerenkov-counter pulse-height distributions. Laser-correlated pulses are associated with second laser pulse. (2.3 units = 3 GeV).

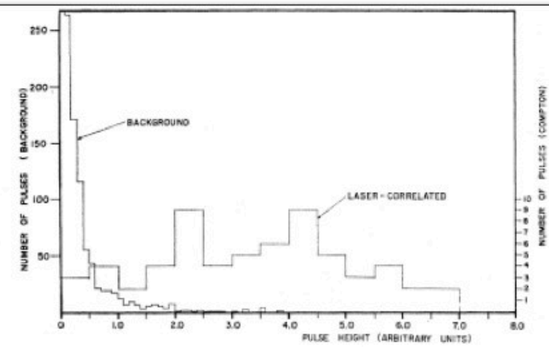

Laser Compton back scattering off of high energy electrons can produce tunable, high energy photons

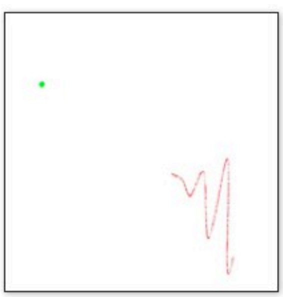

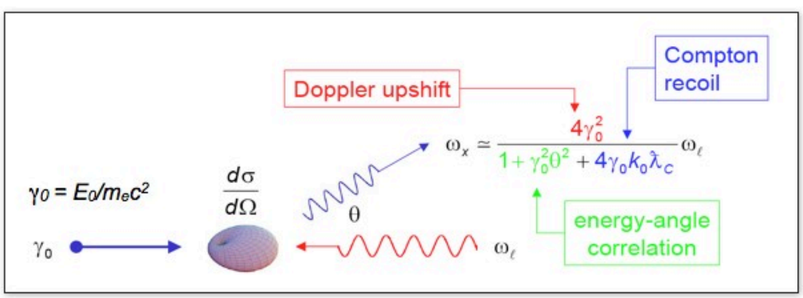

Thomson cross section is very small ~ 6 x 10^{-25} cm^2

High-flux, laser-Compton scattering arrangements aim to produce high photon & electron densities at a common focus

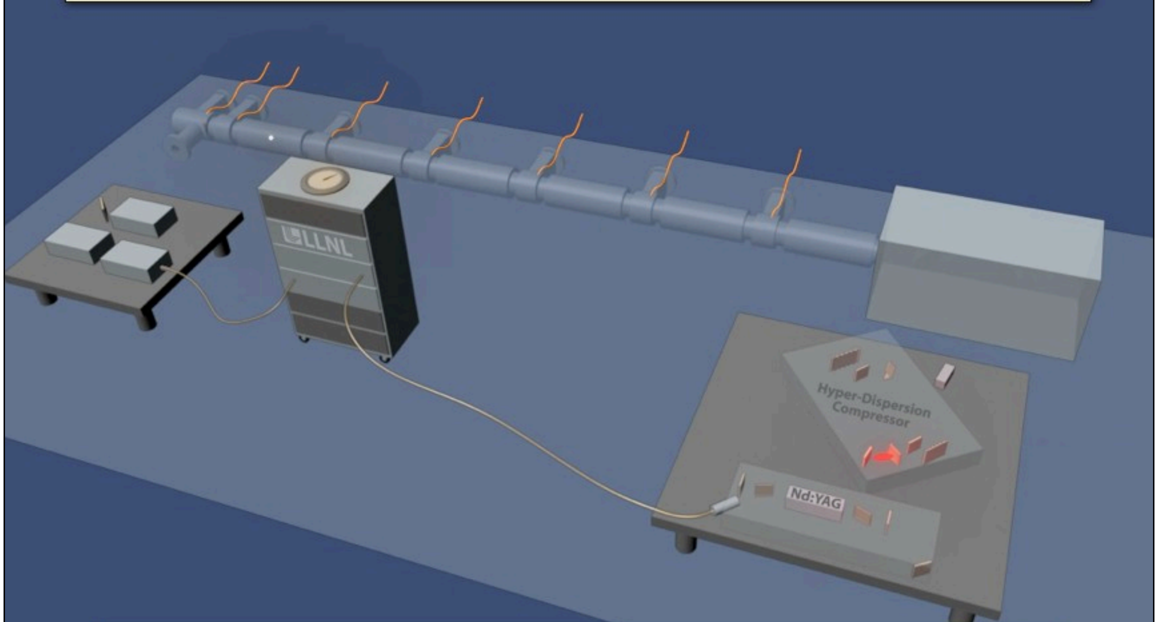

At 250 MeV, scattered radiation is Doppler upshifted by ~1,000,000x and is forwardly-directed in a narrow, polarized, tunable, laser-like, gamma beam

US patent #8,068,522 Barty - Hyperdispersion Chirped Pulse Amplification and Compression

High-flux, laser-Compton scattering arrangements perturb the laser pulse energy very little during the interaction

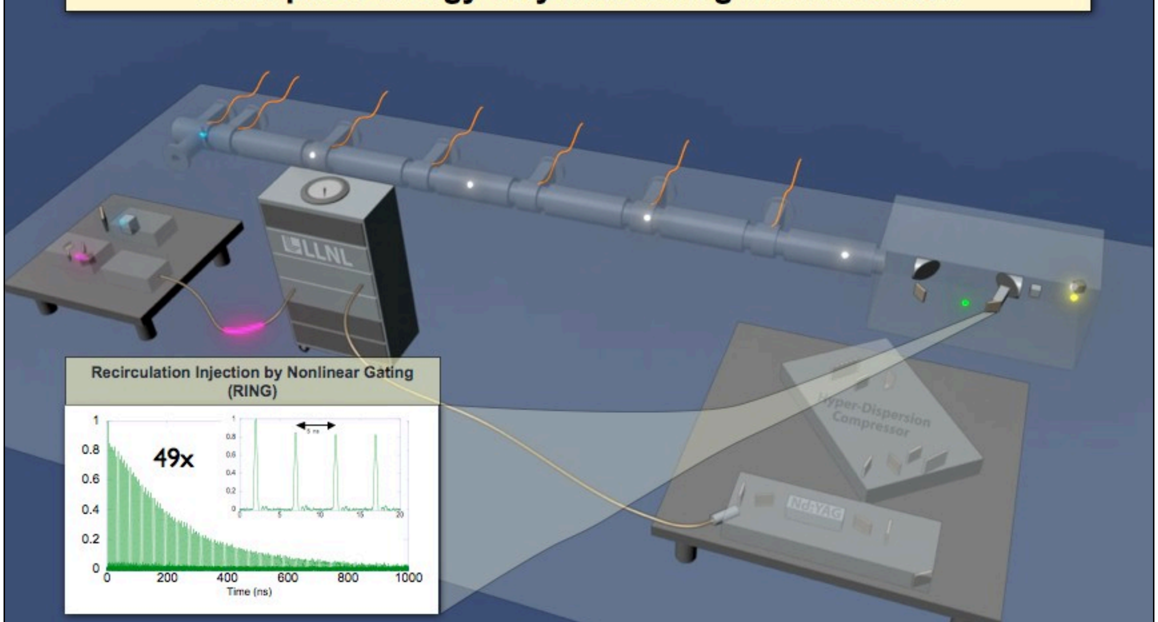

Recirculation can give > 50x increase in Compton photon production for "free"
RING positioning requirements are 10,000x less stringent than 'cavity' schemes

Shverdin, M. Y., I. Jovanovic, V. A. Semenov, S. M. Betts, C. Brown, D. J. Gibson, R. M. Shuttlesworth, F. V. Hartemann, C. W. Siders and C. P. J. Barty., "High-power picosecond laser pulse recirculation." Optics Letters 35(13): 2224-2226. (2010)

Overall Compton scattering is broadband, but it is highly angle correlated and is 'narrowband' on axis

$\Delta\Omega \; ; \; \pi\left(\frac{1}{\gamma}\right)^2$

few mrad

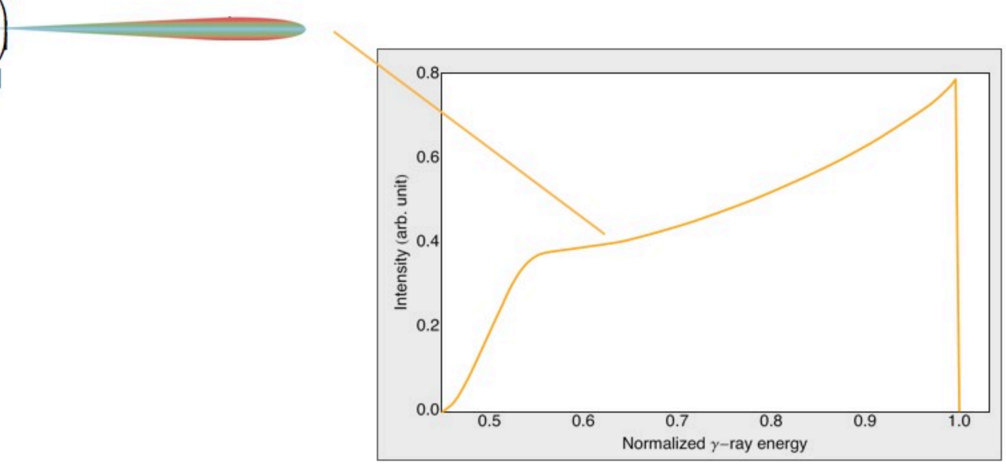

Overall Compton scattering is broadband, but it is highly angle correlated and is 'narrowband' on axis

$\Delta\Omega \; ; \; \pi\left(\frac{1}{\gamma}\right)^2$

few mrad

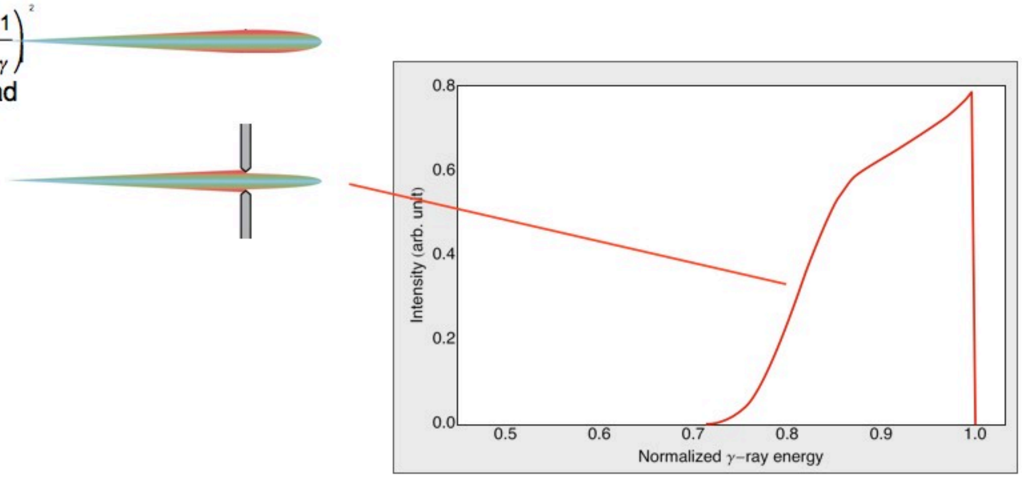

Overall Compton scattering is broadband, but it is highly angle correlated and is 'narrowband' on axis

$\Delta\Omega \;;\; \pi\left(\frac{1}{\gamma}\right)^2$

few mrad

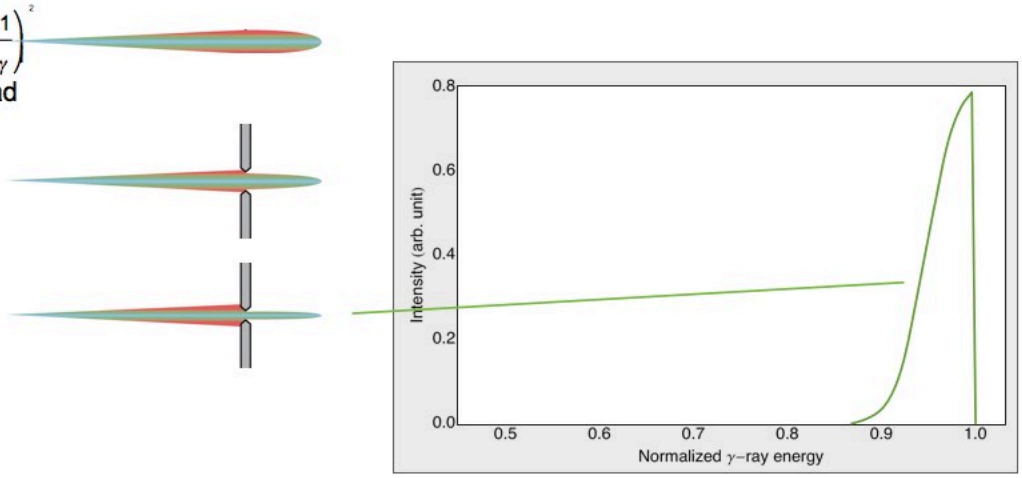

Overall Compton scattering is broadband, but it is highly angle correlated and is 'narrowband' on axis

$\Delta\Omega \;;\; \pi\left(\frac{1}{\gamma}\right)^2$

few mrad

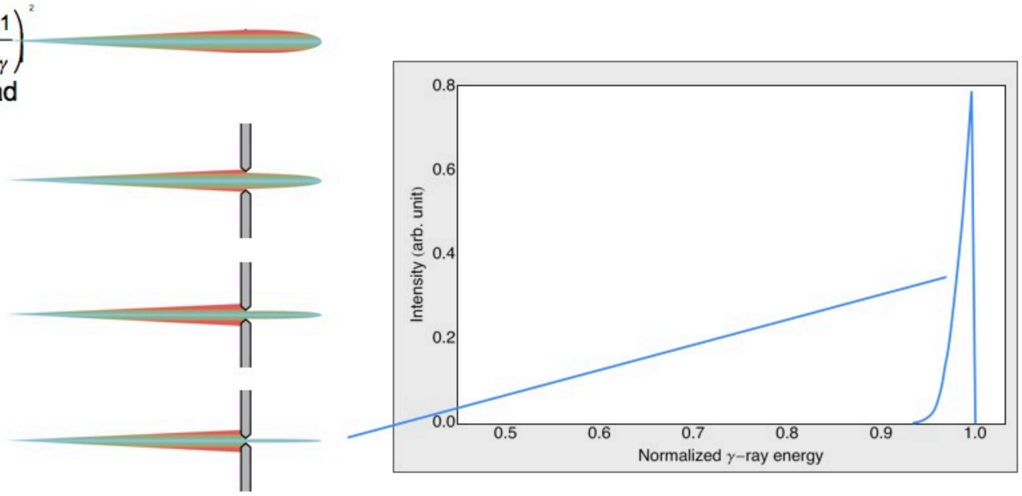

Overall Compton scattering is broadband, but it is highly angle correlated and is 'narrowband' on axis

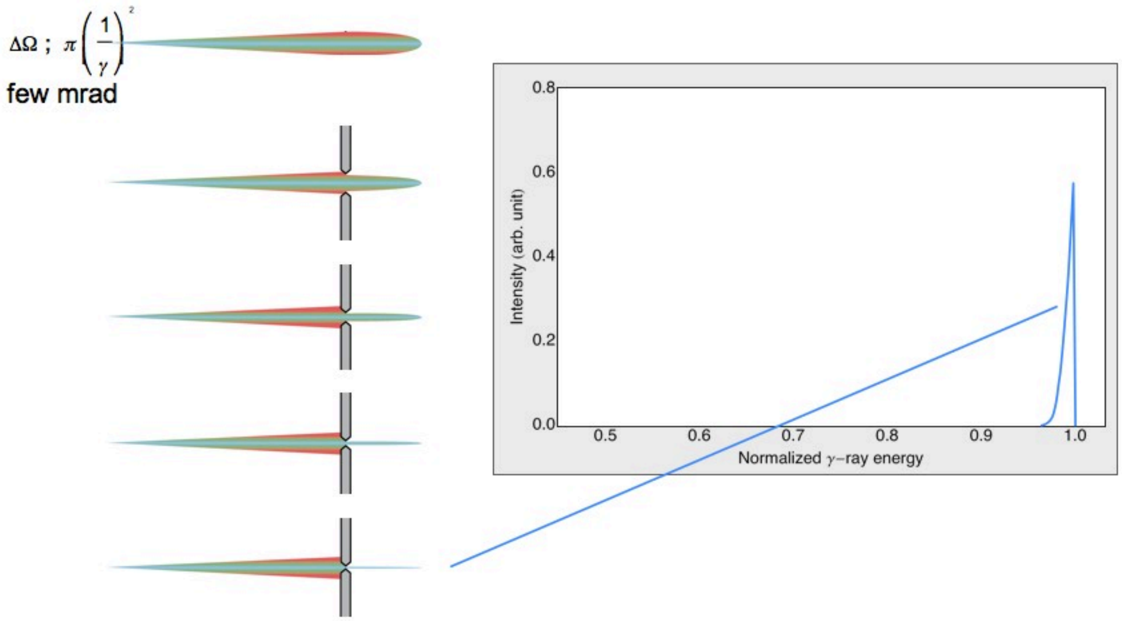

Overall Compton scattering is broadband, but it is highly angle correlated and is 'narrowband' on axis

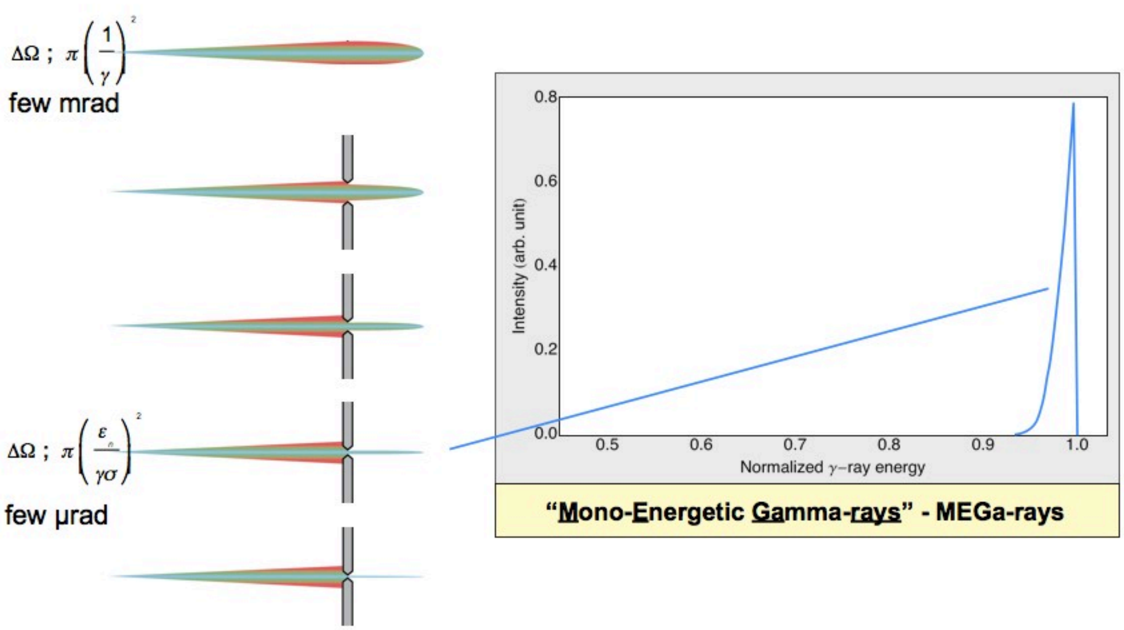

"Mono-Energetic Gamma-rays" - MEGa-rays

Many factors contribute to the minimum possible bandwidth*

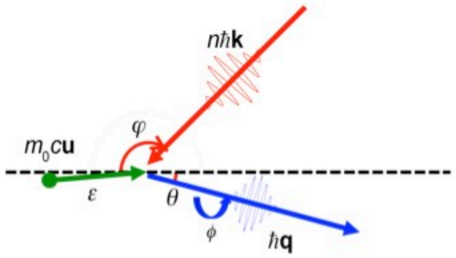

$$q = k\frac{\gamma - u\cos(\varepsilon+\varphi)}{\gamma - u\cos\varepsilon + (1-\cos\varphi)\left\{\frac{A^2}{2\left[\gamma - u\cos(\varepsilon+\varphi)\right]} + \lambda k\right\}}$$

Energy-Momentum Conservation

- **Detection Aperture** $\frac{\Delta q}{q} \simeq -\gamma^2\Delta\theta^2$
- **Laser Bandwidth** $\frac{\Delta q}{q} \simeq \frac{\Delta k}{k}$
- **Laser Focal Spot** $\frac{\Delta q}{q} \simeq -\frac{1}{4}\Delta\varphi^2$
- **Nonlinear Radiation Pressure** $\frac{\Delta q}{q} \simeq -\frac{\Delta A^2}{1+A^2}$
- **Electron Energy Spread** $\frac{\Delta q}{q} \simeq 2\frac{\Delta\gamma}{\gamma}$
- **Electron Beam Emittance** $\frac{\Delta q}{q} \simeq -\gamma^2\Delta\varepsilon^2$

* order-of-magnitude estimated contributions based on 2013 LLNL technology and optimized laser-Compton interaction geometry

Many factors contribute to the minimum possible bandwidth*

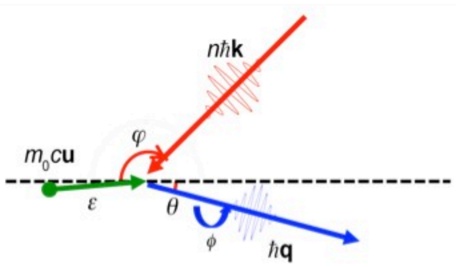

$$q = k\frac{\gamma - u\cos(\varepsilon+\varphi)}{\gamma - u\cos\varepsilon + (1-\cos\varphi)\left\{\frac{A^2}{2\left[\gamma - u\cos(\varepsilon+\varphi)\right]} + \lambda k\right\}}$$

Energy-Momentum Conservation

- **Detection Aperture** $\frac{\Delta q}{q} \simeq -\gamma^2\Delta\theta^2$
- **Laser Bandwidth** ~ 10 ps ~~$\frac{\Delta q}{q} \simeq \frac{\Delta k}{k}$~~ **O($10^{-4}$)**
- **Laser Focal Spot** $\frac{\Delta q}{q} \simeq -\frac{1}{4}\Delta\varphi^2$
- **Nonlinear Radiation Pressure** $\frac{\Delta q}{q} \simeq -\frac{\Delta A^2}{1+A^2}$
- **Electron Energy Spread** $\frac{\Delta q}{q} \simeq 2\frac{\Delta\gamma}{\gamma}$
- **Electron Beam Emittance** $\frac{\Delta q}{q} \simeq -\gamma^2\Delta\varepsilon^2$

* order-of-magnitude estimated contributions based on 2013 LLNL technology and optimized laser-Compton interaction geometry

Many factors contribute to the minimum possible bandwidth*

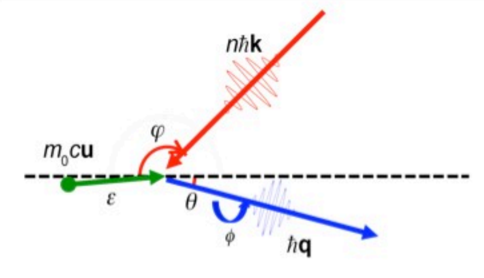

$$q = k\frac{\gamma - u\cos(\varepsilon+\varphi)}{\gamma - u\cos\varepsilon + (1-\cos\varphi)\left\{\frac{A^2}{2\left[\gamma - u\cos(\varepsilon+\varphi)\right]} + \lambda k\right\}}$$

Energy-Momentum Conservation

- **Detection Aperture** $\frac{\Delta q}{q} \simeq -\gamma^2\Delta\theta^2$
- **Laser Bandwidth** ~ 10 ps $\frac{\Delta q}{q} \simeq \frac{\Delta k}{k}$ **O(10^-4)**
- **Laser Focal Spot** ~ 10 microns $\frac{\Delta q}{q} \simeq -\frac{1}{4}\Delta\varphi^2$ **O(10^-4)**
- **Nonlinear Radiation Pressure** $\frac{\Delta q}{q} \simeq -\frac{\Delta A^2}{1+A^2}$
- **Electron Energy Spread** $\frac{\Delta q}{q} \simeq 2\frac{\Delta\gamma}{\gamma}$
- **Electron Beam Emittance** $\frac{\Delta q}{q} \simeq -\gamma^2\Delta\varepsilon^2$

* order-of-magnitude estimated contributions based on 2013 LLNL technology and optimized laser-Compton interaction geometry

Radiation pressure can significantly change the velocity of the electron during scattering

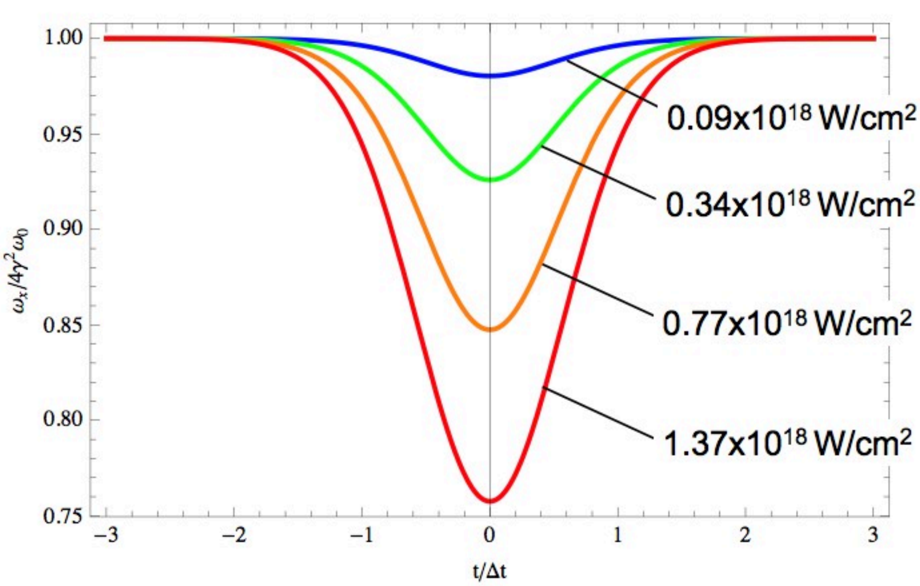

F. V. Hartemann, D. J. Gibson, S. G. Anderson, A. M. Tremaine, P. T. Springer, A. J. Wootton, E. P. Hartouni, and C. P. J. Barty, "High-energy scaling of Compton scattering light sources," Physical Review Special Topics-Accelerators and Beams 8, 100702(100717) (2005)

Nonlinear broadening at low intensity can also be an issue under certain long pulse conditions

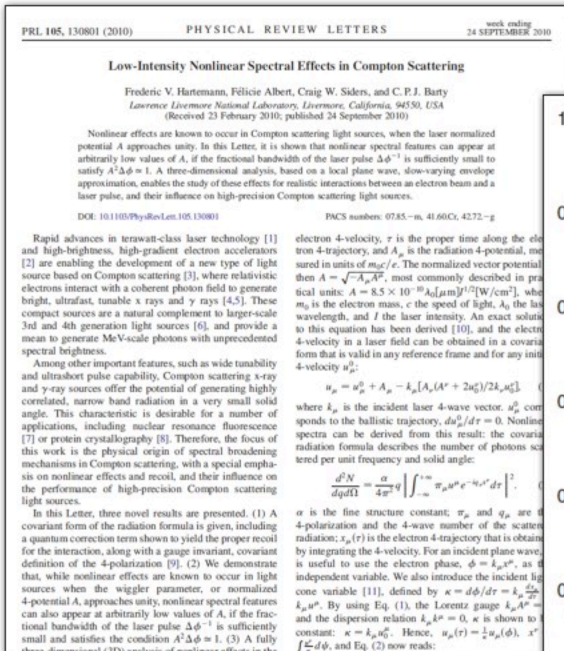
PRL 105, 130801 (2010) PHYSICAL REVIEW LETTERS week ending 24 SEPTEMBER 2010

Low-Intensity Nonlinear Spectral Effects in Compton Scattering

Frederic V. Hartemann, Félicie Albert, Craig W. Siders, and C. P. J. Barty
Lawrence Livermore National Laboratory, Livermore, California, 94550, USA
(Received 23 February 2010; published 24 September 2010)

Nonlinear effects are known to occur in Compton scattering light sources, when the laser normalized potential A approaches unity. In this Letter, it is shown that nonlinear spectral features can appear at arbitrarily low values of A, if the fractional bandwidth of the laser pulse $\Delta\phi^{-1}$ is sufficiently small to satisfy $A^2\Delta\phi \simeq 1$. A three-dimensional analysis, based on a local plane wave, slow-varying envelope approximation, enables the study of these effects for realistic interactions between an electron beam and a laser pulse, and their influence on high-precision Compton scattering light sources.

DOI: 10.1103/PhysRevLett.105.130801 PACS numbers: 07.85.−m, 41.60.Cr, 42.72.−g

Rapid advances in terawatt-class laser technology [1] and high-brightness, high-gradient electron accelerators [2] are enabling the development of a new type of light source based on Compton scattering [3], where relativistic electrons interact with a coherent photon field to generate bright, ultrafast, tunable x rays and γ rays [4,5]. These compact sources are a natural complement to larger-scale 3rd and 4th generation light sources [6], and provide a mean to generate MeV-scale photons with unprecedented spectral brightness.

Among other important features, such as wide tunability and ultrashort pulse capability, Compton scattering x-ray and γ-ray sources offer the potential of generating highly correlated, narrow band radiation in a very small solid angle. This characteristic is desirable for a number of applications, including nuclear resonance fluorescence [7] or protein crystallography [8]. Therefore, the focus of this work is the physical origin of spectral broadening mechanisms in Compton scattering, with a special emphasis on nonlinear effects and recoil, and their influence on the performance of high-precision Compton scattering light sources.

In this Letter, three novel results are presented. (1) A covariant form of the radiation formula is given, including a quantum correction term shown to yield the proper recoil for the interaction, along with a gauge invariant, covariant definition of the 4-polarization [9]. (2) We demonstrate that, while nonlinear effects are known to occur in light sources when the wiggler parameter, or normalized 4-potential A, approaches unity, nonlinear spectral features can also appear at arbitrarily low values of A, if the fractional bandwidth of the laser pulse $\Delta\phi^{-1}$ is sufficiently small and satisfies the condition $A^2\Delta\phi \simeq 1$. (3) A fully three-dimensional (3D) analysis of nonlinear effects in the

electron 4-velocity, τ is the proper time along the ele[ctron] 4-trajectory, and A_μ is the radiation 4-potential, me[a]sured in units of m_0c/e. The normalized vector potential [is] then $A = \sqrt{-A_\mu A^\mu}$, most commonly described in pra[c]tical units: $A = 8.5 \times 10^{-10}\lambda_0[\mu m]I^{1/2}[W/cm^2]$, whe[re] m_0 is the electron mass, c the speed of light, λ_0 the las[er] wavelength, and I the laser intensity. An exact soluti[on] to this equation has been derived [10], and the electr[on] 4-velocity in a laser field can be obtained in a covaria[nt] form that is valid in any reference frame and for any initi[al] 4-velocity u_μ^0:

$$u_\mu = u_\mu^0 + A_\mu - k_\mu[A_\nu(A^\nu + 2u_0^\nu)/2k_\nu u_0^\nu],$$

where k_μ is the incident laser 4-wave vector. u_μ^0 corr[e]sponds to the ballistic trajectory, $du_\mu^0/d\tau = 0$. Nonline[ar] spectra can be derived from this result: the covaria[nt] radiation formula describes the number of photons sca[t]tered per unit frequency and solid angle:

$$\frac{d^2N}{dq d\Omega} = \frac{\alpha}{4\pi^2} q \left| \int_{-\infty}^{+\infty} \pi_\mu u^\mu e^{-iq_\nu x^\nu} d\tau \right|^2.$$

α is the fine structure constant; π_μ and q_μ are t[he] 4-polarization and the 4-wave number of the scatter[ed] radiation; $x_\mu(\tau)$ is the electron 4-trajectory that is obtain[ed] by integrating the 4-velocity. For an incident plane wave, [it] is useful to use the electron phase, $\phi = k_\mu x^\mu$, as t[he] independent variable. We also introduce the incident lig[ht] cone variable [11], defined by $\kappa = d\phi/d\tau = k_\mu \frac{dx_\mu}{d\tau}$ $k_\mu u^\mu$. By using Eq. (1), the Lorentz gauge $k_\mu A^\mu =$ and the dispersion relation $k_\mu k^\mu = 0$, κ is shown to [be] constant: $\kappa = k_\mu u_0^\mu$. Hence, $u_\mu(\tau) = \frac{1}{\kappa}u_\mu(\phi)$, x^ν $\int \frac{u^\nu}{\kappa} d\phi$, and Eq. (2) now reads:

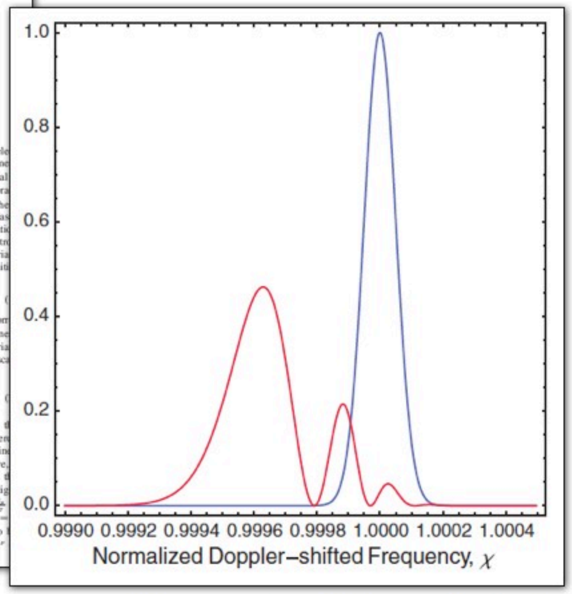

Hartemann, F. V., F. Albert, C. W. Siders and C. P. J. Barty. "Low-intensity nonlinear spectral effects in Compton scattering." Physical Review Letters 105(13): 130801. (2010)

Many factors contribute to the minimum possible bandwidth*

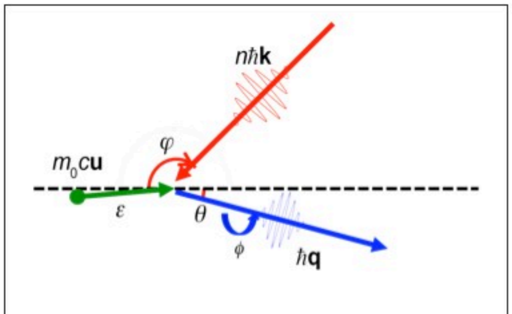

$$q = k\frac{\gamma - u\cos(\varepsilon+\varphi)}{\gamma - u\cos\varepsilon + (1-\cos\varphi)\left\{\frac{A^2}{2[\gamma - u\cos(\varepsilon+\varphi)]} + \lambda k\right\}}$$

Energy-Momentum Conservation

- **Detection Aperture** $\frac{\Delta q}{q} \simeq -\gamma^2\Delta\theta^2$
- **Laser Bandwidth** ~ 10 ps ~~$\frac{\Delta q}{q} \simeq \frac{\Delta k}{k}$~~ O(10-4)
- **Laser Focal Spot** ~ 10 microns ~~$\frac{\Delta q}{q} \simeq -\frac{1}{4}\Delta\varphi^2$~~ O(10-4)
- **Nonlinear Radiation Pressure** ~~$\frac{\Delta q}{q} \simeq -\frac{\Delta A^2}{1+A^2}$~~ < 10-4
- **Electron Energy Spread** $\frac{\Delta q}{q} \simeq 2\frac{\Delta\gamma}{\gamma}$
- **Electron Beam Emittance** $\frac{\Delta q}{q} \simeq -\gamma^2\Delta\varepsilon^2$

* order-of-magnitude estimated contributions based on 2013 LLNL technology and optimized laser-Compton interaction geometry

Modern, high gradient accelerators can create very small emittance and energy spread at low charge

25 pC electron beam phase space

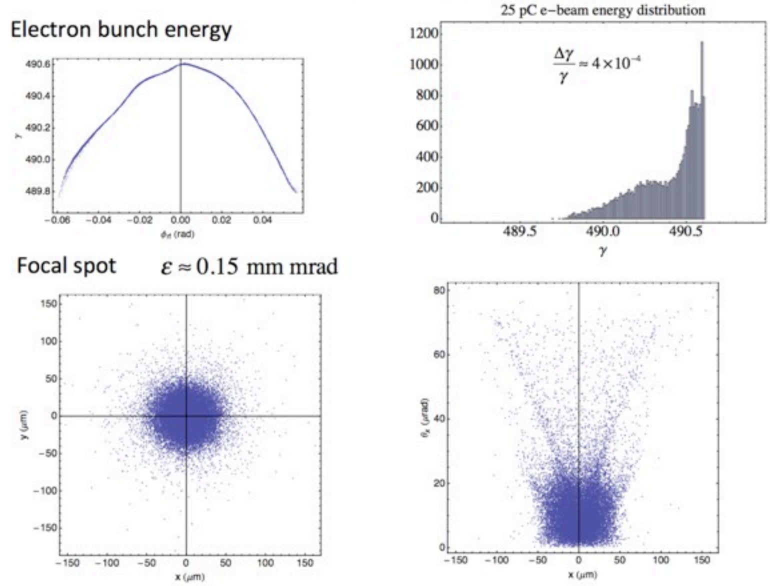

Marsh, R. A., F. Albert, S. G. Anderson, G. Beer, T. S. Chu, R. R. Cross, G. A. Deis, C. A. Ebbers, D. J. Gibson, T. L. Houck, F. V. Hartemann, C. P. J. Barty, et al. "Modeling and design of an X-band RF photoinjector." Physical Review Special Topics: Accelerators and Beams 15(10): 102001 (2012)

Many factors contribute to the minimum possible bandwidth*

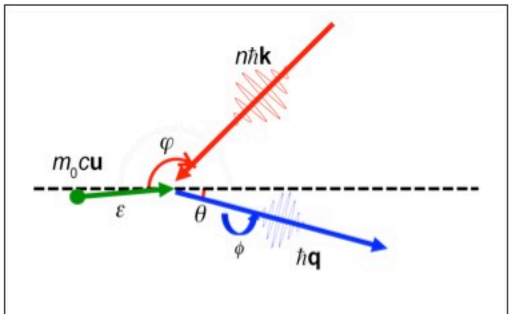

$$q = k\frac{\gamma - u\cos(\varepsilon+\varphi)}{\gamma - u\cos\varepsilon + (1-\cos\varphi)\left\{\frac{A^2}{2\left[\gamma - u\cos(\varepsilon+\varphi)\right]} + \lambda k\right\}}$$

Energy-Momentum Conservation

- **Detection Aperture** $\frac{\Delta q}{q} \simeq -\gamma^2\Delta\theta^2$
- **Laser Bandwidth** ~ 10 ps $\frac{\Delta q}{q} \simeq \frac{\Delta k}{k}$ O(10⁻⁴)
- **Laser Focal Spot** ~ 10 microns $\frac{\Delta q}{q} \simeq -\frac{1}{4}\Delta\varphi^2$ O(10⁻⁴)
- **Nonlinear Radiation Pressure** $\frac{\Delta q}{q} \simeq -\frac{\Delta A^2}{1+A^2}$ < 10⁻⁴
- **Electron Energy Spread** $\frac{\Delta q}{q} \simeq 2\frac{\Delta\gamma}{\gamma}$
- **Electron Beam Emittance** $\frac{\Delta q}{q} \simeq -\gamma^2\Delta\varepsilon^2$

* order-of-magnitude estimated contributions based on 2013 LLNL technology and optimized laser-Compton interaction geometry

Many factors contribute to the minimum possible bandwidth*

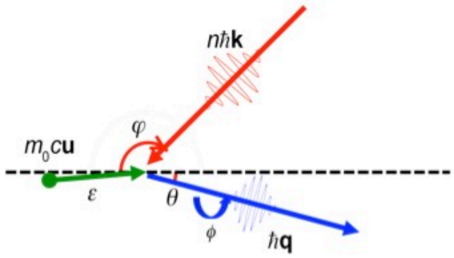

$$q = k\frac{\gamma - u\cos(\varepsilon+\varphi)}{\gamma - u\cos\varepsilon + (1-\cos\varphi)\left\{\frac{A^2}{2[\gamma - u\cos(\varepsilon+\varphi)]} + \lambda k\right\}}$$

Energy-Momentum Conservation

- **Detection Aperture** $\frac{\Delta q}{q} \simeq -\gamma^2\Delta\theta^2$ **< 10^{-3}**
- **Laser Bandwidth** ~ 10 ps $\frac{\Delta q}{q} \simeq \frac{\Delta k}{k}$ **O(10^{-4})**
- **Laser Focal Spot** ~ 10 microns $\frac{\Delta q}{q} \simeq -\frac{1}{4}\Delta\varphi^2$ **O(10^{-4})**
- **Nonlinear Radiation Pressure** $\frac{\Delta q}{q} \simeq -\frac{\Delta A^2}{1+A^2}$ **< 10^{-4}**
- **Electron Energy Spread** $\frac{\Delta q}{q} \simeq 2\frac{\Delta\gamma}{\gamma}$ **< 10^{-3}**
- **Electron Beam Emittance** $\frac{\Delta q}{q} \simeq -\gamma^2\Delta\varepsilon^2$ **< 10^{-3}**

* order-of-magnitude estimated contributions based on 2013 LLNL technology and optimized laser-Compton interaction geometry

Many factors contribute to the minimum possible bandwidth*

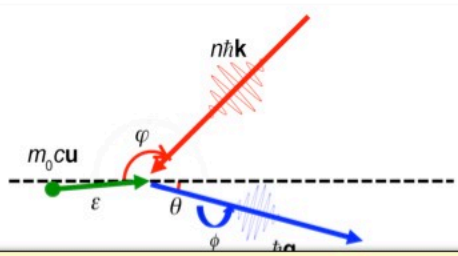

Optimally designed sources can have fractional bandwidths of <10^{-3} FWHM

$$q = k\frac{\gamma - u\cos(\varepsilon+\varphi)}{\gamma - u\cos\varepsilon + (1-\cos\varphi)\left\{\frac{A^2}{2[\gamma - u\cos(\varepsilon+\varphi)]} + \lambda k\right\}}$$

Energy-Momentum Conservation

- **Detection Aperture** $\frac{\Delta q}{q} \simeq -\gamma^2\Delta\theta^2$ **< 10^{-3}**
- **Laser Bandwidth** ~ 10 ps $\frac{\Delta q}{q} \simeq \frac{\Delta k}{k}$ **O(10^{-4})**
- **Laser Focal Spot** ~ 10 microns $\frac{\Delta q}{q} \simeq -\frac{1}{4}\Delta\varphi^2$ **O(10^{-4})**
- **Nonlinear Radiation Pressure** $\frac{\Delta q}{q} \simeq -\frac{\Delta A^2}{1+A^2}$ **< 10^{-4}**
- **Electron Energy Spread** $\frac{\Delta q}{q} \simeq 2\frac{\Delta\gamma}{\gamma}$ **< 10^{-3}**
- **Electron Beam Emittance** $\frac{\Delta q}{q} \simeq -\gamma^2\Delta\varepsilon^2$ **< 10^{-3}**

* order-of-magnitude estimated contributions based on 2013 LLNL technology and optimized laser-Compton interaction geometry

Optimized laser-Compton sources enable "lab-scale" x-ray science and "nuclear" photonics

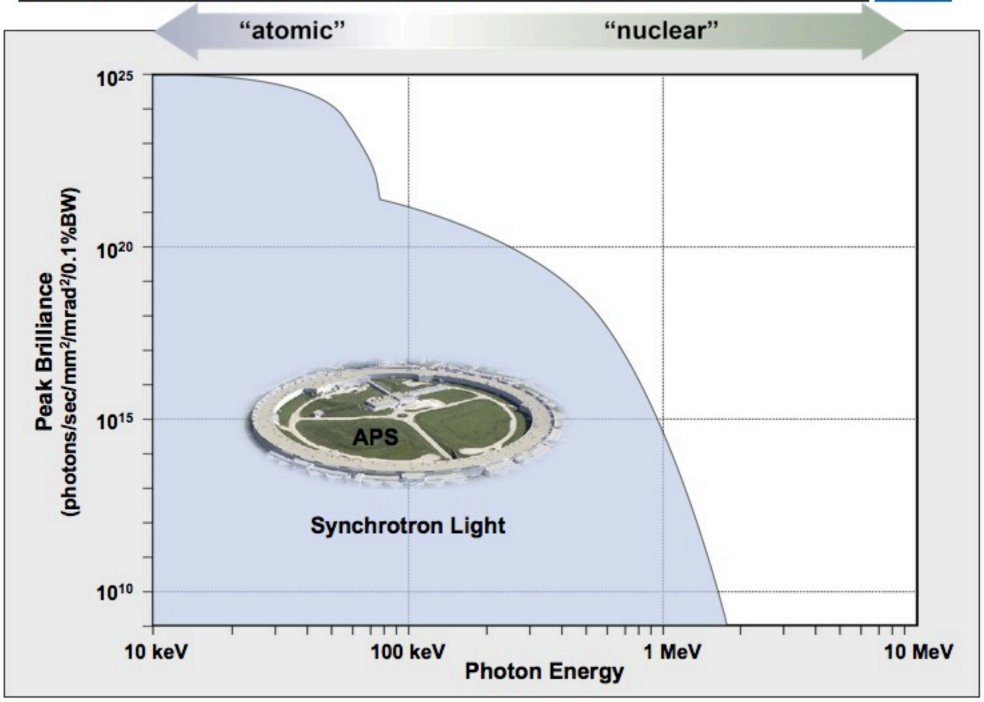

Optimized laser-Compton sources enable "lab-scale" x-ray science and "nuclear" photonics

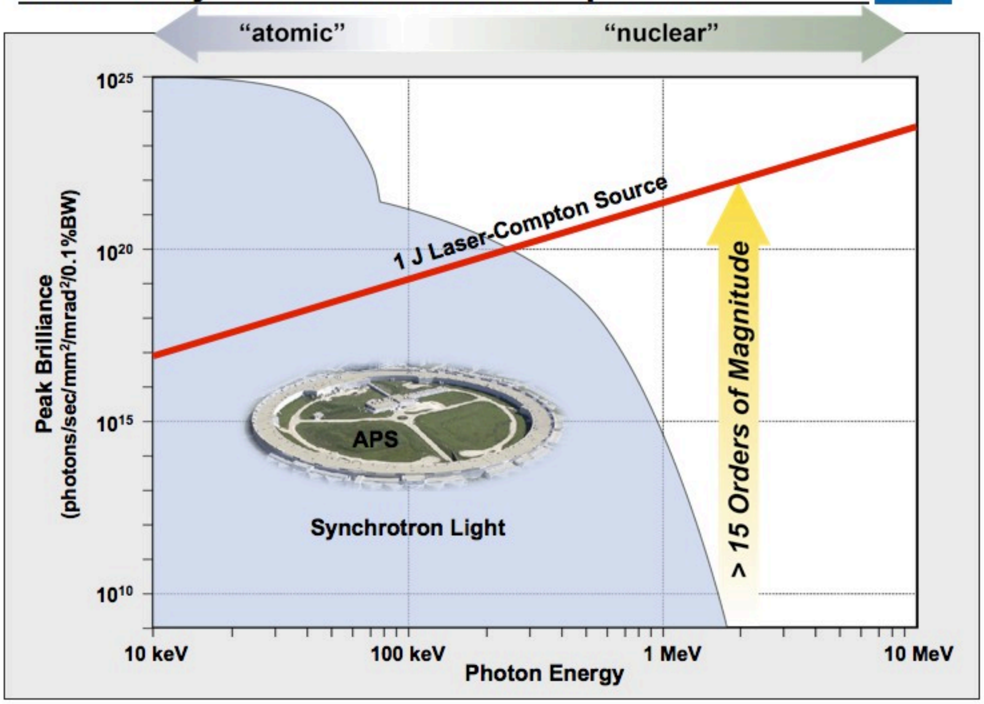

Optimized laser-Compton sources enable “lab-scale” x-ray science and “nuclear” photonics

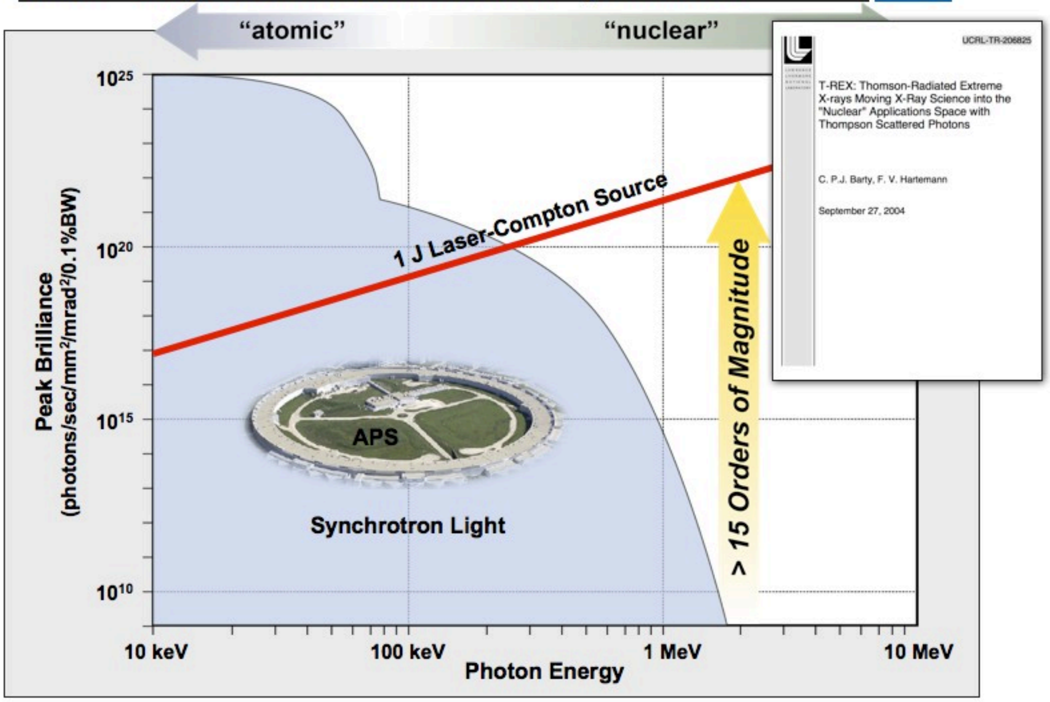

Optimized laser-Compton sources enable “lab-scale” x-ray science and “nuclear” photonics

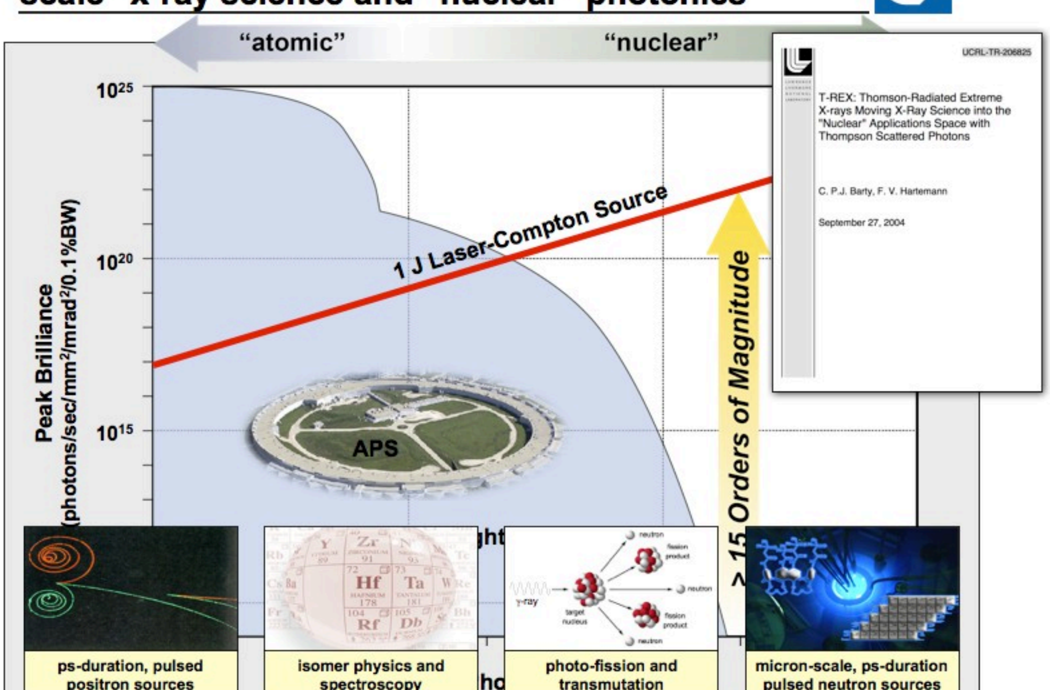

D. Habs, T. Tajima, J. Schreiber, C. P. J. Barty, M. Fujiwara, and P. G. Thirolf, "Vision of nuclear physics with photo-nuclear reactions by laser-driven gamma beams," EPJ D 55, '09

Gamma-ray absorption & radiation by the nucleus is an "isotope-specific" signature of the material

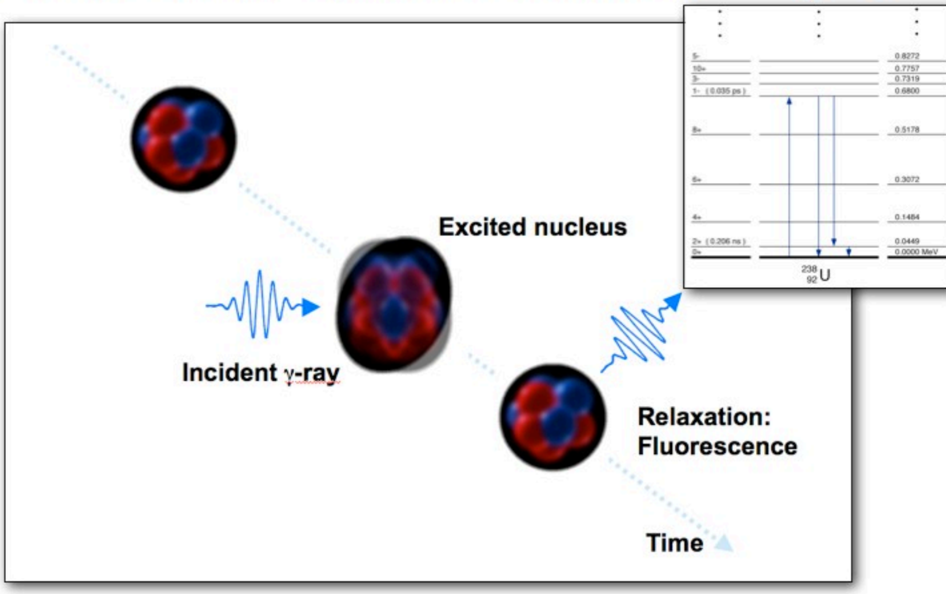

Nuclear Resonance Fluorescence (NRF) is analogous to atomic resonance fluorescence but depends upon the number of protons AND the number of neutrons in the nucleus

Selective excitation of NRF is possible with narrow bandwidth gamma-rays ($\Delta E/E \sim 10^{-3}$)

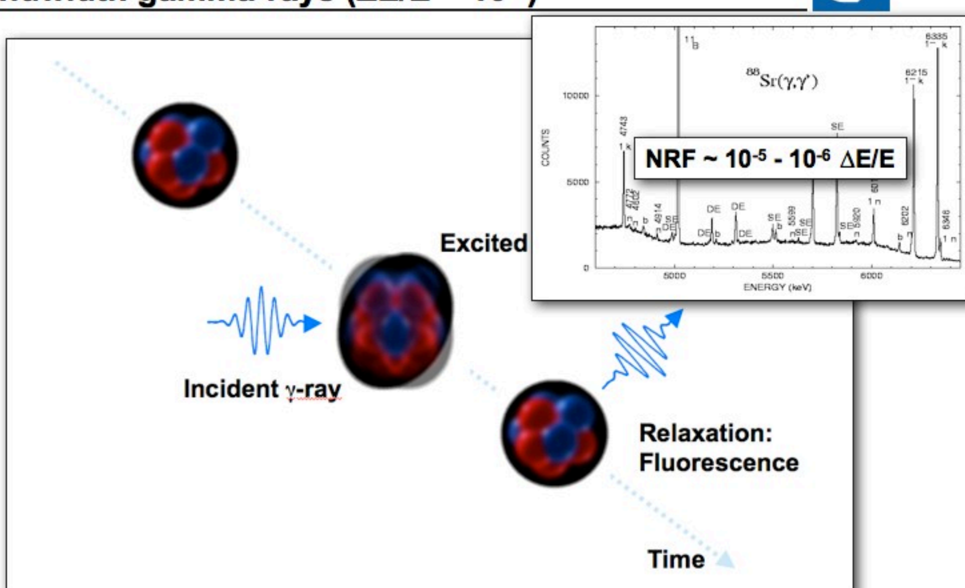

Nuclear Resonance Fluorescence (NRF) is analogous to atomic resonance fluorescence but depends upon the number of protons AND the number of neutrons in the nucleus

NRF transitions are common and many have cross sections larger than the atomic background

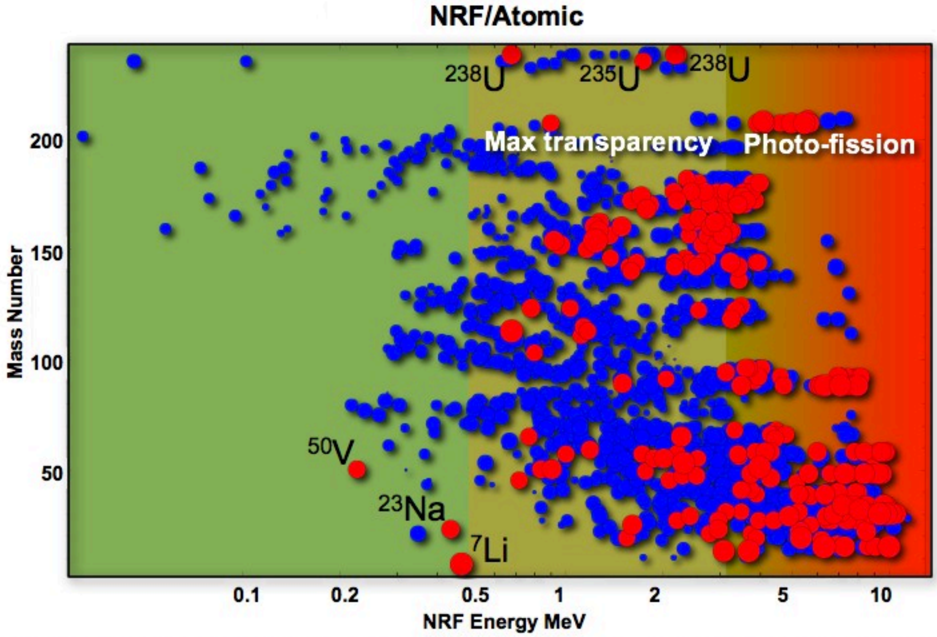

Gammas in the 1 MeV to 3 MeV range are both highly penetrating and non-activating

NRF transitions are common and many have cross sections larger than the atomic background

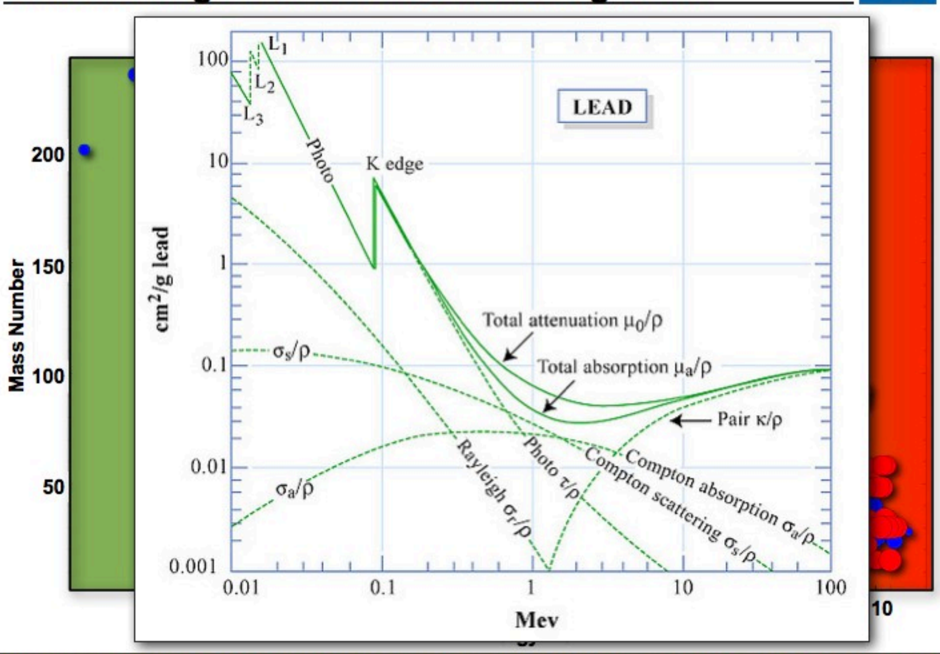

Gammas in the 1 MeV to 3 MeV range are both highly penetrating and non-activating

Bright, mono-energetic, gamma-ray sources enable new possibilities: "Inverse Density" radiography

- X-ray absorption is proportional to electron density/atomic number
- IF the x-ray can penetrate the high-Z material, it is not stopped by the low-Z material
- Low-Z materials are effectively shielded by dense, high-Z material

Precision imaging of low density material features inside of high density components is not feasible with conventional x-ray radiography

Monte Carlo simulations using COG

Imaging simulations (shielded low-Z material)

Shielded low-Z NRF test object (a)

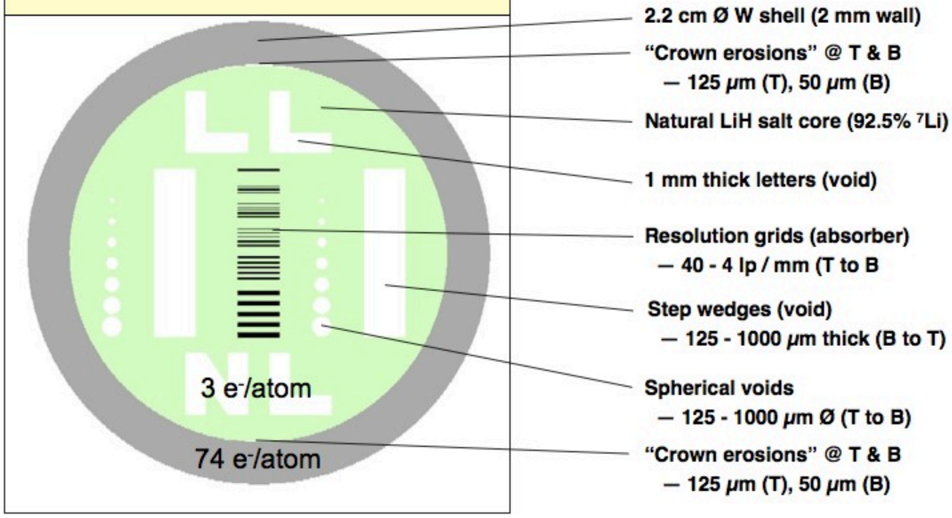

Monte Carlo simulations using COG

Imaging simulations (shielded low-Z material)

Shielded low-Z NRF test object (a)

- 2.2 cm Ø W shell (2 mm wall)
- "Crown erosions" @ T & B
  - 125 μm (T), 50 μm (B)
- Natural LiH salt core (92.5% ^{7}Li)
- 1 mm thick letters (void)
- Resolution grids (absorber)
  - 40 - 4 lp / mm (T to B
- Step wedges (void)
  - 125 - 1000 μm thick (B to T)
- Spherical voids
  - 125 - 1000 μm Ø (T to B)
- "Crown erosions" @ T & B
  - 125 μm (T), 50 μm (B)

Monte Carlo simulations using COG

Simulation of 0.478 MeV NRF image vs. 9 MeV e-Brem x-ray image (normalized*)

0.478 MeV NRF Image Simulation (Enhanced ^{7}Li Density)

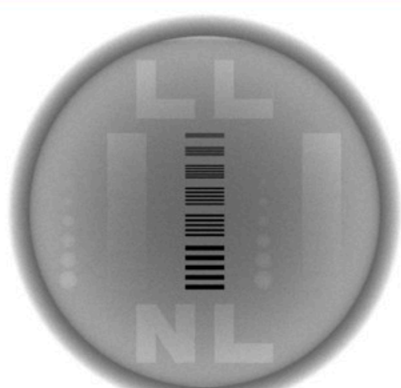

High-Z shell:

EDep ~ 0.117 MeV/γ

RDose ~ 1.060E-07 μSv/γ

9 MeV e-Brem X-Ray Image Simulation

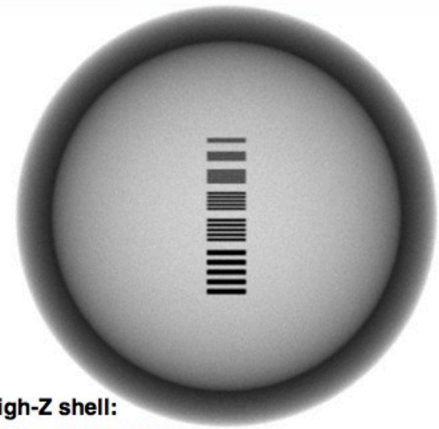

High-Z shell:

EDep ~ 0.215 MeV/γ

RDose ~ 4.276E-07 μSv/γ

* The images have been normalized such that the open-field intensity in each case is ≈ 1 (arbitrary units)

Hall, J., V. Semenov, F. Albert and C. P. J. Barty. "Numerical Simulation of Nuclear Materials Detection, Imaging and Assay with MEGa-rays." Proceedings of the 52nd Annual Meeting of the Institute for Nuclear Materials Management Vol 3. 2673-2682. (2011)

Potential NRF-based Applications of Bright Gamma Sources are Numerous

HEU Grand Challenge
detection of shielded material

Nuclear Fuel Assay
100 parts per million per isotope

Waste Imaging & Assay
non-invasive content certification

Industrial NDE
micron-scale & isotope specific

Medical Imaging
low density & isotope specific

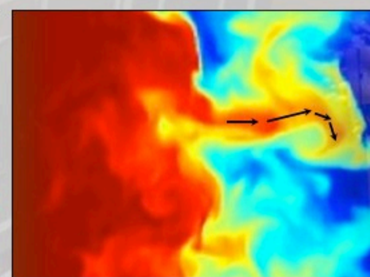

Dense Plasma Science
isotope mass, position & velocity

US patent #7,564,241 Barty, Hartemann, McNabb & Pruet - detection, assay and imaging with laser-Compton gamma-rays

Finding shielded Highly Enriched Uranium (HEU) is a grand challenge

Lead Attenuation

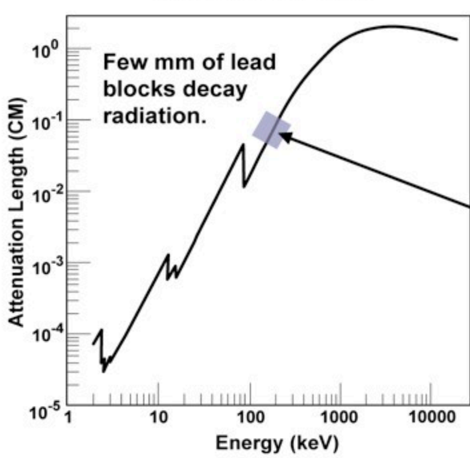

Long half-life: 7×10^8 y
Low-energy signal: 186 keV

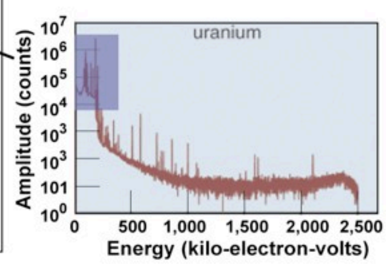

Passive detection of decay signature is easily defeated by mm's of lead shielding

Conventional MeV-range radiographic inspection can image through thick objects

Visually powerful but unable to distinguish one material from another, i.e. cannot tell if SNM (special nuclear material) is present

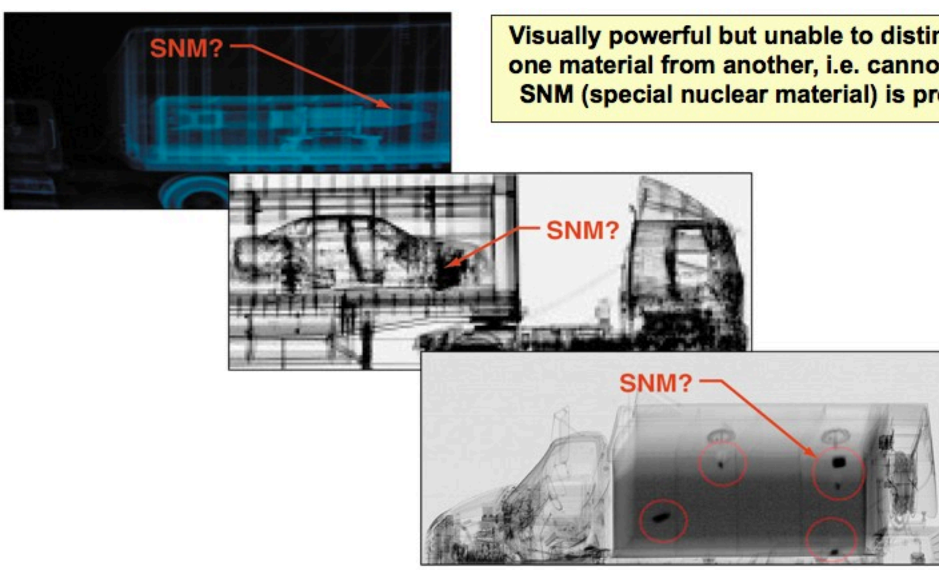

MEGa-ray beam absorption could be used to rapidly & safely distinguish SNM from background materials

Using MEGa-ray technologies currently under development, identification of a ~5mm thick piece of 235U would take << 1s

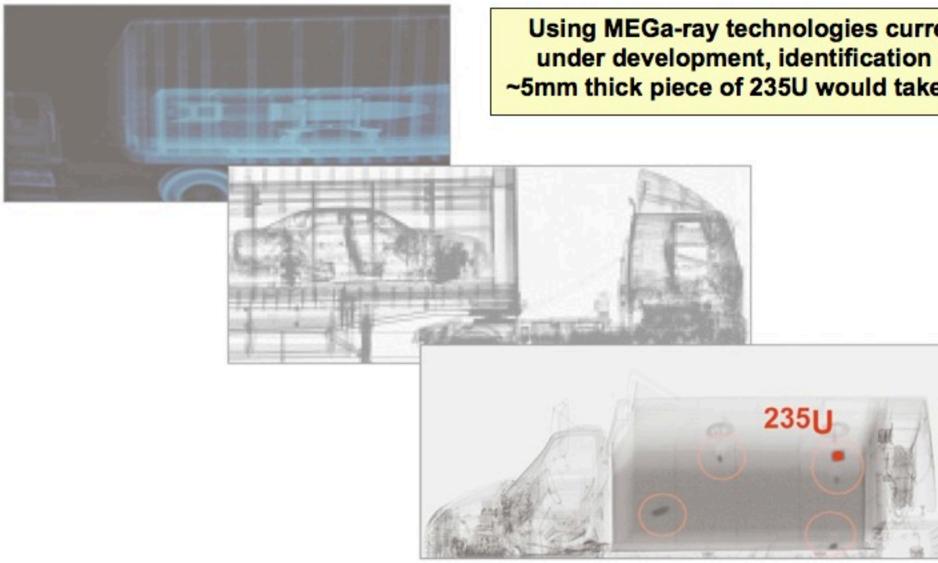

Numerical analysis suggests that active (but not "activating") SNM detection could be accomplished with MEGa-rays at doses that are 100x below allowable human limits

US patent #7,564,241 Barty, Hartemann, McNabb & Pruet - detection, assay and imaging with MEGa-rays

MEGa-ray beam absorption could be used to rapidly & safely distinguish SNM from background materials

Using MEGa-ray technologies currently under development, identification of a ~5mm thick piece of 235U would take << 1s

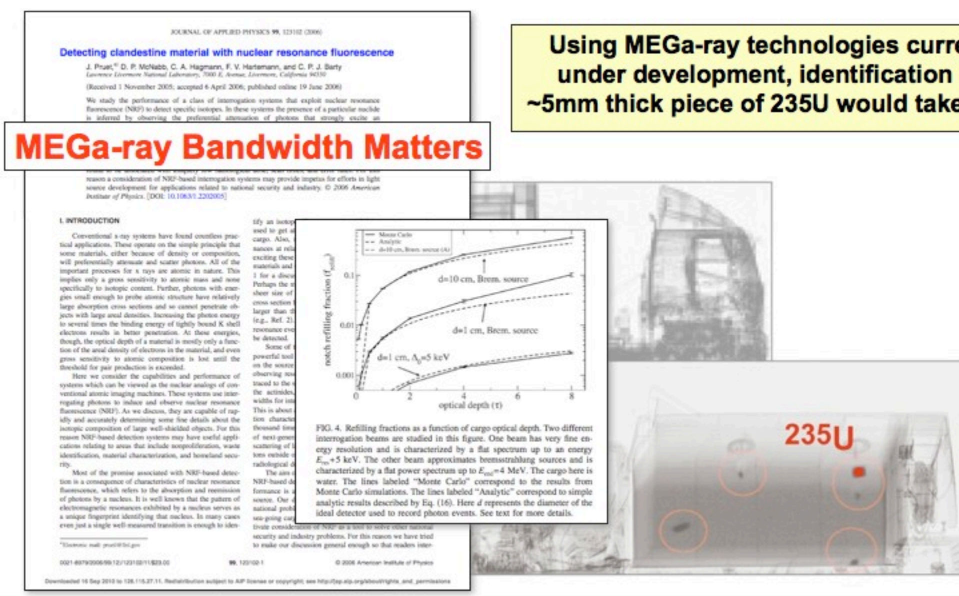

Numerical analysis suggests that active (but not "activating") SNM detection could be accomplished with MEGa-rays at doses that are 100x below allowable human limits

J. Pruet, D. P. McNabb, C. A. Hagmann, F. V. Hartemann, and C. P. J. Barty, "Detecting clandestine material with nuclear resonance fluorescence," JAP 99, 123102-123111 (2006)

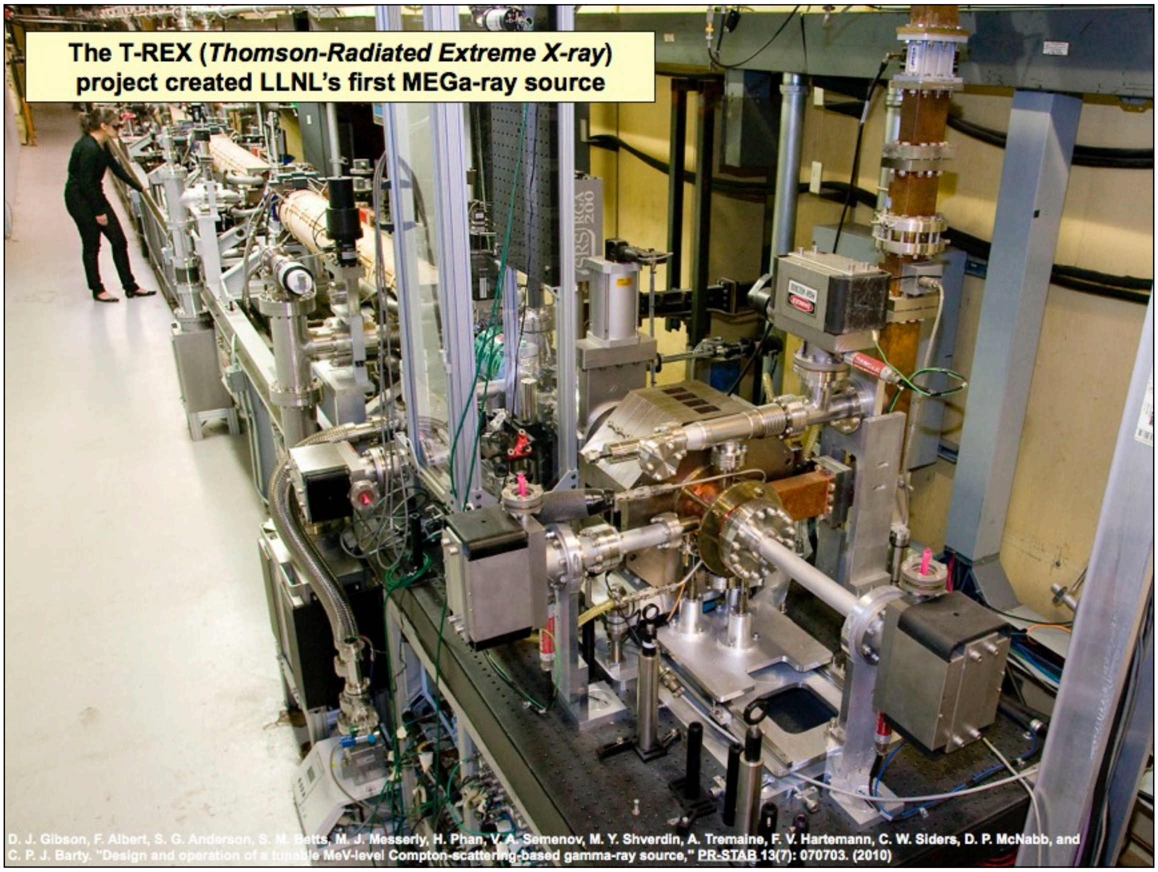
The T-REX (*Thomson-Radiated Extreme X-ray*)
project created LLNL's first MEGa-ray source
D. J. Gibson, F. Albert, S. G. Anderson, S. M. Betts, M. J. Messerly, H. Phan, V. A. Semenov, M. Y. Shverdin, A. Tremaine, F. V. Hartemann, C. W. Siders, D. P. McNabb, and
C. P. J. Barty. "Design and operation of a tunable MeV-level Compton-scattering-based gamma-ray source," PR-STAB 13(7): 070703. (2010)

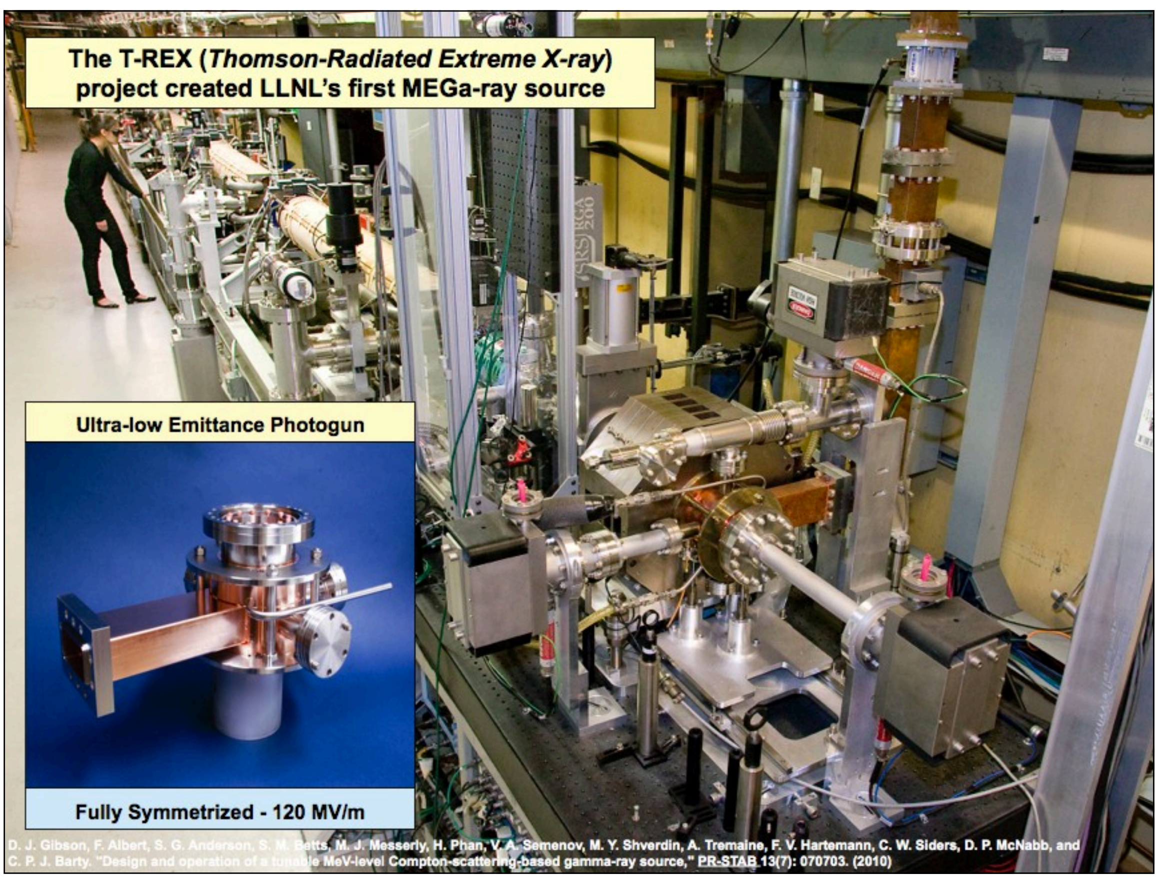
The T-REX (*Thomson-Radiated Extreme X-ray*)
project created LLNL's first MEGa-ray source
Ultra-low Emittance Photogun
Fully Symmetrized - 120 MV/m
D. J. Gibson, F. Albert, S. G. Anderson, S. M. Betts, M. J. Messerly, H. Phan, V. A. Semenov, M. Y. Shverdin, A. Tremaine, F. V. Hartemann, C. W. Siders, D. P. McNabb, and
C. P. J. Barty. "Design and operation of a tunable MeV-level Compton-scattering-based gamma-ray source," PR-STAB 13(7): 070703. (2010)

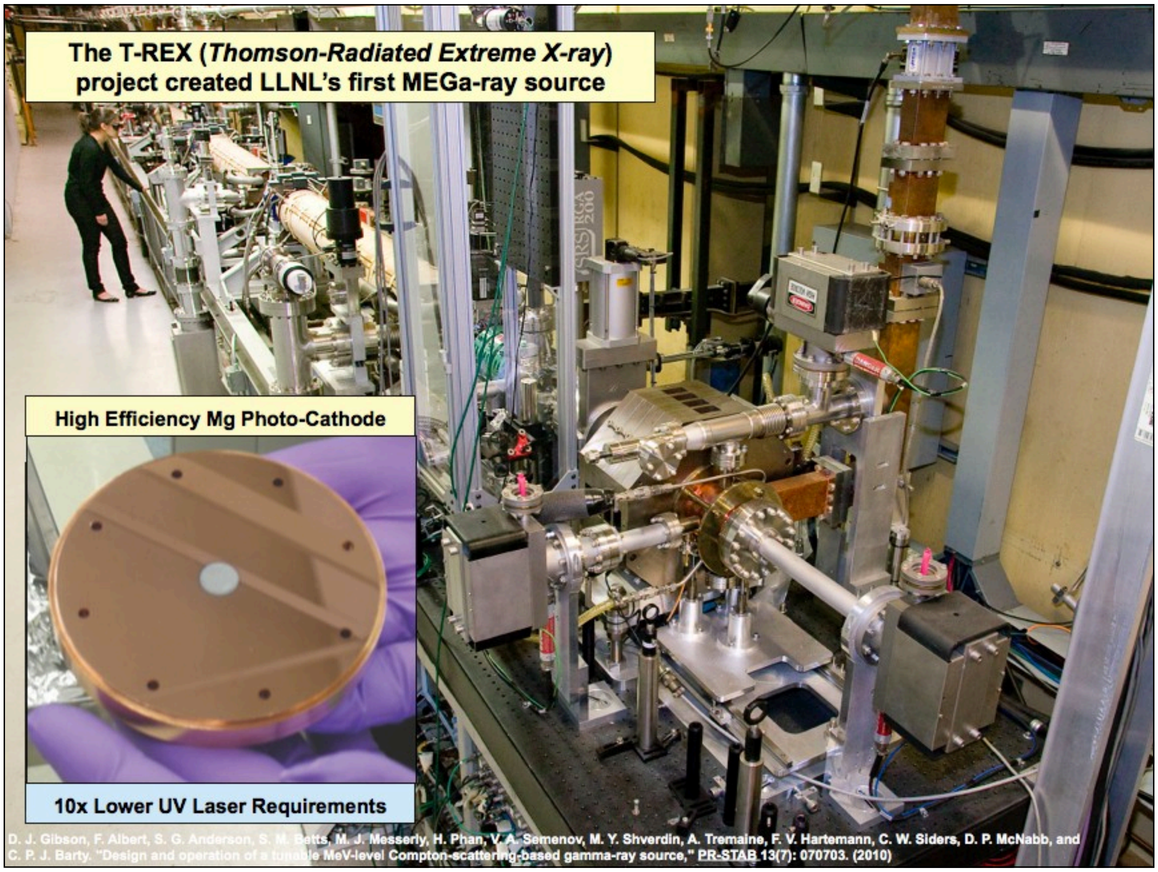
The T-REX (Thomson-Radiated Extreme X-ray)
project created LLNL's first MEGa-ray source
High Efficiency Mg Photo-Cathode
10x Lower UV Laser Requirements
D. J. Gibson, F. Albert, S. G. Anderson, S. M. Betts, M. J. Messerly, H. Phan, V. A. Semenov, M. Y. Shverdin, A. Tremaine, F. V. Hartemann, C. W. Siders, D. P. McNabb, and C. P. J. Barty. "Design and operation of a tunable MeV-level Compton-scattering-based gamma-ray source," PR-STAB 13(7): 070703. (2010)

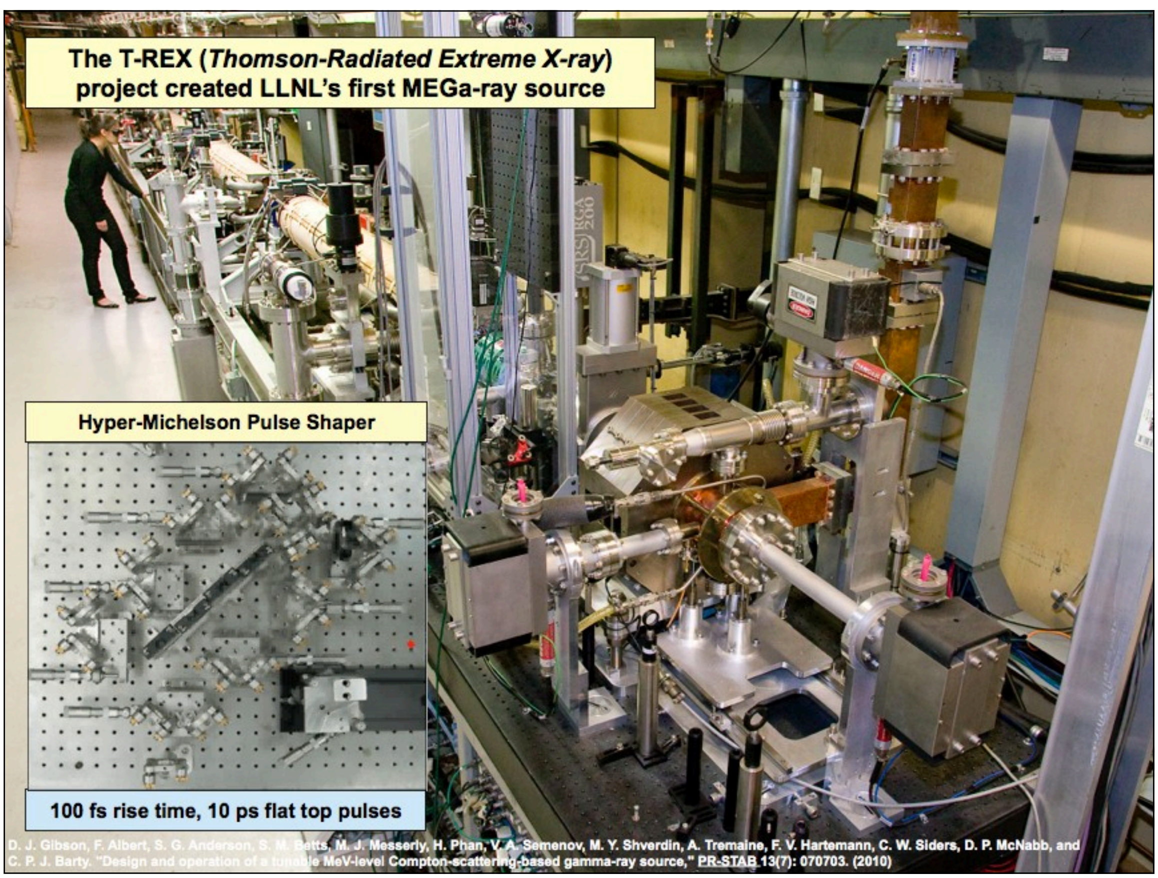
The T-REX (Thomson-Radiated Extreme X-ray)
project created LLNL's first MEGa-ray source
Hyper-Michelson Pulse Shaper
100 fs rise time, 10 ps flat top pulses
D. J. Gibson, F. Albert, S. G. Anderson, S. M. Betts, M. J. Messerly, H. Phan, V. A. Semenov, M. Y. Shverdin, A. Tremaine, F. V. Hartemann, C. W. Siders, D. P. McNabb, and C. P. J. Barty. "Design and operation of a tunable MeV-level Compton-scattering-based gamma-ray source," PR-STAB 13(7): 070703. (2010)

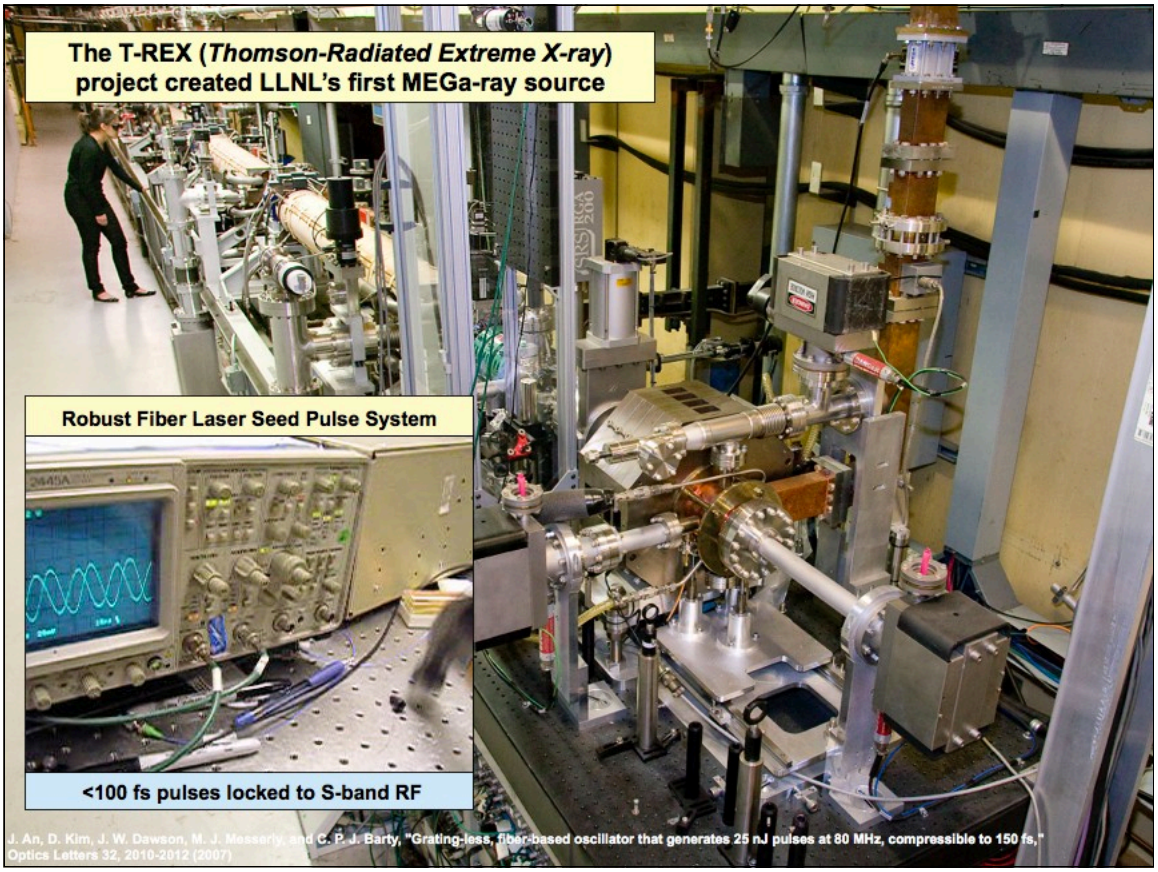
The T-REX (*Thomson-Radiated Extreme X-ray*) project created LLNL's first MEGa-ray source
Robust Fiber Laser Seed Pulse System
<100 fs pulses locked to S-band RF
J. An, D. Kim, J. W. Dawson, M. J. Messerly, and C. P. J. Barty, "Grating-less, fiber-based oscillator that generates 25 nJ pulses at 80 MHz, compressible to 150 fs," Optics Letters 32, 2010-2012 (2007)

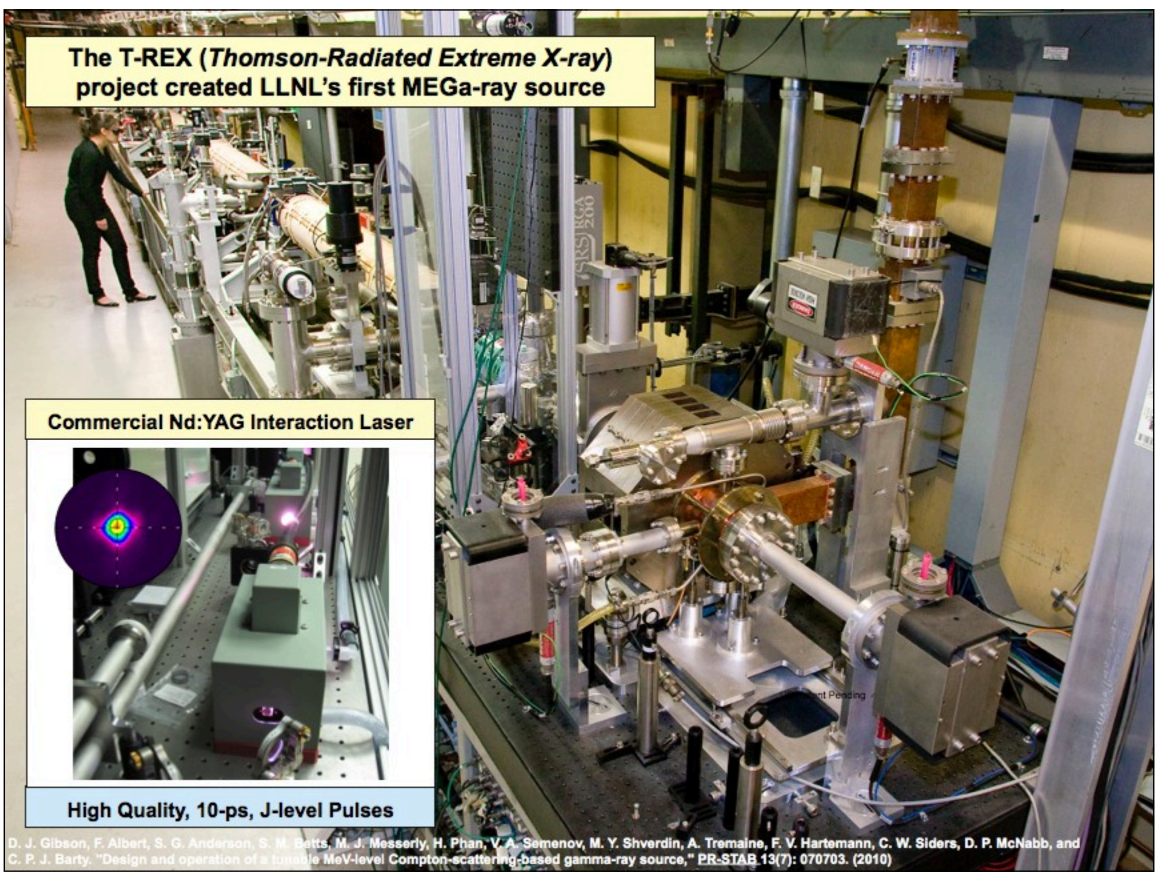
The T-REX (*Thomson-Radiated Extreme X-ray*) project created LLNL's first MEGa-ray source
Commercial Nd:YAG Interaction Laser
High Quality, 10-ps, J-level Pulses
D. J. Gibson, F. Albert, S. G. Anderson, S. M. Betts, M. J. Messerly, H. Phan, V. A. Semenov, M. Y. Shverdin, A. Tremaine, F. V. Hartemann, C. W. Siders, D. P. McNabb, and C. P. J. Barty. "Design and operation of a tunable MeV-level Compton-scattering-based gamma-ray source," PR-STAB 13(7): 070703. (2010)

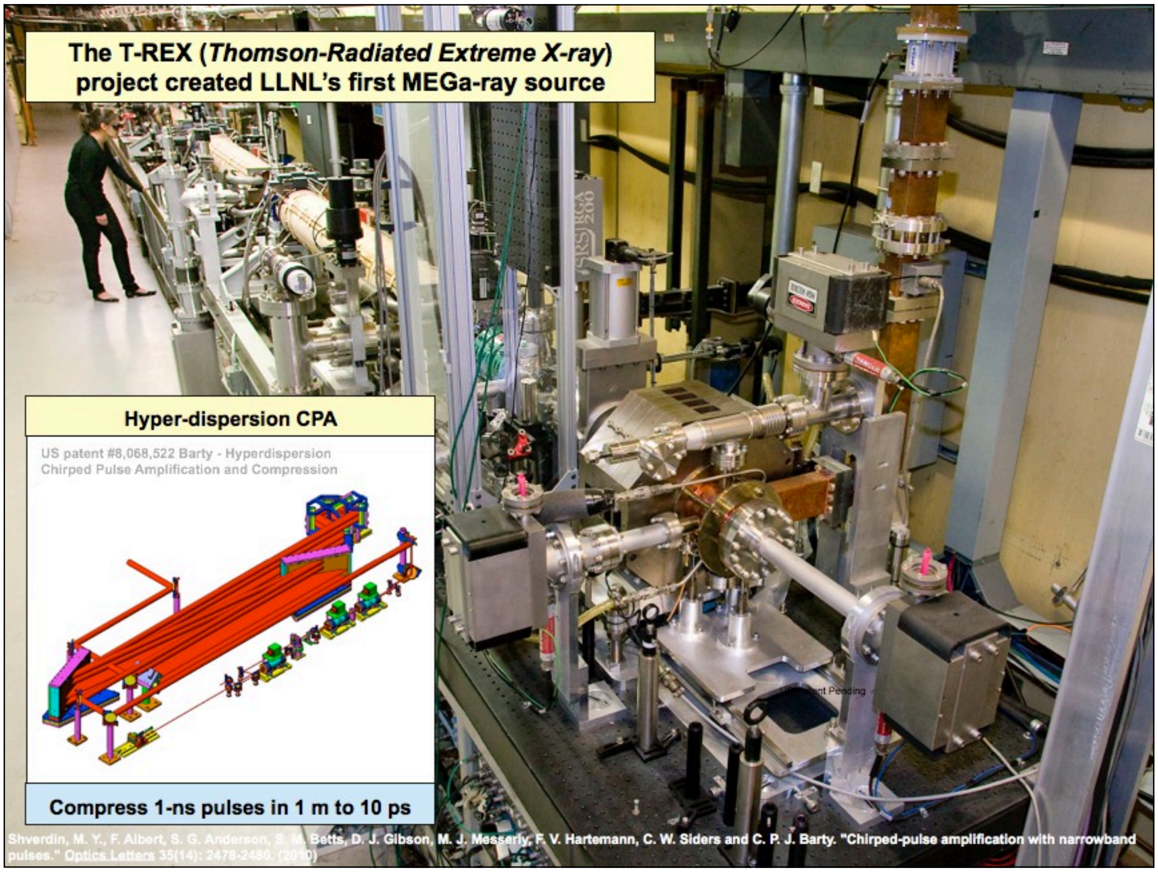
The T-REX (*Thomson-Radiated Extreme X-ray*) project created LLNL's first MEGa-ray source
Hyper-dispersion CPA
US patent #8,068,522 Barty - Hyperdispersion Chirped Pulse Amplification and Compression
Compress 1-ns pulses in 1 m to 10 ps
Shverdin, M. Y., F. Albert, S. G. Anderson, S. M. Betts, D. J. Gibson, M. J. Messerly, F. V. Hartemann, C. W. Siders and C. P. J. Barty. "Chirped-pulse amplification with narrowband pulses." Optics Letters 35(14): 2478-2480. (2010)

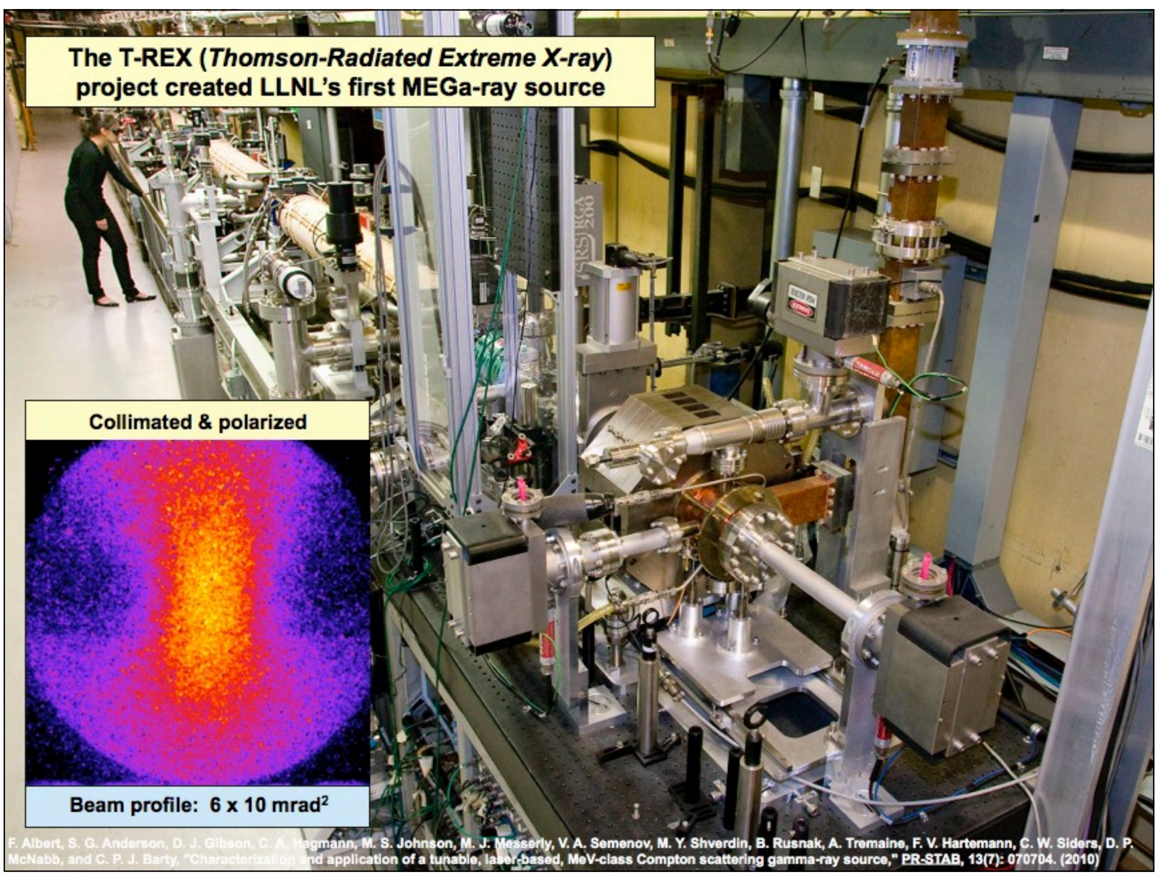
The T-REX (*Thomson-Radiated Extreme X-ray*) project created LLNL's first MEGa-ray source
Collimated & polarized
Beam profile: 6 x 10 mrad^2
F. Albert, S. G. Anderson, D. J. Gibson, C. A. Hagmann, M. S. Johnson, M. J. Messerly, V. A. Semenov, M. Y. Shverdin, B. Rusnak, A. Tremaine, F. V. Hartemann, C. W. Siders, D. P. McNabb, and C. P. J. Barty, "Characterization and application of a tunable, laser-based, MeV-class Compton scattering gamma-ray source," PR-STAB, 13(7): 070704. (2010)

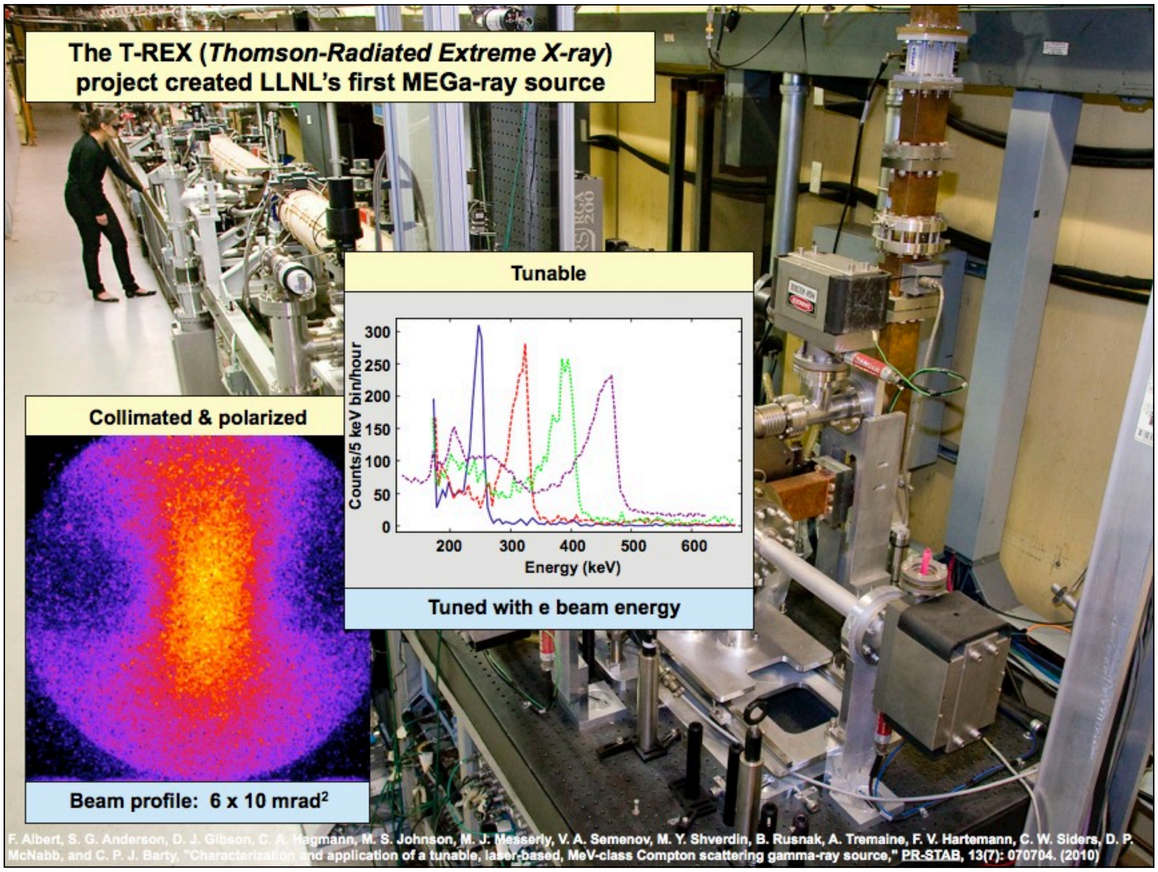
The T-REX (Thomson-Radiated Extreme X-ray) project created LLNL's first MEGa-ray source
Tunable
Counts/5 keV bin/hour
Energy (keV)
Tuned with e beam energy
Collimated & polarized
Beam profile: 6 x 10 mrad²
F. Albert, S. G. Anderson, D. J. Gibson, C. A. Hagmann, M. S. Johnson, M. J. Messerly, V. A. Semenov, M. Y. Shverdin, B. Rusnak, A. Tremaine, F. V. Hartemann, C. W. Siders, D. P. McNabb, and C. P. J. Barty, "Characterization and application of a tunable, laser-based, MeV-class Compton scattering gamma-ray source," PR-STAB, 13(7): 070704. (2010)

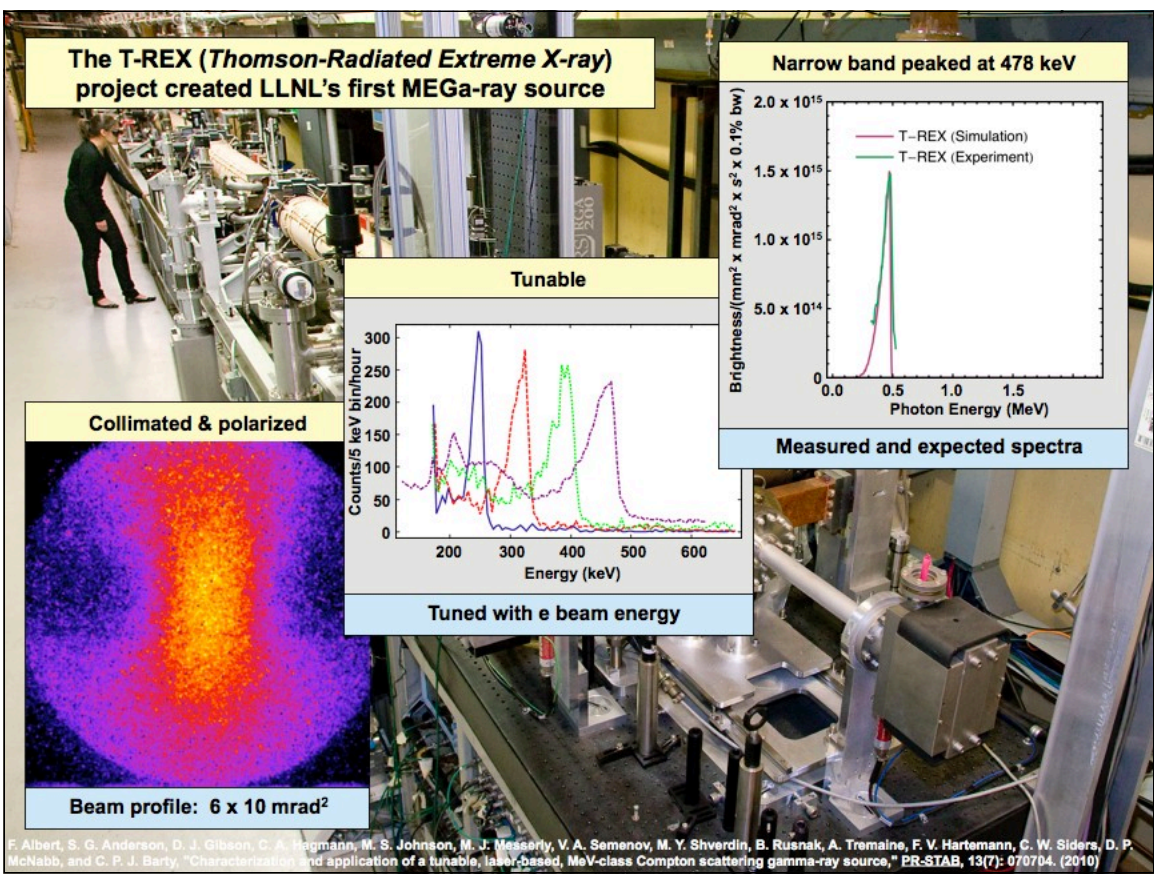
The T-REX (Thomson-Radiated Extreme X-ray) project created LLNL's first MEGa-ray source
Narrow band peaked at 478 keV
Brightness/(mm² x mrad² x s² x 0.1% bw)
T-REX (Simulation)
T-REX (Experiment)
Photon Energy (MeV)
Measured and expected spectra
Tunable
Counts/5 keV bin/hour
Energy (keV)
Tuned with e beam energy
Collimated & polarized
Beam profile: 6 x 10 mrad²
F. Albert, S. G. Anderson, D. J. Gibson, C. A. Hagmann, M. S. Johnson, M. J. Messerly, V. A. Semenov, M. Y. Shverdin, B. Rusnak, A. Tremaine, F. V. Hartemann, C. W. Siders, D. P. McNabb, and C. P. J. Barty, "Characterization and application of a tunable, laser-based, MeV-class Compton scattering gamma-ray source," PR-STAB, 13(7): 070704. (2010)

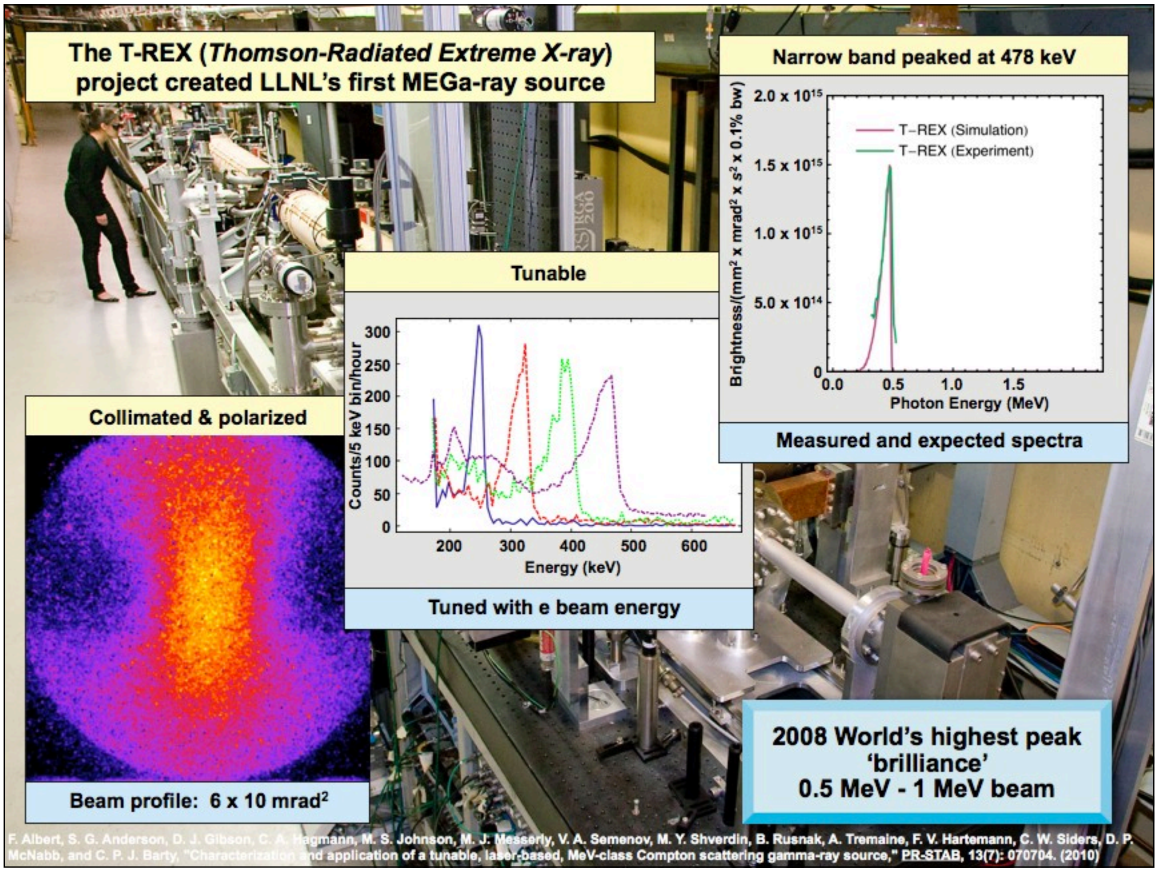

The T-REX (*Thomson-Radiated Extreme X-ray*) project created LLNL's first MEGa-ray source
Narrow band peaked at 478 keV
T-REX (Simulation)
T-REX (Experiment)
Brightness/(mm² x mrad² x s² x 0.1% bw)
2.0 x 10^15
1.5 x 10^15
1.0 x 10^15
5.0 x 10^14
0
0.0 0.5 1.0 1.5
Photon Energy (MeV)
Measured and expected spectra
Tunable
Counts/5 keV bin/hour
300 250 200 150 100 50 0
200 300 400 500 600
Energy (keV)
Tuned with e beam energy
Collimated & polarized
Beam profile: 6 x 10 mrad²
2008 World's highest peak 'brilliance' 0.5 MeV - 1 MeV beam
F. Albert, S. G. Anderson, D. J. Gibson, C. A. Hagmann, M. S. Johnson, M. J. Messerly, V. A. Semenov, M. Y. Shverdin, B. Rusnak, A. Tremaine, F. V. Hartemann, C. W. Siders, D. P. McNabb, and C. P. J. Barty, "Characterization and application of a tunable, laser-based, MeV-class Compton scattering gamma-ray source," PR-STAB, 13(7): 070704. (2010)

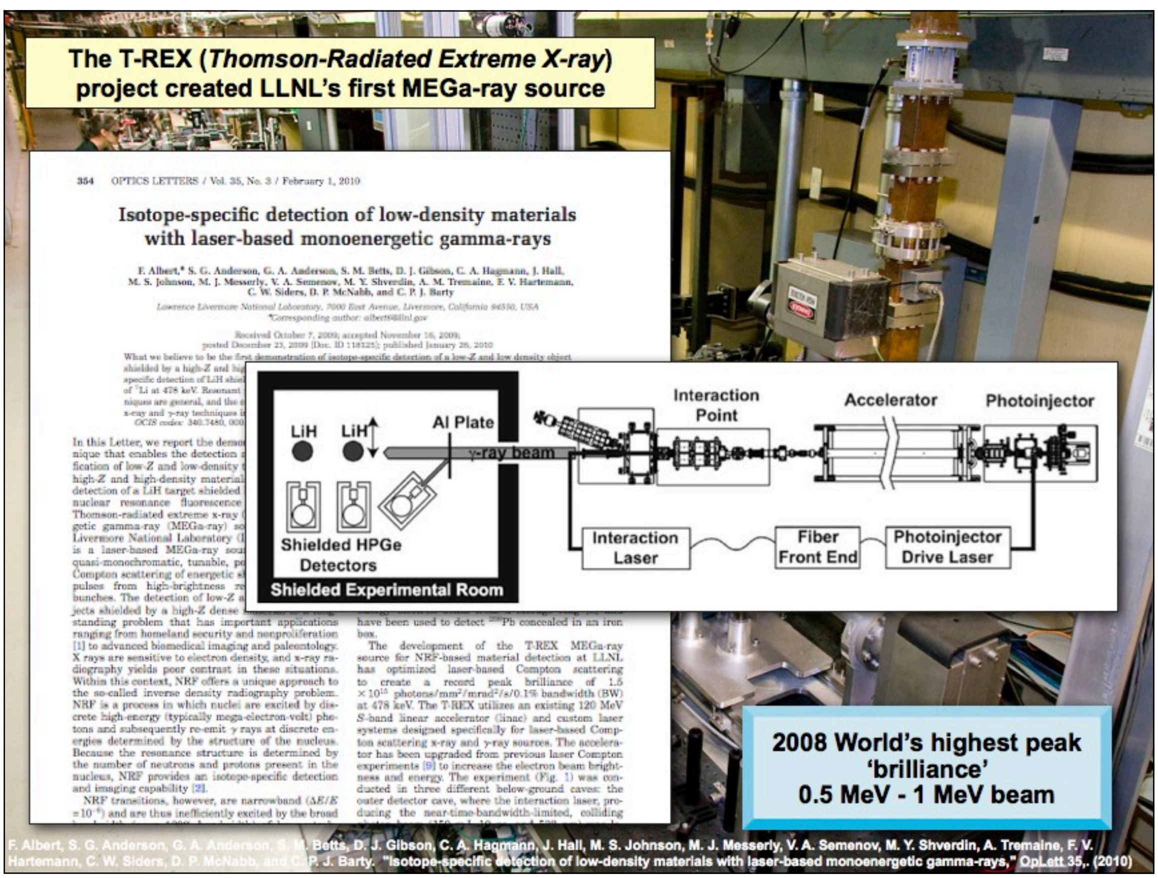

The T-REX (*Thomson-Radiated Extreme X-ray*) project created LLNL's first MEGa-ray source
354 OPTICS LETTERS / Vol. 35, No. 3 / February 1, 2010
Isotope-specific detection of low-density materials with laser-based monoenergetic gamma-rays
F. Albert,* S. G. Anderson, G. A. Anderson, S. M. Betts, D. J. Gibson, C. A. Hagmann, J. Hall, M. S. Johnson, M. J. Messerly, V. A. Semenov, M. Y. Shverdin, A. M. Tremaine, F. V. Hartemann, C. W. Siders, D. P. McNabb, and C. P. J. Barty
Lawrence Livermore National Laboratory, 7000 East Avenue, Livermore, California 94550, USA
*Corresponding author: albert6@llnl.gov
have been used to detect Pb concealed in an iron box.
The development of the T-REX MEGa-ray source for NRF-based material detection at LLNL has optimized laser-based Compton scattering to create a record peak brilliance of 1.5 × 10^15 photons/mm²/mrad²/s/0.1% bandwidth (BW) at 478 keV. The T-REX utilizes an existing 120 MeV S-band linear accelerator (linac) and custom laser systems designed specifically for laser-based Compton scattering x-ray and γ-ray sources. The accelerator has been upgraded from previous laser Compton experiments [9] to increase the electron beam brightness and energy. The experiment (Fig. 1) was conducted in three different below-ground caves: the outer detector cave, where the interaction laser, producing the near-time-bandwidth-limited, colliding
LiH
LiH
Al Plate
γ-ray beam
Shielded HPGe Detectors
Shielded Experimental Room
Interaction Point
Accelerator
Photoinjector
Interaction Laser
Fiber Front End
Photoinjector Drive Laser
2008 World's highest peak 'brilliance' 0.5 MeV - 1 MeV beam
F. Albert, S. G. Anderson, G. A. Anderson, S. M. Betts, D. J. Gibson, C. A. Hagmann, J. Hall, M. S. Johnson, M. J. Messerly, V. A. Semenov, M. Y. Shverdin, A. Tremaine, F. V. Hartemann, C. W. Siders, D. P. McNabb, and C. P. J. Barty. "Isotope-specific detection of low-density materials with laser-based monoenergetic gamma-rays," OpLett 35,. (2010)

Transmission-based detection was used for our initial material detection experiments

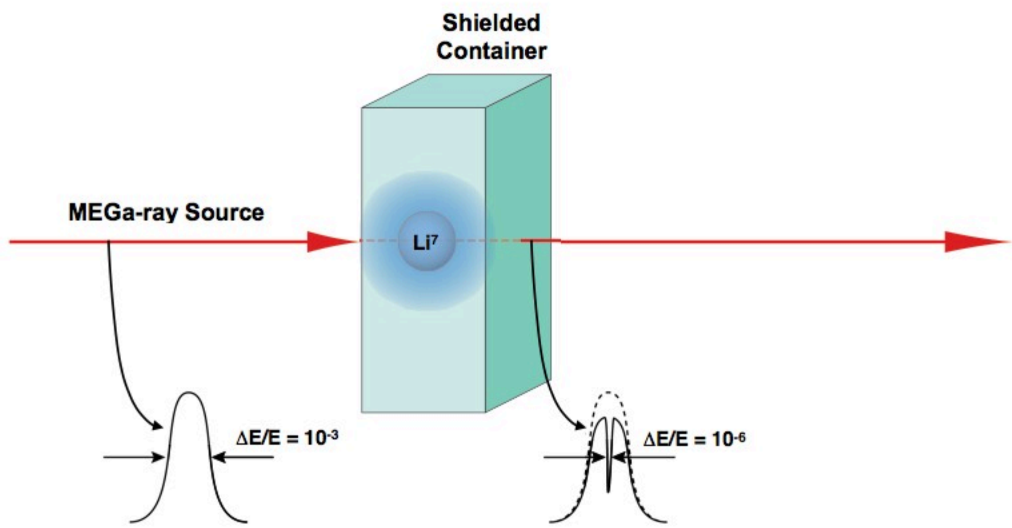

Transmission-based detection was used for our initial material detection experiments

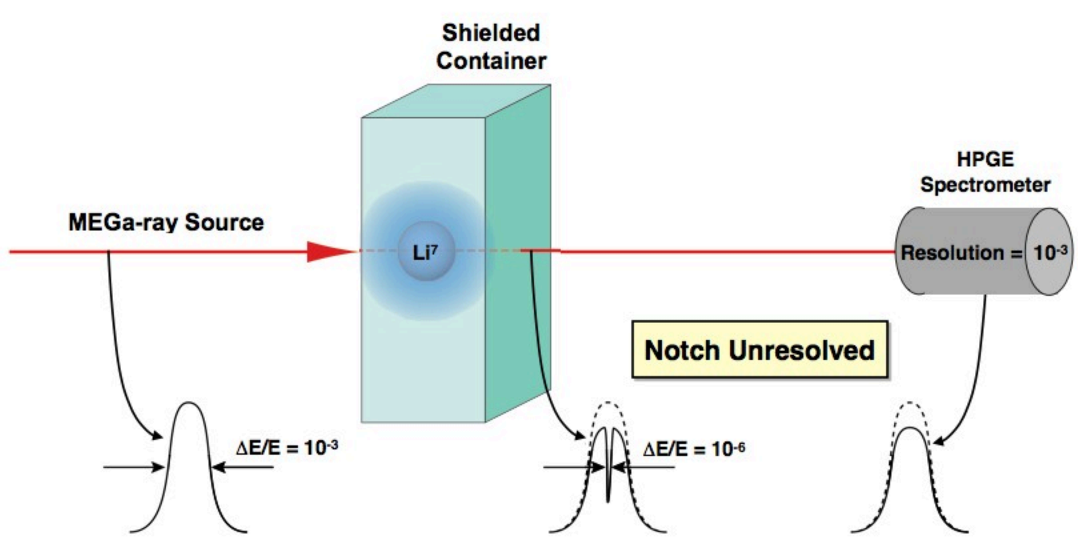

Transmission-based detection was used for our initial material detection experiments

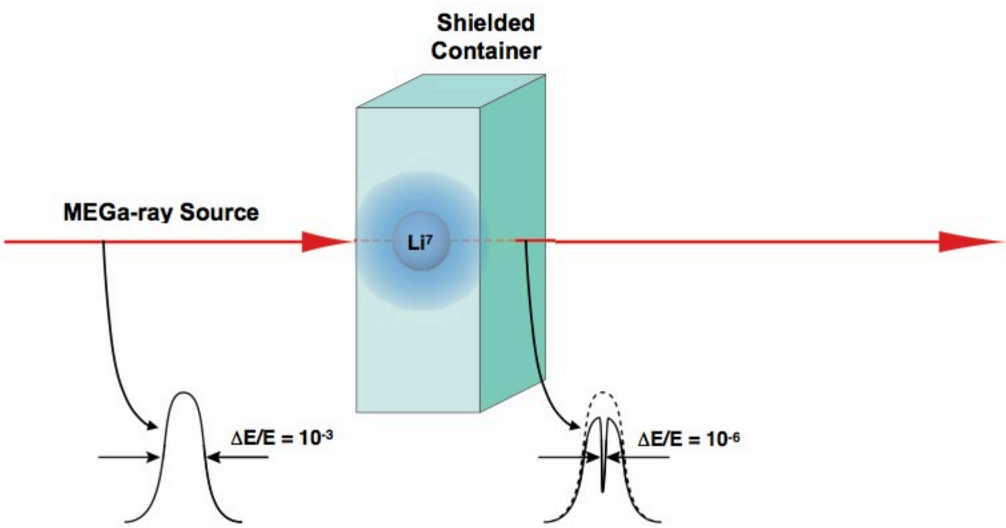

Transmission-based detection was used for our initial material detection experiments

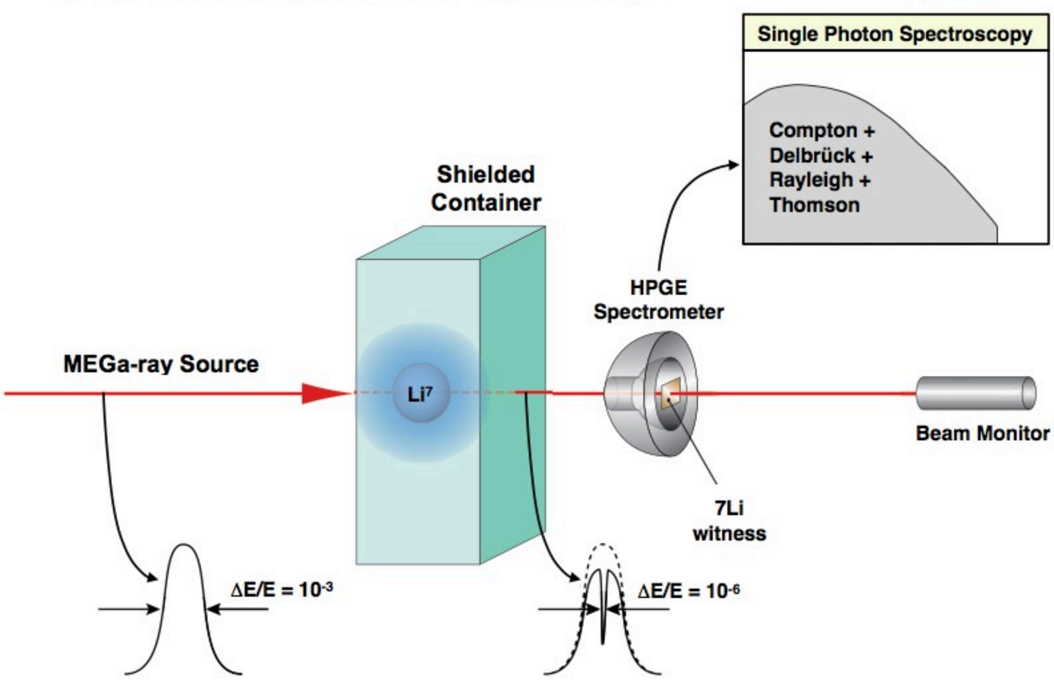

Nuclear Thomson, Rayleigh and Delbrück coherent scattering channels must also be considered

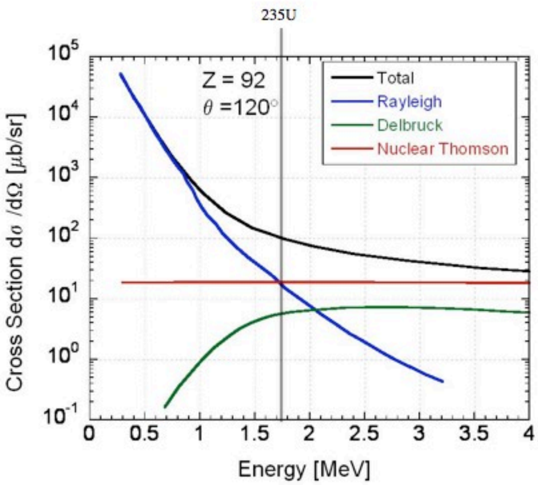

- **Magnitude of nuclear Thomson and Delbrück cross sections are important at 1 MeV and comparable to Rayleigh near 2 MeV**
- **Must be properly treated for MEGa-ray applications and detector design, especially for high Z**

Nuclear Thomson, Rayleigh and Delbrück coherent scattering channels must also be considered

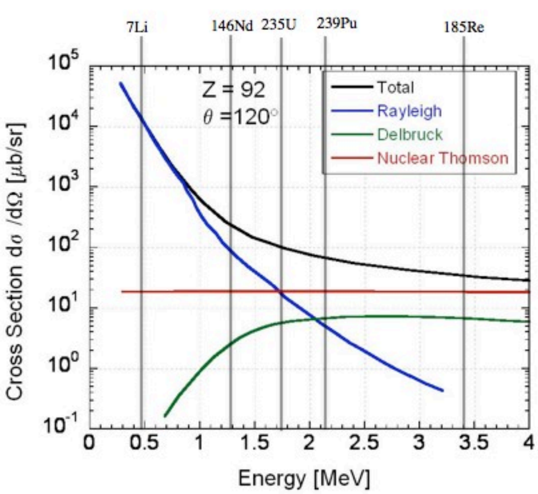

- **Magnitude of nuclear Thomson and Delbrück cross sections are important at 1 MeV and comparable to Rayleigh near 2 MeV**
- **Must be properly treated for MEGa-ray applications and detector design, especially for high Z**

Transmission-based detection was used for our initial material detection experiments

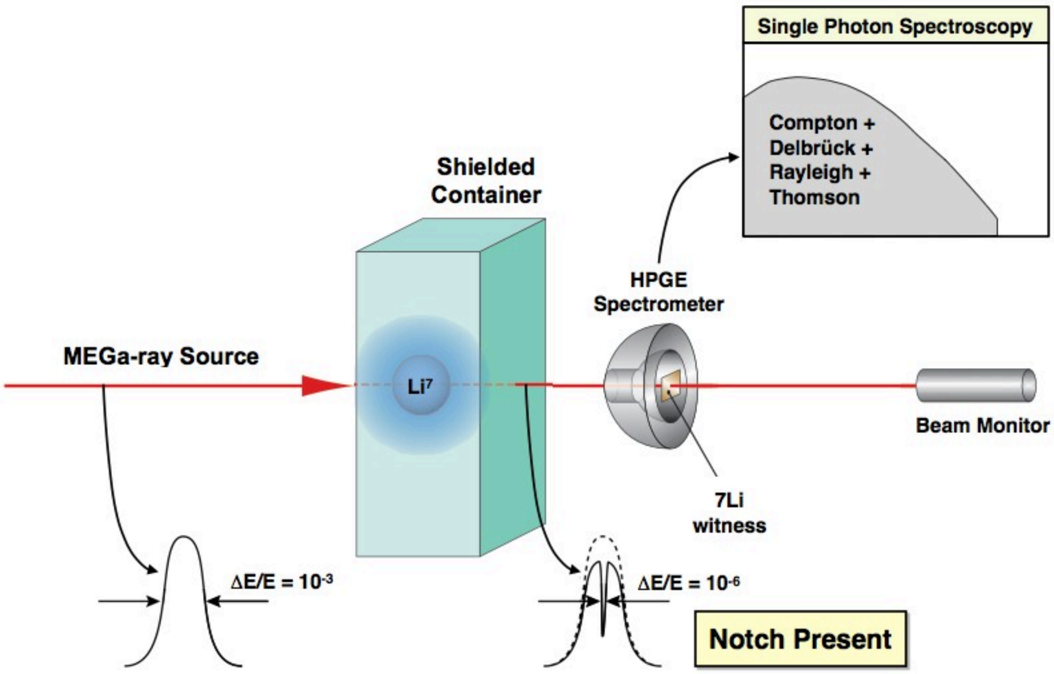

Transmission-based detection was used for our initial material detection experiments

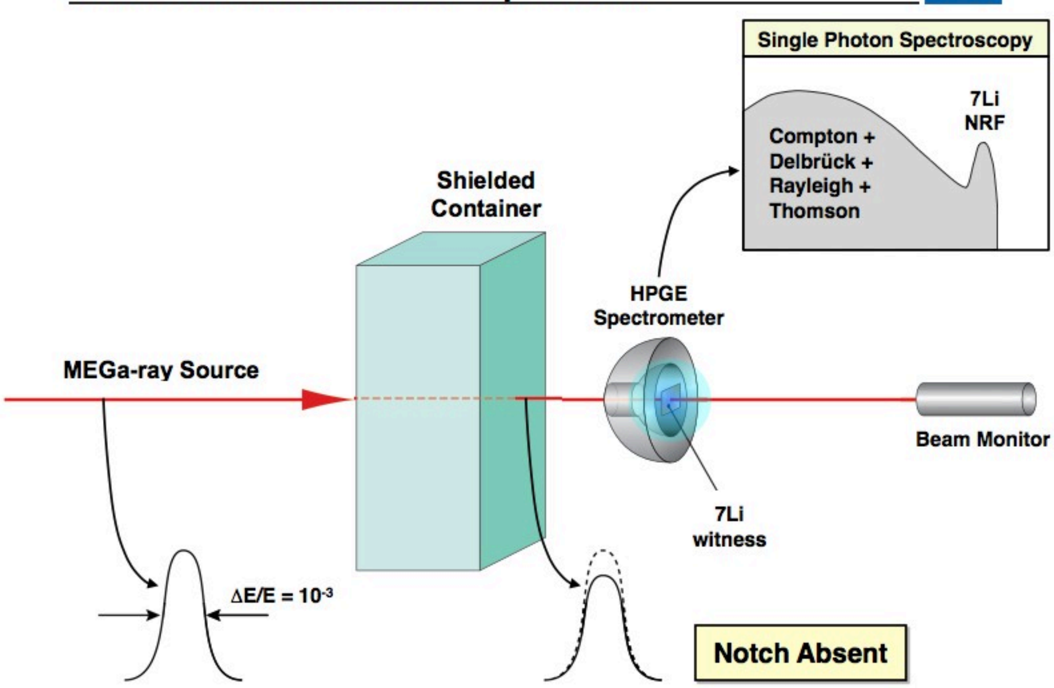

originally suggested by Prof. W. Bertozzi of MIT

Transmission-based detection was used for our initial material detection experiments

However, single-photon-counting spectroscopy is not well suited to high-flux/pulse, MEGa-ray sources

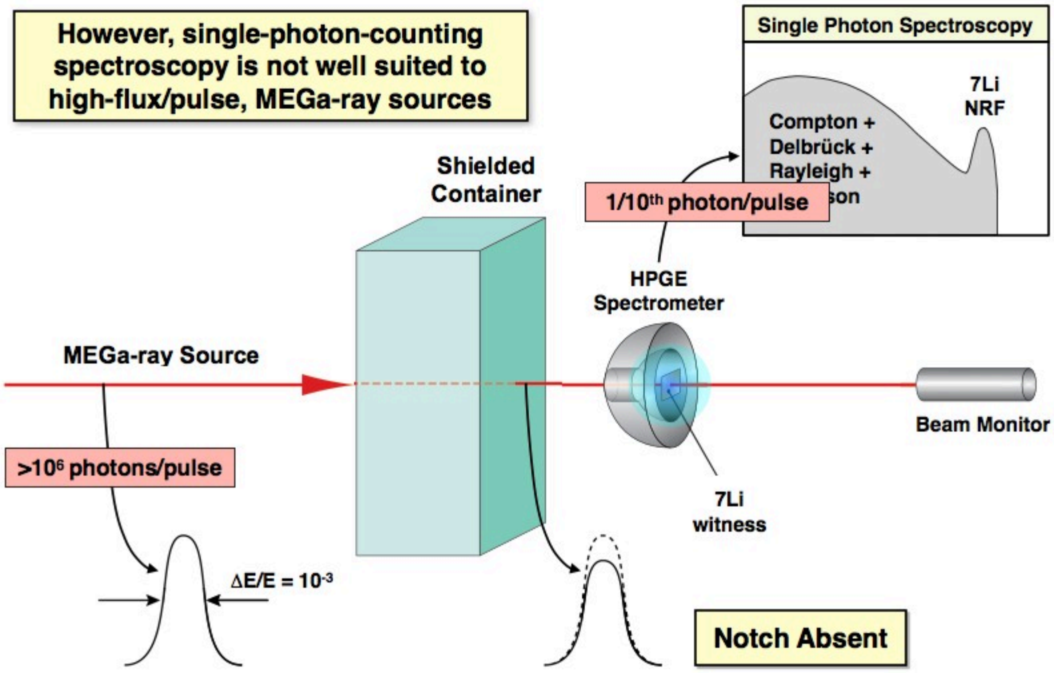

originally suggested by Prof. W. Bertozzi of MIT

Transmission-based detection was used for our initial material detection experiments

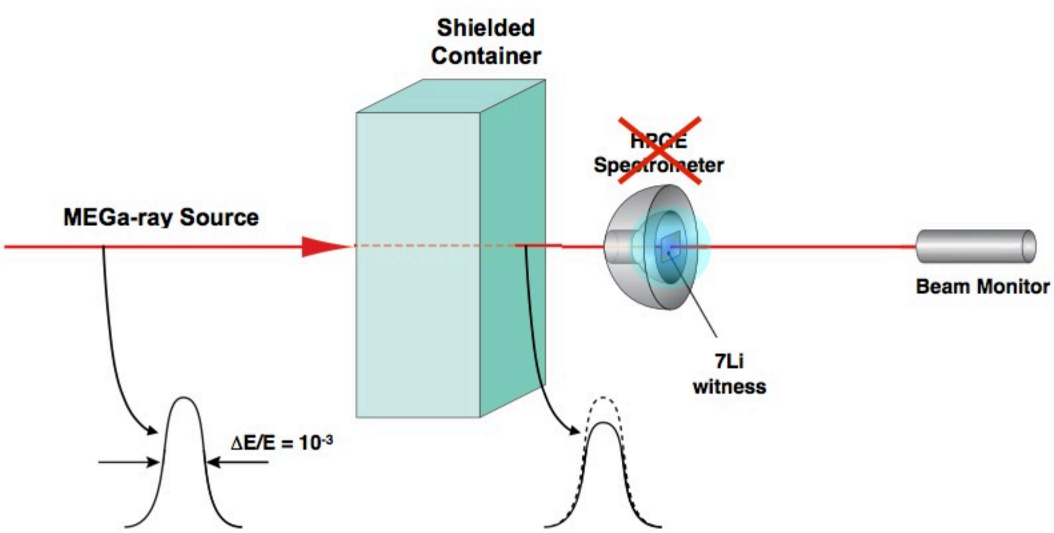

Dual Isotope Notch Observation (DINO) eliminates the need for high resolution spectroscopy

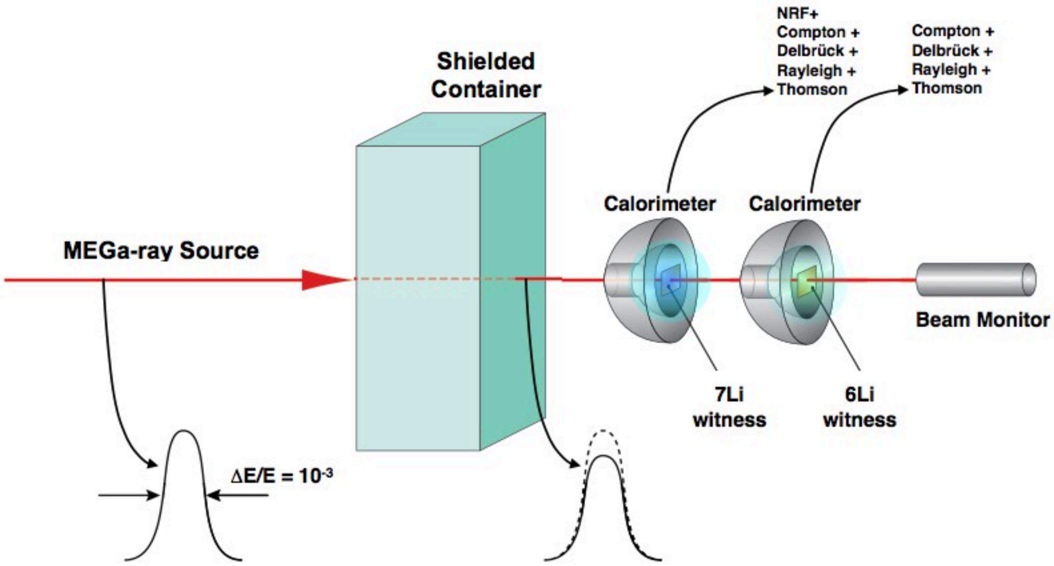

US patent #8,369,480 Barty, C. P. J. - Dual isotope notch observer for material identification, assay and imaging

Dual Isotope Notch Observation (DINO) eliminates the need for high resolution spectroscopy

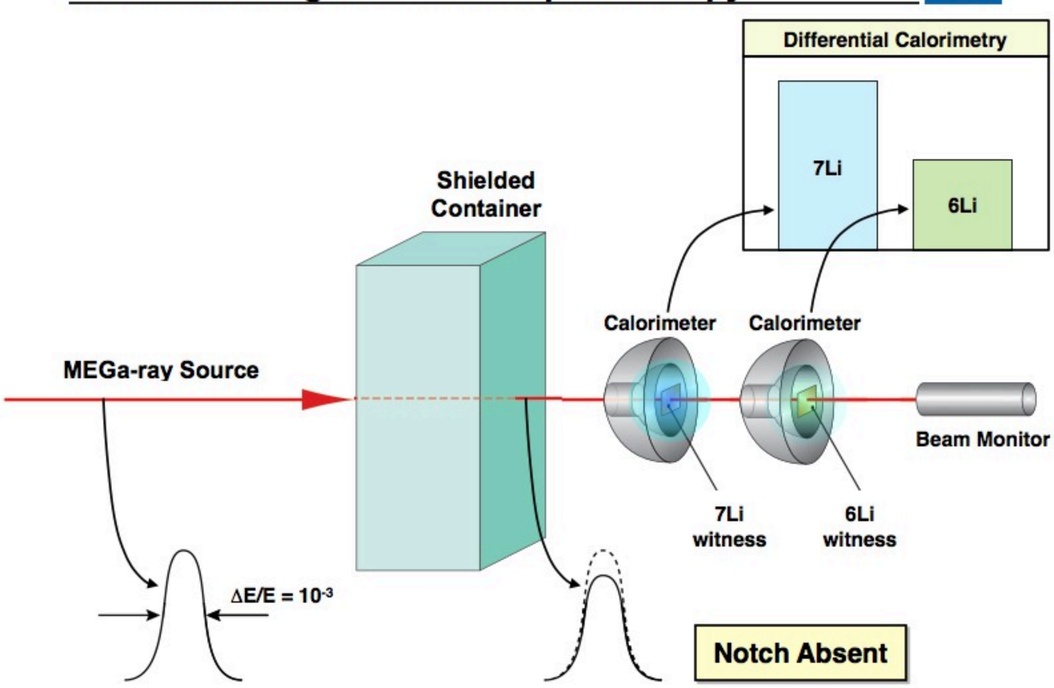

US patent #8,369,480 Barty, C. P. J. - Dual isotope notch observer for material identification, assay and imaging

Dual Isotope Notch Observation (DINO) eliminates the need for high resolution spectroscopy

This technique not only avoids single photon spectroscopy but also enables precision ASSAY as well as detection

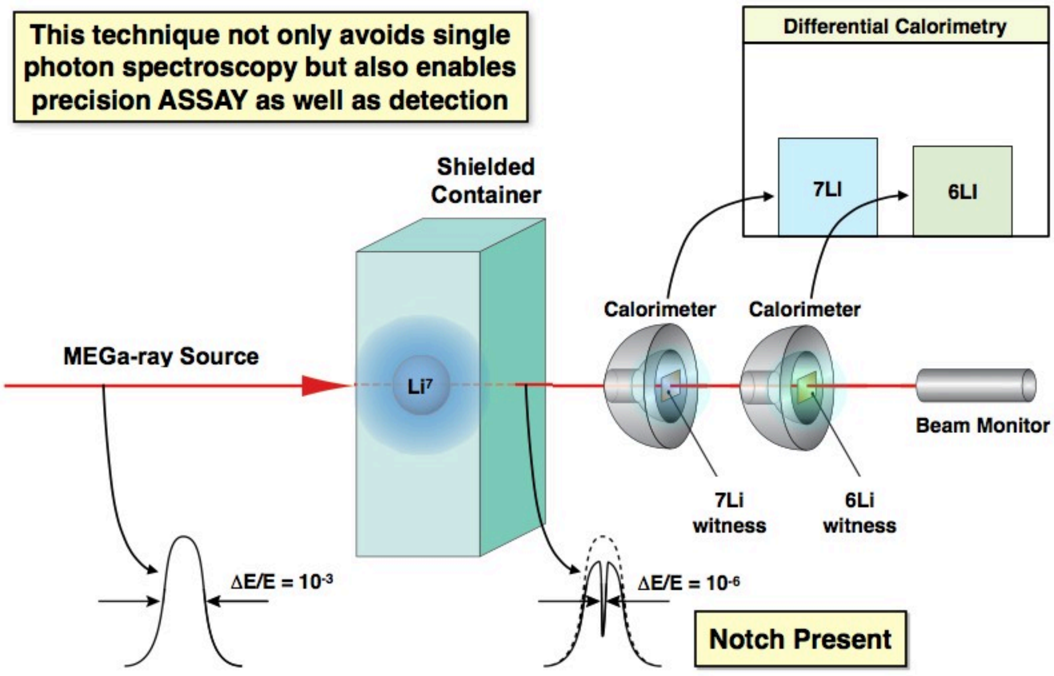

US patent #8,369,480 Barty, C. P. J. - Dual isotope notch observer for material identification, assay and imaging

We are currently designing and simulating DINO systems for U & Pu detection and assay applications

Strongest ^{235}U NRF resonance = 1733 keV

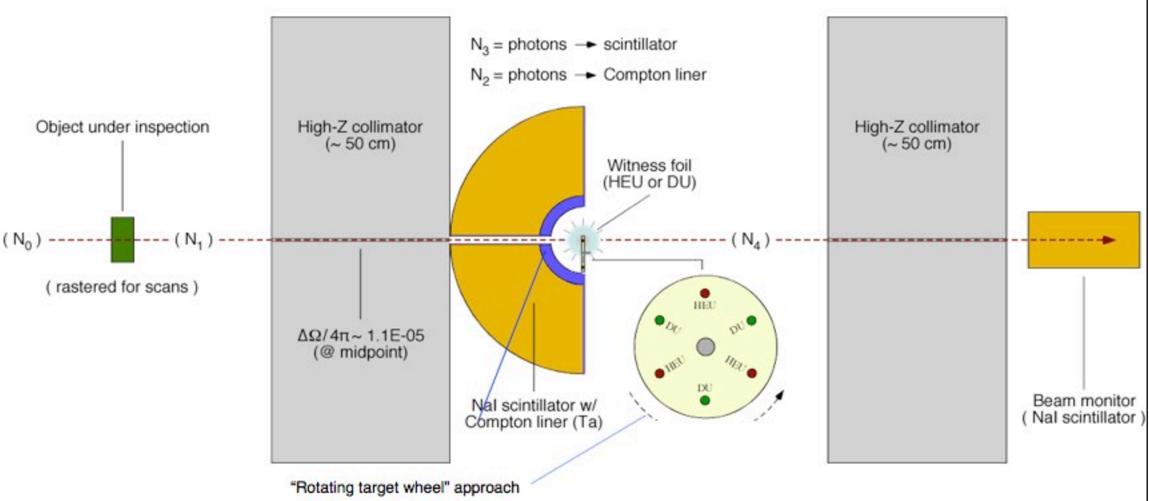

* Note: The total dwell (object inspection) time is assumed to be equally divided between exposures of the HEU & DU witness foils in this case.

MC model of single-stage DINO detector system* (COG):

There are numerous design considerations for isotopic-specific applications of DINO detectors

- Dimensions of the witness "foils" or more accurately the witness "pins"
- Configuration of the witness "pins"
- Solid angle subtended by the calorimeter
- Methods for rejection of non-resonant scattering
- Composition and efficiency of the "calorimeter"
- Collimation of the MEGa-ray illumination source
- Bandwidth of the MEGa-ray illumination source
- "Stability" of the MEGa-ray illumination source
- Choice of DINO "decision metric"
- etc....

There are numerous design considerations for isotopic-specific applications of DINO detectors

- Dimensions of the witness "foils" or more accurately the witness "pins"
- Configuration of the witness "pins"
- Solid angle subtended by the calorimeter

- **Methods for rejection of non-resonant scattering**

- Composition and efficiency of the "calorimeter"
- Collimation of the MEGa-ray illumination source
- Bandwidth of the MEGa-ray illumination source
- "Stability" of the MEGa-ray illumination source
- Choice of DINO "decision metric"
- etc....

Monte Carlo simulations using COG

Design of the Compton liner can greatly increase the ratio of NRF to background in the scintillator

Strongest ^{235}U NRF resonance = 1733 keV

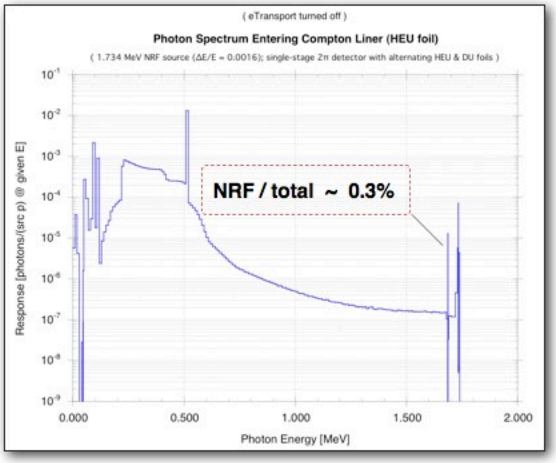

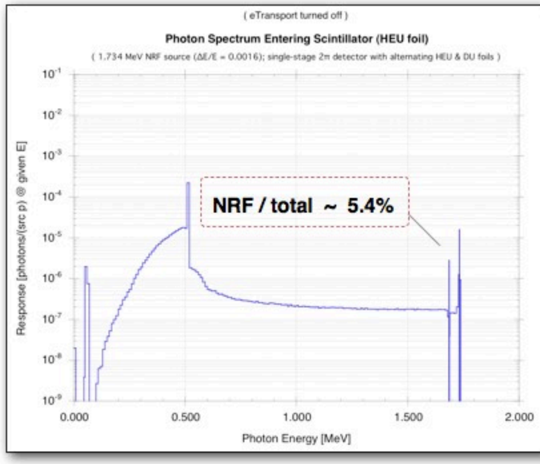

Hall, J., V. Semenov, F. Albert and C. P. J. Barty. "Numerical Simulation of Nuclear Materials Detection, Imaging and Assay with MEGa-rays." Proceedings of the 52nd Annual Meeting of the Institute for Nuclear Materials Management Vol 3. 2673-2682. (2011)

Monte Carlo simulations using COG

Sensitivity of the detector decreases rapidly with respect to source bandwidth

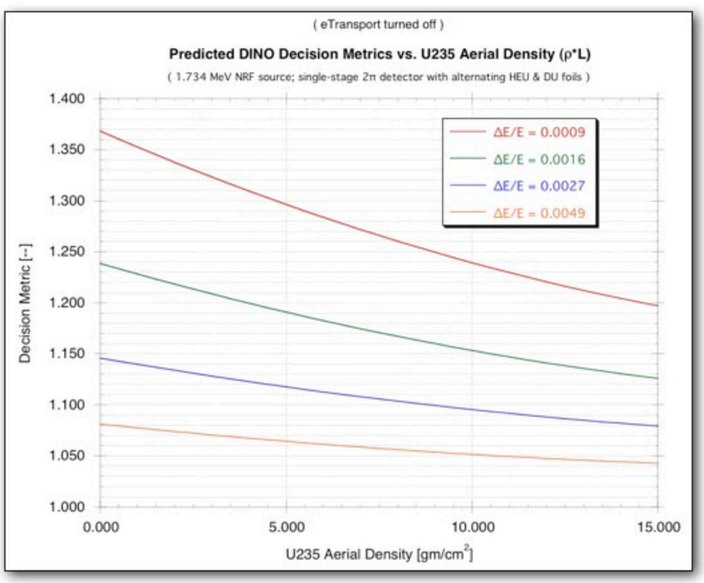

Hall, J., V. Semenov, F. Albert and C. P. J. Barty. "Numerical Simulation of Nuclear Materials Detection, Imaging and Assay with MEGa-rays." Proceedings of the 52nd Annual Meeting of the Institute for Nuclear Materials Management Vol 3. 2673-2682. (2011)

Monte Carlo simulations using COG

Precision assay and imaging of nuclear fuel would be possible with MEGa-rays and DINO

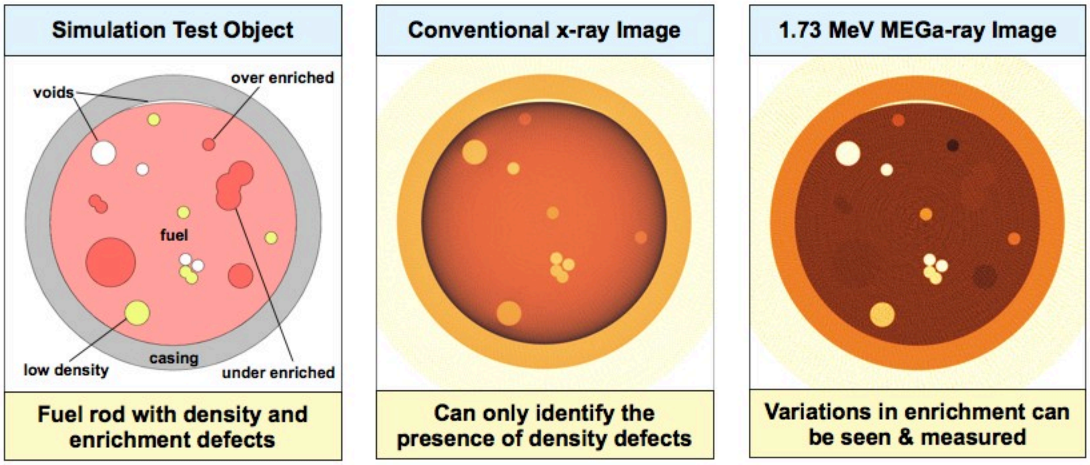

Hall, J., V. Semenov, F. Albert and C. P. J. Barty. "Numerical Simulation of Nuclear Materials Detection, Imaging and Assay with MEGa-rays." Proceedings of the 52nd Annual Meeting of the Institute for Nuclear Materials Management Vol 3. 2673-2682. (2011)

Monte Carlo simulations using COG

Simulations indicate that the enrichment of fuel rods could be measured to ~3% in 5 to 6 minutes

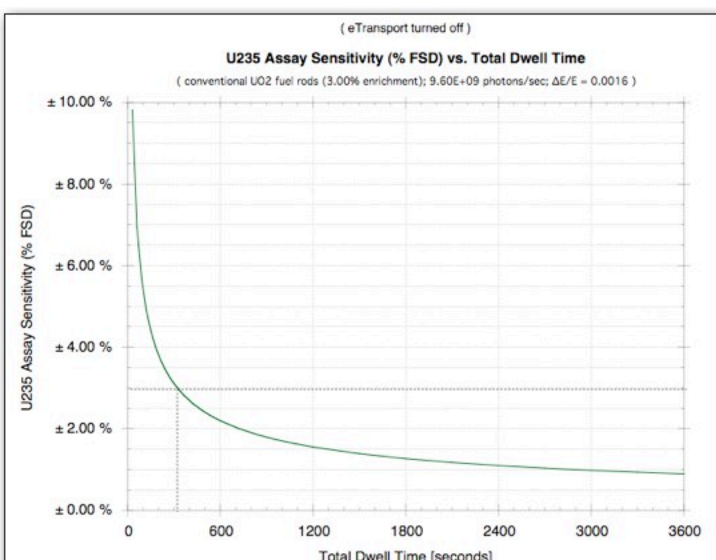

Hall, J., V. Semenov, F. Albert and C. P. J. Barty. "Numerical Simulation of Nuclear Materials Detection, Imaging and Assay with MEGa-rays." Proceedings of the 52nd Annual Meeting of the Institute for Nuclear Materials Management Vol 3. 2673-2682. (2011)

NRF-based materials evaluation will be much easier elsewhere in the periodic table

atomic number	isotope	oxide	natural isotopic abundance (%)	REE-Oxide weight % at Mountain Pass	REE Atomic % at Mountain Pass	REE Isotope % at Mountain Pass	cost per kg in 2009 (US$)	NRF gamma energy (keV)	NRF cross section (barns)	Background cross section (barns)	NRF to background cross section ratio
92	235U	UO_2	90.0	na	na	na	na	1733	26.0	20.0	1.3
39	89Y	Y_2O_3	100.0	0.130	0.0092	0.0092	$13.50	1507	24.5	6.9	3.6
40	90Zr	na	51.5	na	na	na	na	2186	5.5	6.1	0.9
57	138La	La_2O_3	0.1	33.784	2.5925	0.0023	$5.85	no data	no data	no data	no data
57	139La	La_2O_3	99.9	33.784	2.5925	2.5902	$5.85	1538	7.2	10.6	0.7
58	136Ce	Ce_2O_3	0.19	49.581	3.8096	0.0070	$4.15	552	5.4	23	0.2
58	138Ce	Ce_2O_3	0.25	49.581	3.8096	0.0096	$4.15	789	6.2	16	0.4
58	140Ce	Ce_2O_3	88.45	49.581	3.8096	3.3696	$4.15	1596	16.9	10.5	1.6
58	142Ce	Ce_2O_3	11.11	49.581	3.8096	0.4234	$4.15	2187	19.3	9.4	2.1
59	141Pr	Pr_2O_3	100.0	4.119	0.3168	0.3168	$15.15	no data	no data	no data	no data
60	142Nd	Nd_2O_3	27.2	11.158	0.8610	0.2342	$15.25	3424	46.8	9.1	5.1
60	143Nd	Nd_2O_3	12.2	11.158	0.8610	0.1050	$15.25	1407	10.8	12	0.9
60	144Nd	Nd_2O_3	23.8	11.158	0.8610	0.2049	$15.25	2186	17.4	9.8	1.8
60	145Nd	Nd_2O_3	8.3						1.8	15	0.1
60	146Nd	Nd_2O_3	17.2						14.9	19	0.8
60	148Nd	Nd_2O_3	5.7						5.4	9.1	0.6
60	150Nd	Nd_2O_3	5.6						1.8	14	0.1
62	144Sm	Sm_2O_3	3.1						55.2	9.5	5.8
62	144Sm	Sm_2O_3	3.1						16.6	11.5	1.4
62	147Sm	Sm_2O_3	15.0						2.2	20	0.1
62	148Sm	Sm_2O_3	11.2						8.4	12	0.7
62	149Sm	Sm_2O_3	13.8						2.2	23	0.1
62	150Sm	Sm_2O_3	7.4						23.1	13.6	1.7
62	152Sm	Sm_2O_3	26.8						18.0	9.7	1.9
62	152Sm	Sm_2O_3	26.8						70.5	15	4.7
62	154Sm	Sm_2O_3	22.8	0.850	0.0660	0.0150	$4.50	921	95.1	16	5.9
62	154Sm	Sm_2O_3	22.8	0.850	0.0660	0.0150	$4.50	1440	3.8	12.1	0.3
63	151Eu	Eu_2O_3	47.8	0.105	0.0082	0.0039	$465.00	908	16.7	60	0.3
63	153Eu	Eu_2O_3	52.2	0.105	0.0082	0.0043	$465.00	no data	no data	no data	no data
64	152Gd	Gd_2O_3	0.2	0.210	0.0164	0.0000	$6.50	344	5.0	50	0.1
64	154Gd	Gd_2O_3	2.2	0.210	0.0164	0.0004	$6.50	1241	735.3	13.8	53.3
64	155Gd	Gd_2O_3	14.8	0.210	0.0164	0.0024	$6.50	615	0.2	90	0.0
64	156Gd	Gd_2O_3	20.5	0.210	0.0164	0.0034	$6.50	1243	33.1	13.7	2.4
64	156Gd	Gd_2O_3	20.5	0.210	0.0164	0.0034	$6.50	1367	32.4	13	2.5
64	156Gd	Gd_2O_3	20.5	0.210	0.0164	0.0034	$6.50	2745	16.1	10.2	1.6
64	156Gd	Gd_2O_3	20.5	0.210	0.0164	0.0034	$6.50	3071	41.2	10	4.1
64	157Gd	Gd_2O_3	15.7	0.210	0.0164	0.0026	$6.50	131	2.8	500	0.0
64	158Gd	Gd_2O_3	24.8	0.210	0.0164	0.0041	$6.50	1264	60.9	13.7	4.4
64	158Gd	Gd_2O_3	24.8	0.210	0.0164	0.0041	$6.50	3201	25.0	9.9	2.5
64	160Gd	Gd_2O_3	21.9	0.210	0.0164	0.0036	$6.50	1224	56.5	13.7	4.1
65	159Tb	Tb_2O_3	100.0	0.016	0.0013	0.0013	$350.00	58	192.7	3800	0.1
65	159Tb	Tb_2O_3	100.0	0.016	0.0013	0.0013	$350.00	581	4.4	28	0.2

The ratio of the NRF to background cross section for many materials is significantly greater than that for the actinides

Specific Spectral Density is the key laser-Compton source metric

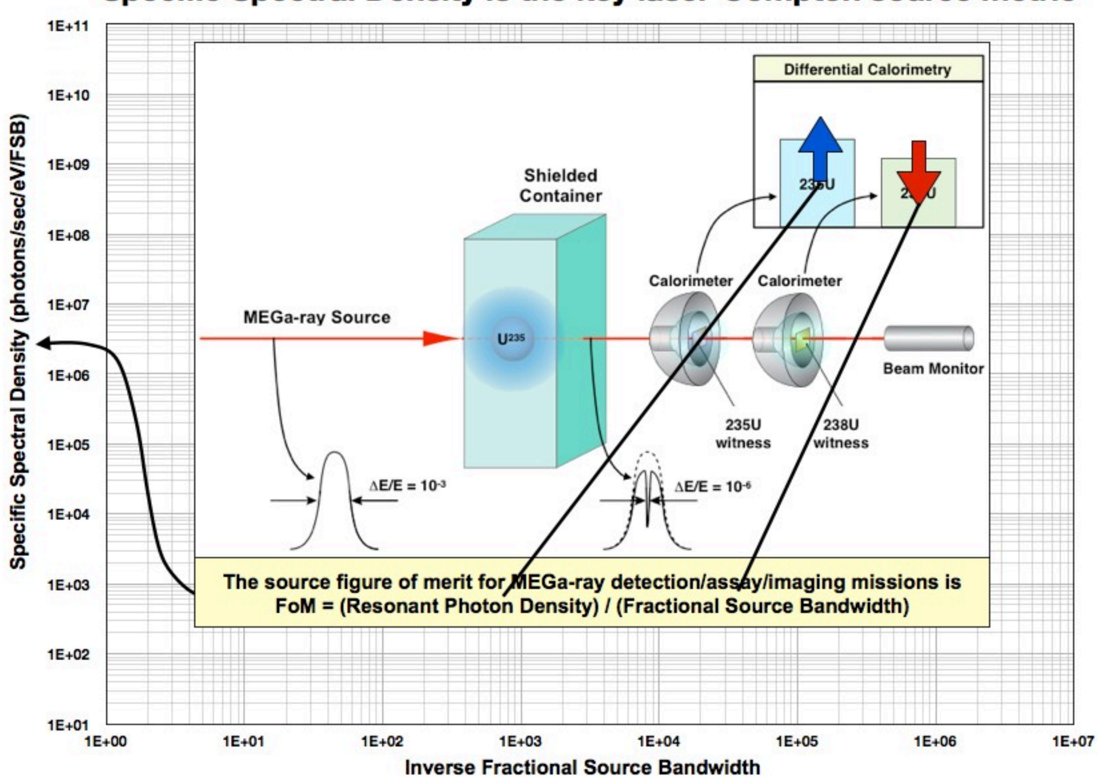

Monte Carlo simulations using COG

Simulations indicate that the enrichment of fuel rods could be measured to ~3% in 5 to 6 minutes

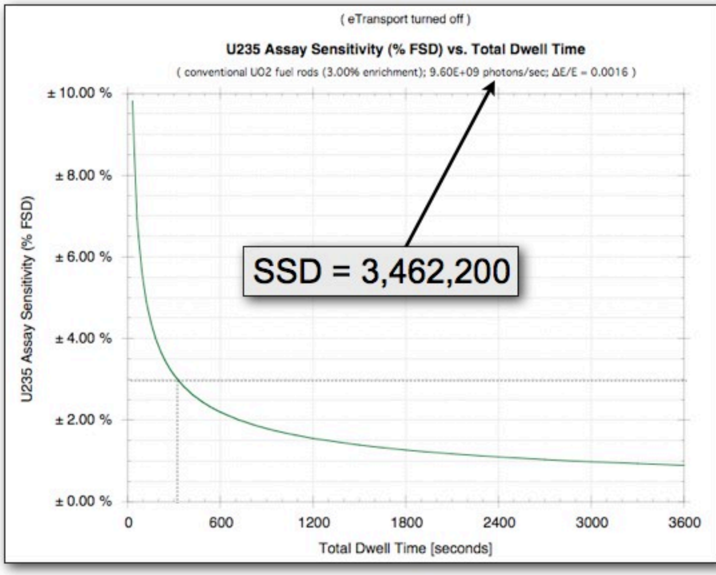

Hall, J., V. Semenov, F. Albert and C. P. J. Barty. "Numerical Simulation of Nuclear Materials Detection, Imaging and Assay with MEGa-rays." Proceedings of the 52nd Annual Meeting of the Institute for Nuclear Materials Management Vol 3. 2673-2682. (2011)

Specific Spectral Density is the key source metric

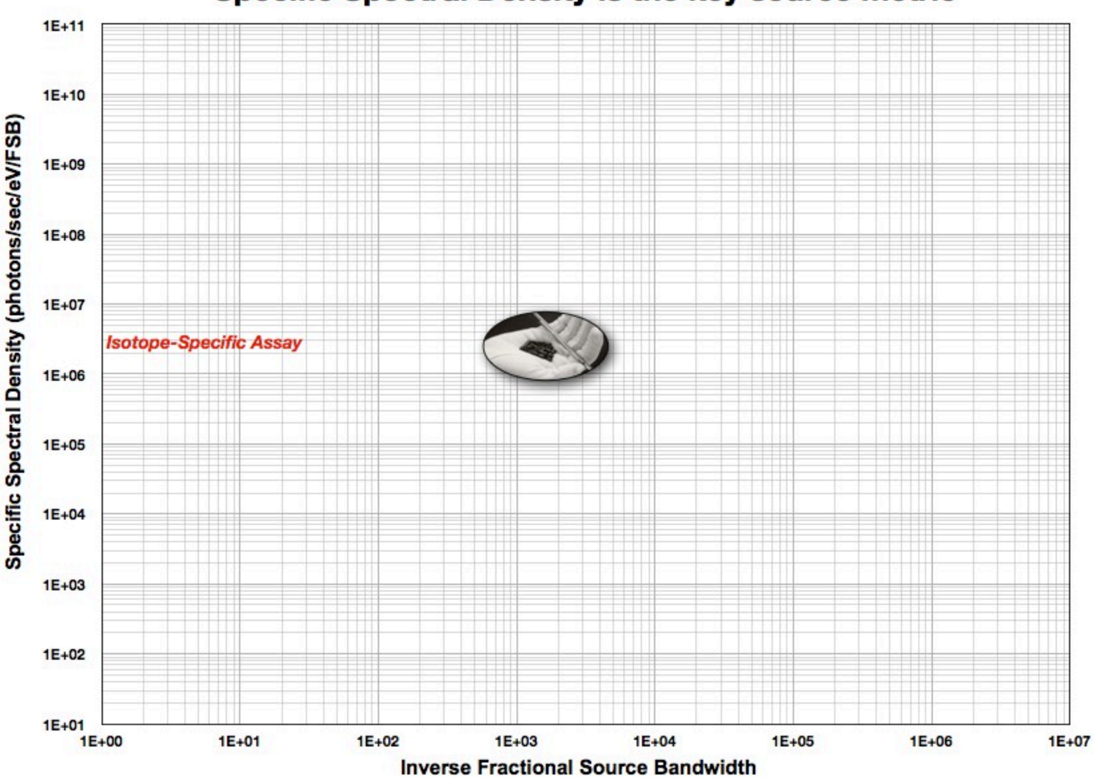

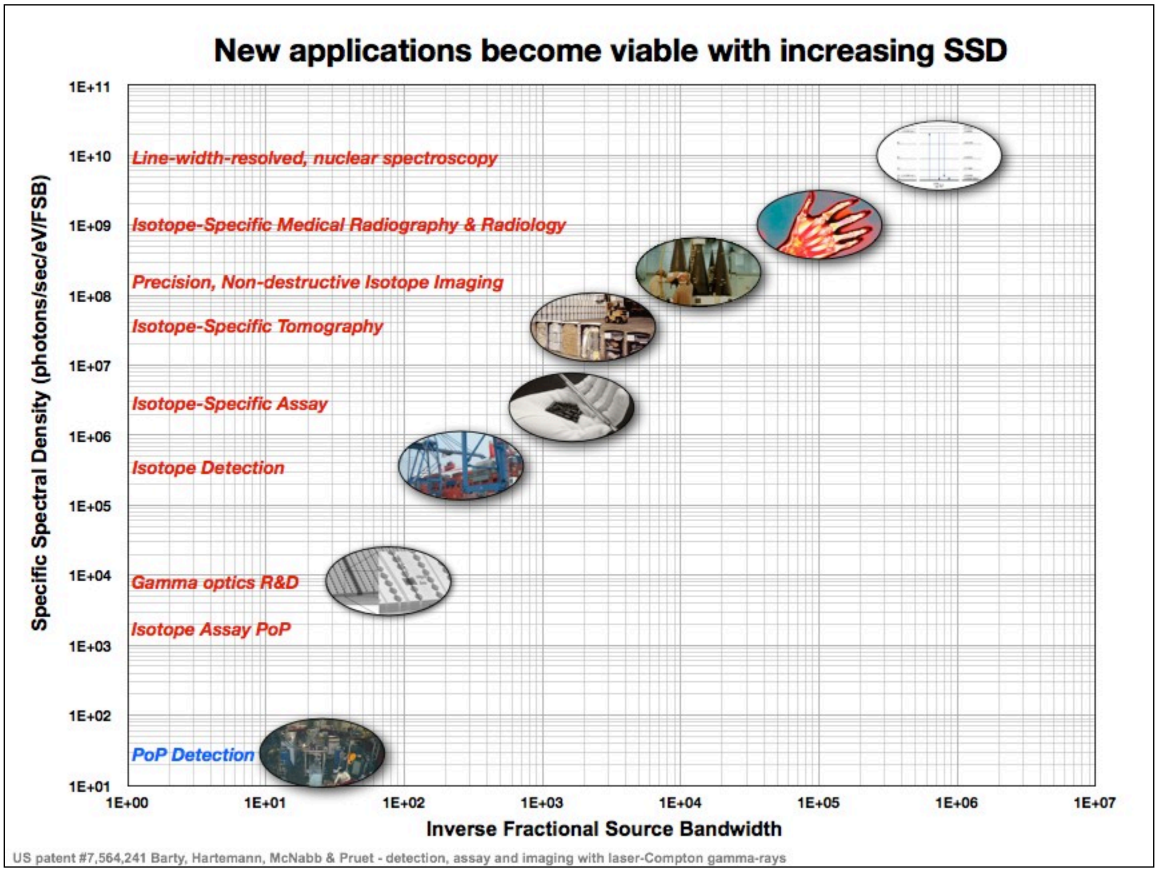
New applications become viable with increasing SSD
Specific Spectral Density (photons/sec/eV/FSB)
Inverse Fractional Source Bandwidth
1E+11
1E+10
1E+09
1E+08
1E+07
1E+06
1E+05
1E+04
1E+03
1E+02
1E+01
1E+00
1E+01
1E+02
1E+03
1E+04
1E+05
1E+06
1E+07
Line-width-resolved, nuclear spectroscopy
Isotope-Specific Medical Radiography & Radiology
Precision, Non-destructive Isotope Imaging
Isotope-Specific Tomography
Isotope-Specific Assay
Isotope Detection
Gamma optics R&D
Isotope Assay PoP
PoP Detection
US patent #7,564,241 Barty, Hartemann, McNabb & Pruet - detection, assay and imaging with laser-Compton gamma-rays

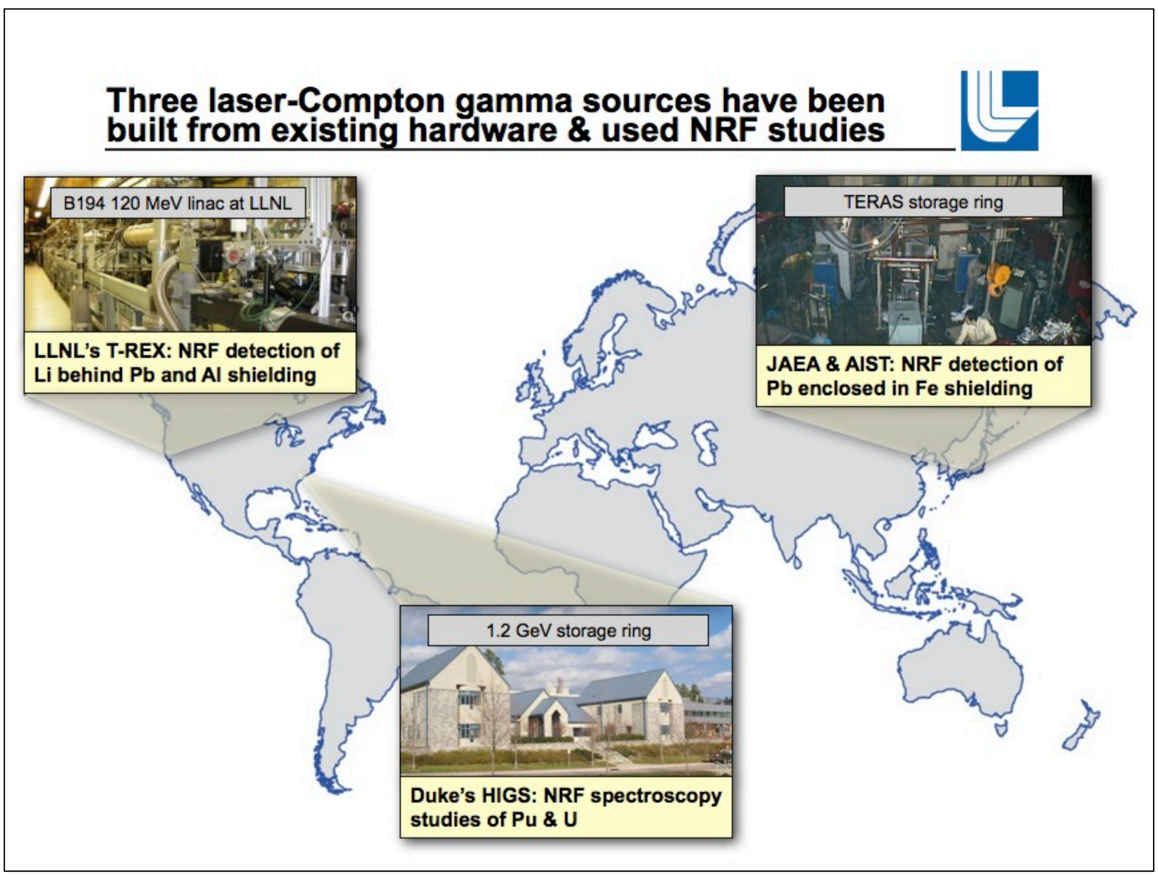
Three laser-Compton gamma sources have been built from existing hardware & used NRF studies
B194 120 MeV linac at LLNL
LLNL's T-REX: NRF detection of Li behind Pb and Al shielding
TERAS storage ring
JAEA & AIST: NRF detection of Pb enclosed in Fe shielding
1.2 GeV storage ring
Duke's HIGS: NRF spectroscopy studies of Pu & U

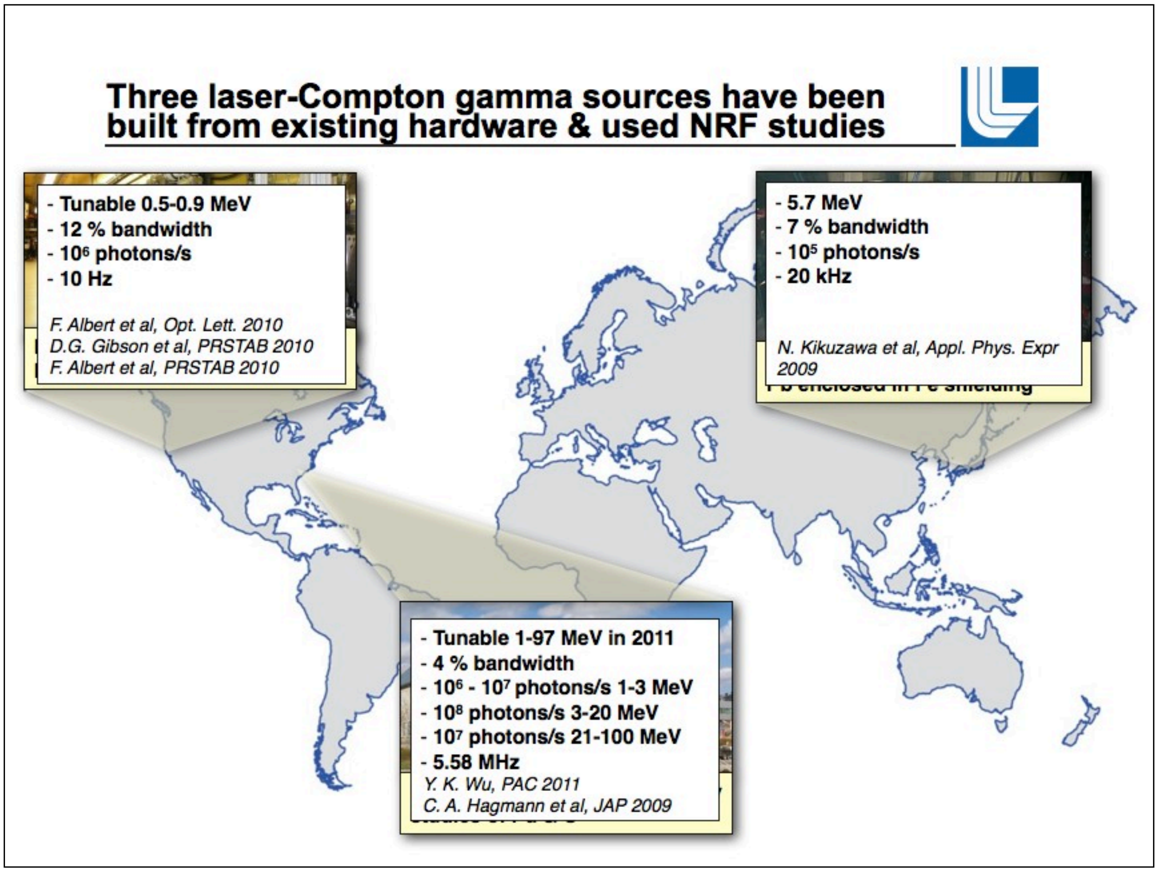
Three laser-Compton gamma sources have been built from existing hardware & used NRF studies
- Tunable 0.5-0.9 MeV
- 12 % bandwidth
- 10^6 photons/s
- 10 Hz
F. Albert et al, Opt. Lett. 2010
D.G. Gibson et al, PRSTAB 2010
F. Albert et al, PRSTAB 2010
- 5.7 MeV
- 7 % bandwidth
- 10^5 photons/s
- 20 kHz
N. Kikuzawa et al, Appl. Phys. Expr 2009
- Tunable 1-97 MeV in 2011
- 4 % bandwidth
- 10^6 - 10^7 photons/s 1-3 MeV
- 10^8 photons/s 3-20 MeV
- 10^7 photons/s 21-100 MeV
- 5.58 MHz
Y. K. Wu, PAC 2011
C. A. Hagmann et al, JAP 2009

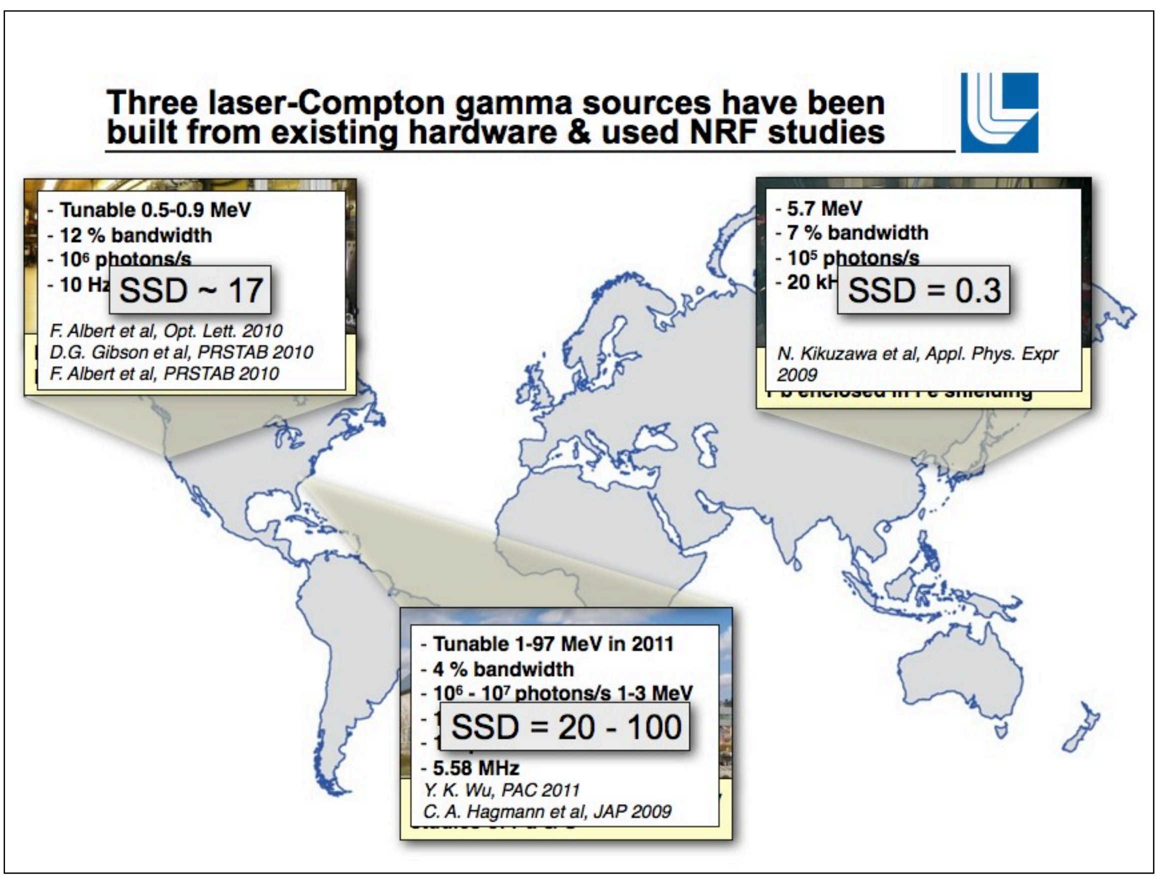
Three laser-Compton gamma sources have been built from existing hardware & used NRF studies
- Tunable 0.5-0.9 MeV
- 12 % bandwidth
- 10^6 photons/s
SSD ~ 17
F. Albert et al, Opt. Lett. 2010
D.G. Gibson et al, PRSTAB 2010
F. Albert et al, PRSTAB 2010
- 5.7 MeV
- 7 % bandwidth
- 10^5 photons/s
SSD = 0.3
N. Kikuzawa et al, Appl. Phys. Expr 2009
- Tunable 1-97 MeV in 2011
- 4 % bandwidth
- 10^6 - 10^7 photons/s 1-3 MeV
SSD = 20 - 100
- 5.58 MHz
Y. K. Wu, PAC 2011
C. A. Hagmann et al, JAP 2009

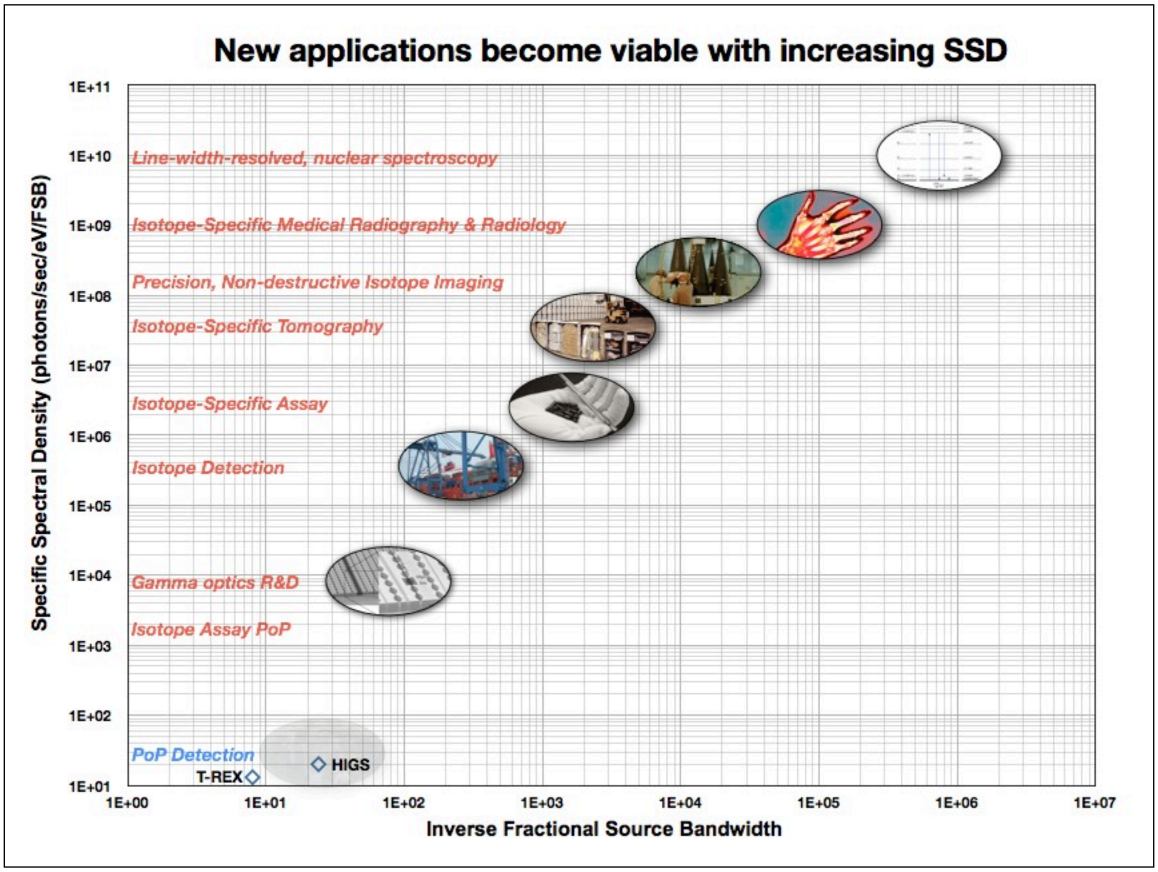
New applications become viable with increasing SSD
Specific Spectral Density (photons/sec/eV/FSB)
Inverse Fractional Source Bandwidth
1E+11
1E+10
1E+09
1E+08
1E+07
1E+06
1E+05
1E+04
1E+03
1E+02
1E+01
1E+00
1E+01
1E+02
1E+03
1E+04
1E+05
1E+06
1E+07
Line-width-resolved, nuclear spectroscopy
Isotope-Specific Medical Radiography & Radiology
Precision, Non-destructive Isotope Imaging
Isotope-Specific Tomography
Isotope-Specific Assay
Isotope Detection
Gamma optics R&D
Isotope Assay PoP
PoP Detection
T-REX
HIGS


many applications require one to take the source to the object and not vice versa
Desired Capability:
1.73 MeV photons
(250 MeV electrons)
100,000 SSD
0.1% bandwidth
Truck size or smaller

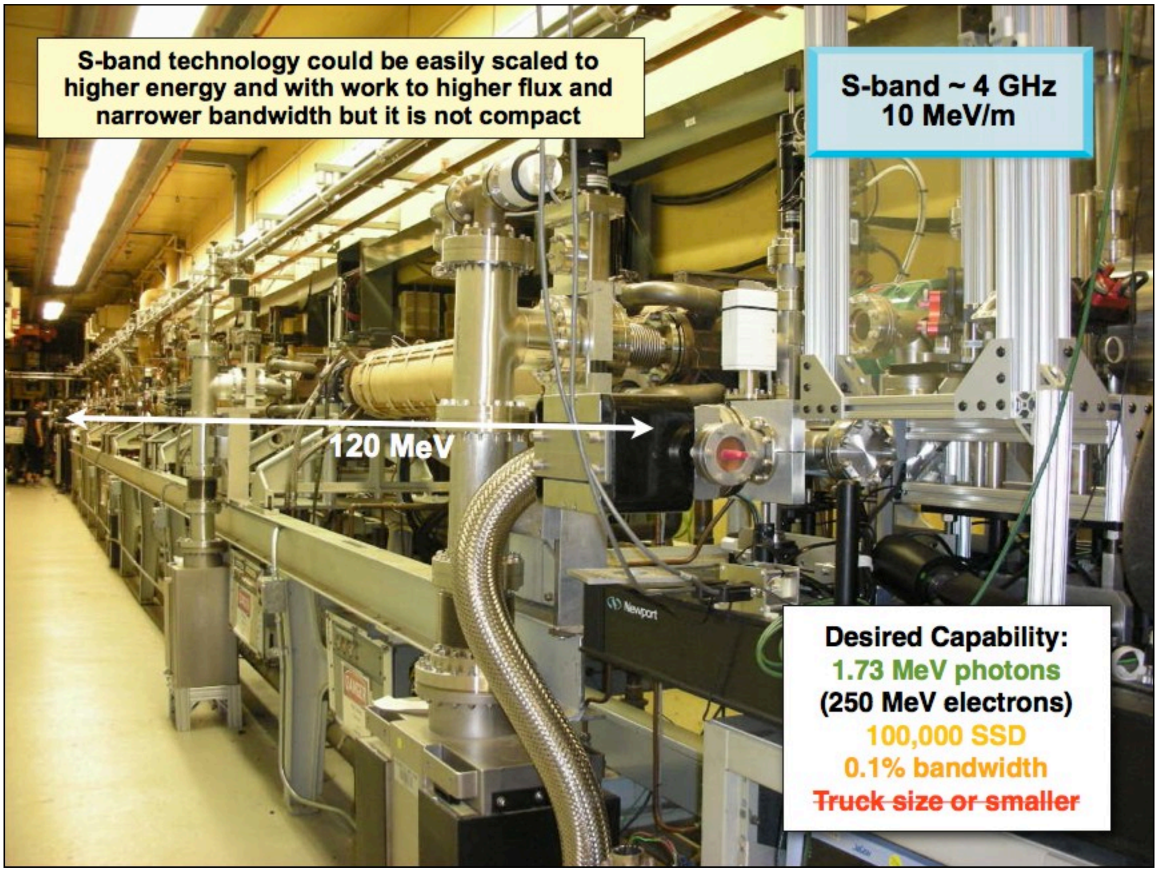
S-band technology could be easily scaled to higher energy and with work to higher flux and narrower bandwidth but it is not compact
S-band ~ 4 GHz
10 MeV/m
120 MeV
Newport
Desired Capability:
1.73 MeV photons
(250 MeV electrons)
100,000 SSD
0.1% bandwidth
~~Truck size or smaller~~


High gradient x-band technology developed at DOE's SLAC National Accelerator Lab provides a path to future compact MEGa-ray machines
X-Band ~ 12 GHz
Grad > 120 MeV/m
70 MeV
Desired Capability:
1.73 MeV photons
(250 MeV electrons)
>100,000,000 SSD
0.1% bandwidth
Truck size or smaller


LLNL B194
S-band modulators
10 required for
250 MeV system

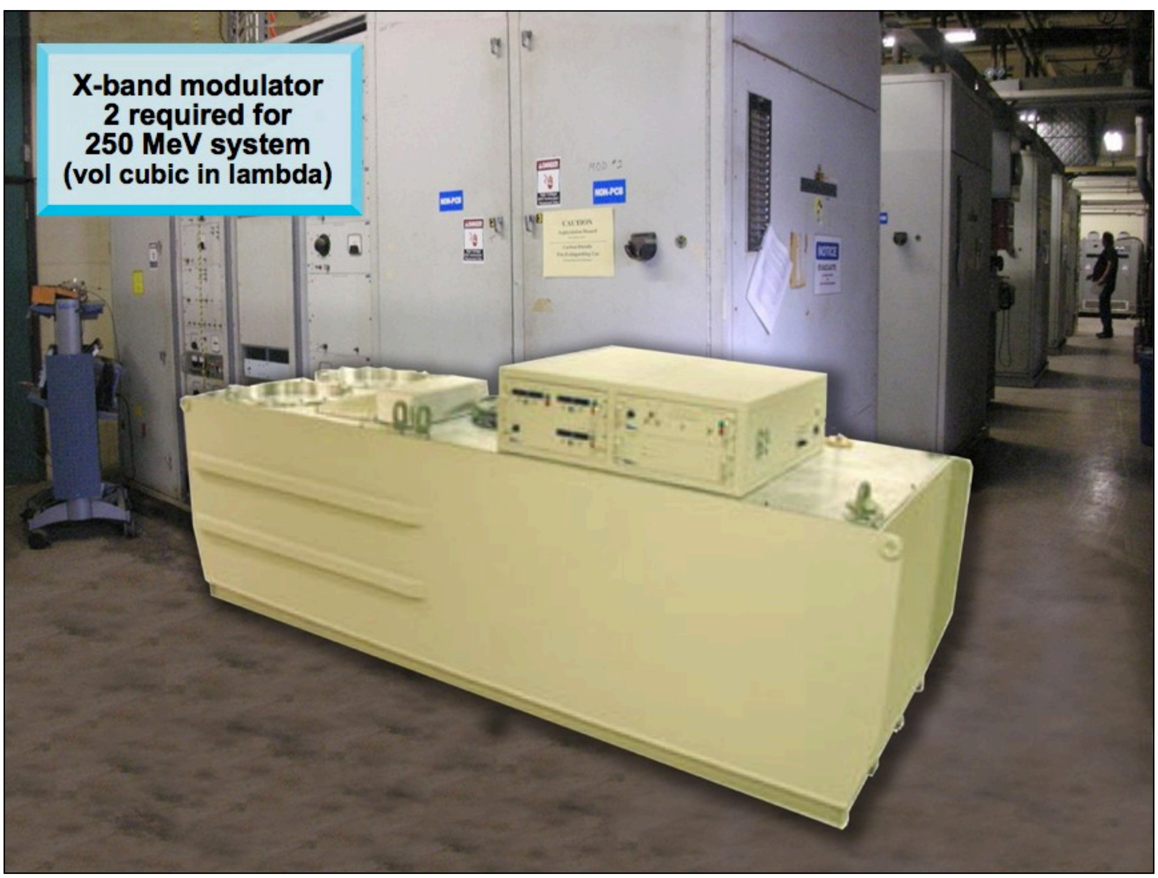
X-band modulator
2 required for
250 MeV system
(vol cubic in lambda)

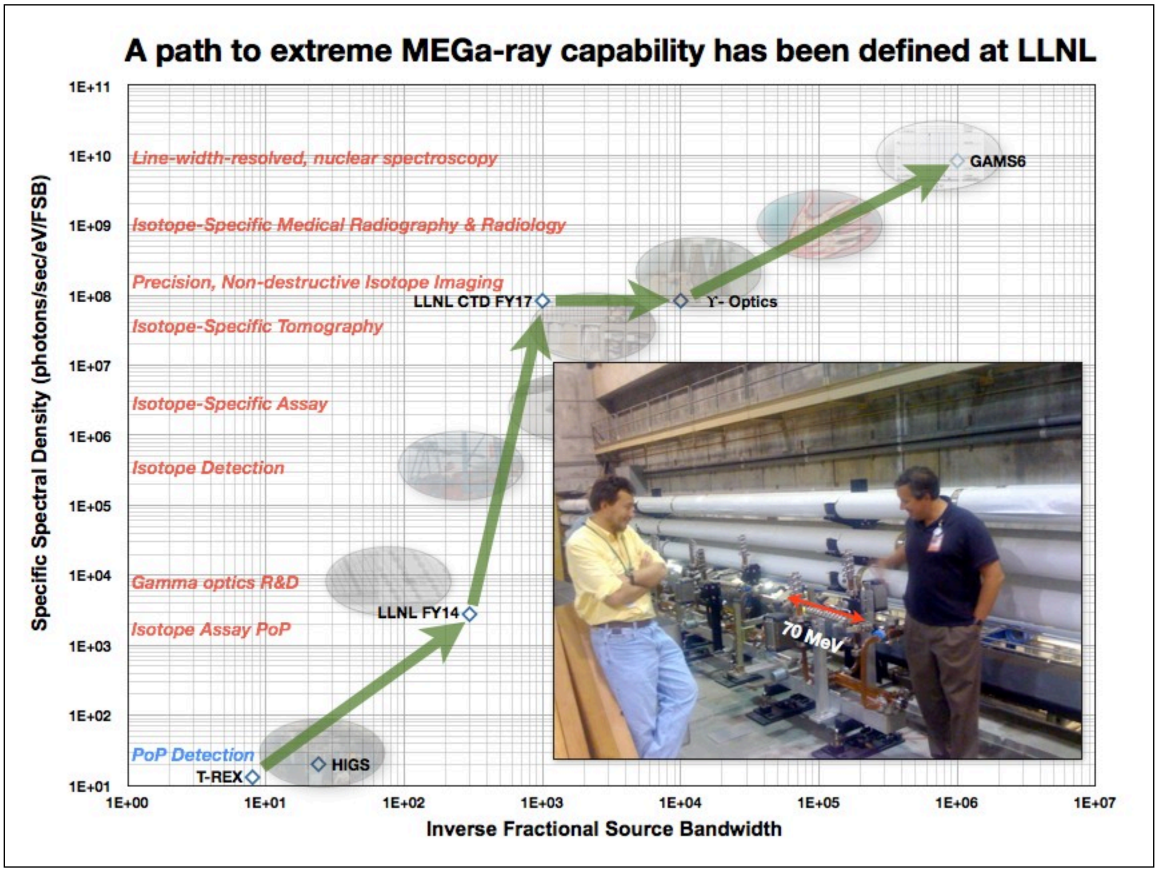
A path to extreme MEGa-ray capability has been defined at LLNL
Specific Spectral Density (photons/sec/eV/FSB)
Inverse Fractional Source Bandwidth
1E+11
1E+10
1E+09
1E+08
1E+07
1E+06
1E+05
1E+04
1E+03
1E+02
1E+01
1E+00
1E+01
1E+02
1E+03
1E+04
1E+05
1E+06
1E+07
Line-width-resolved, nuclear spectroscopy
Isotope-Specific Medical Radiography & Radiology
Precision, Non-destructive Isotope Imaging
Isotope-Specific Tomography
Isotope-Specific Assay
Isotope Detection
Gamma optics R&D
Isotope Assay PoP
PoP Detection
T-REX
HIGS
LLNL FY14
LLNL CTD FY17
ϒ- Optics
GAMS6
70 MeV

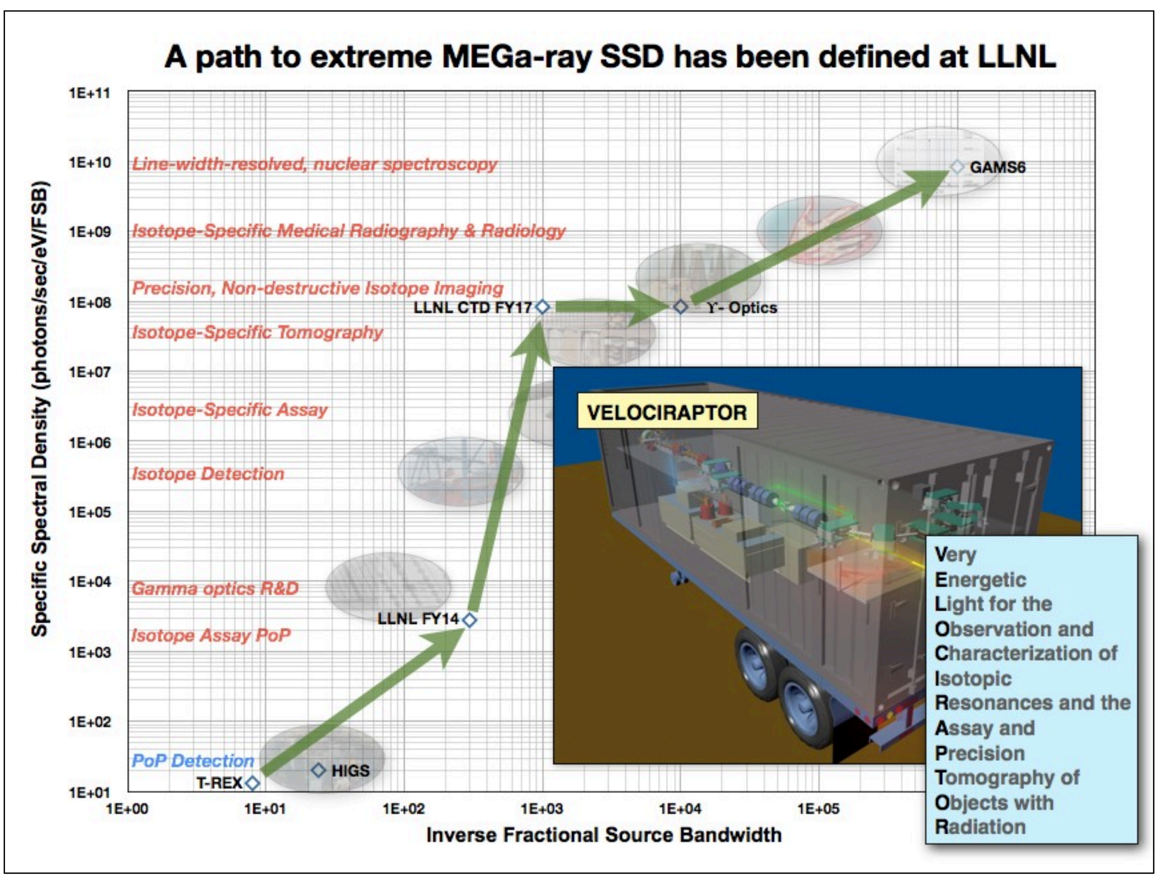
A path to extreme MEGa-ray SSD has been defined at LLNL
Specific Spectral Density (photons/sec/eV/FSB)
Inverse Fractional Source Bandwidth
1E+11
1E+10
1E+09
1E+08
1E+07
1E+06
1E+05
1E+04
1E+03
1E+02
1E+01
1E+00
1E+01
1E+02
1E+03
1E+04
1E+05
Line-width-resolved, nuclear spectroscopy
Isotope-Specific Medical Radiography & Radiology
Precision, Non-destructive Isotope Imaging
Isotope-Specific Tomography
Isotope-Specific Assay
Isotope Detection
Gamma optics R&D
Isotope Assay PoP
PoP Detection
T-REX
HIGS
LLNL FY14
LLNL CTD FY17
ϒ- Optics
GAMS6
VELOCIRAPTOR
Very
Energetic
Light for the
Observation and
Characterization of
Isotopic
Resonances and the
Assay and
Precision
Tomography of
Objects with
Radiation

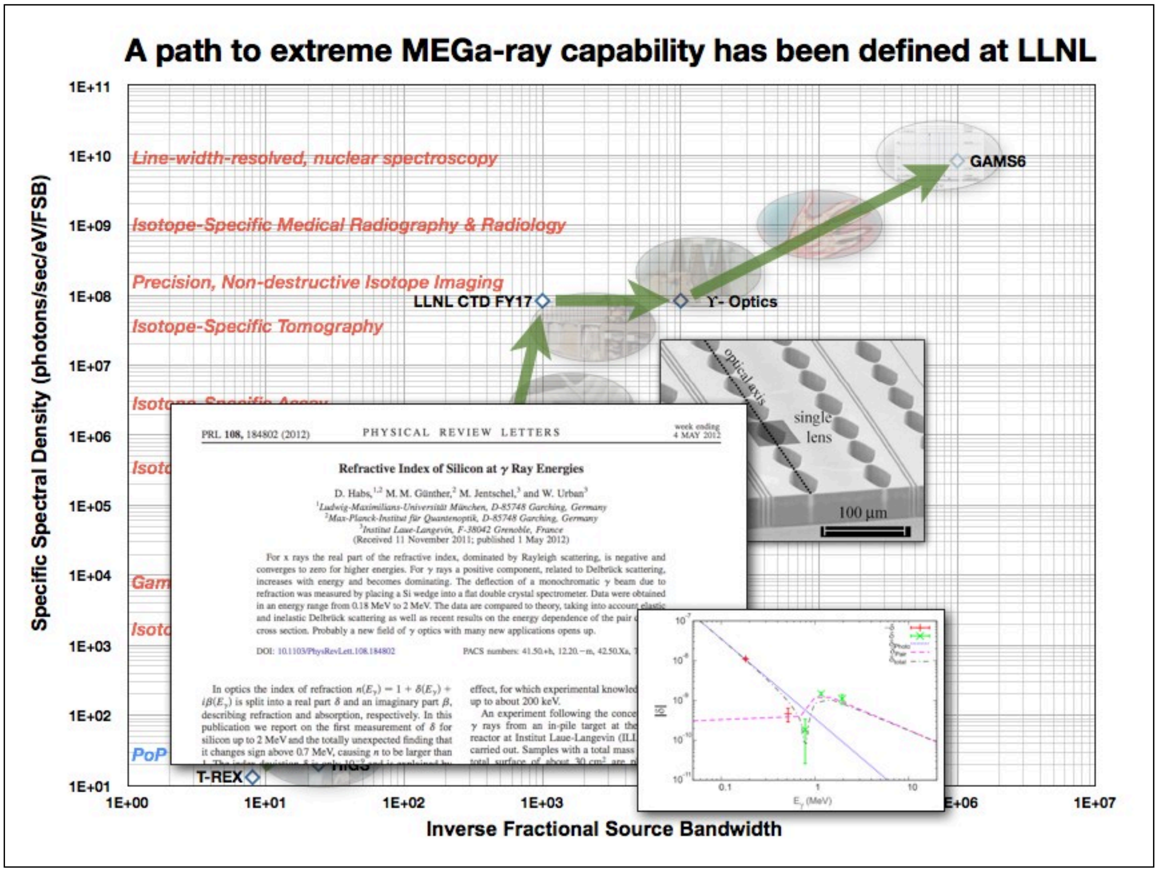

A path to extreme MEGa-ray capability has been defined at LLNL
Specific Spectral Density (photons/sec/eV/FSB)
Inverse Fractional Source Bandwidth
1E+11
1E+10
1E+09
1E+08
1E+07
1E+06
1E+05
1E+04
1E+03
1E+02
1E+01
1E+00
1E+01
1E+02
1E+03
1E+06
1E+07
Line-width-resolved, nuclear spectroscopy
Isotope-Specific Medical Radiography & Radiology
Precision, Non-destructive Isotope Imaging
Isotope-Specific Tomography
GAMS6
LLNL CTD FY17
ϒ- Optics
T-REX
HIGS
optical axis
single lens
100 µm
PRL 108, 184802 (2012)
PHYSICAL REVIEW LETTERS
week ending 4 MAY 2012
Refractive Index of Silicon at γ Ray Energies
D. Habs,[1,2] M. M. Günther,[2] M. Jentschel,[3] and W. Urban[3]
[1]Ludwig-Maximilians-Universität München, D-85748 Garching, Germany
[2]Max-Planck-Institut für Quantenoptik, D-85748 Garching, Germany
[3]Institut Laue-Langevin, F-38042 Grenoble, France
(Received 11 November 2011; published 1 May 2012)
DOI: 10.1103/PhysRevLett.108.184802
E$_\gamma$ (MeV)

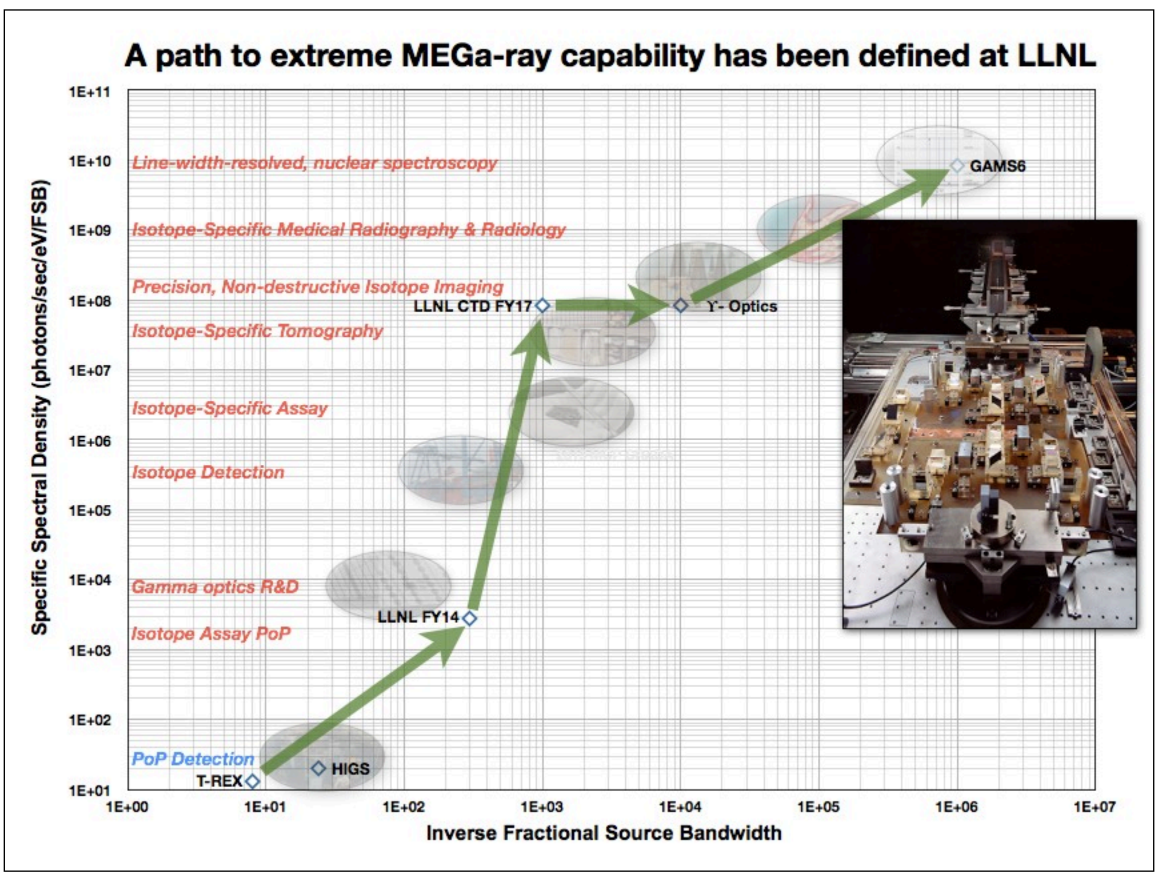

A path to extreme MEGa-ray capability has been defined at LLNL
Specific Spectral Density (photons/sec/eV/FSB)
Inverse Fractional Source Bandwidth
1E+11
1E+10
1E+09
1E+08
1E+07
1E+06
1E+05
1E+04
1E+03
1E+02
1E+01
1E+00
1E+01
1E+02
1E+03
1E+04
1E+05
1E+06
1E+07
Line-width-resolved, nuclear spectroscopy
Isotope-Specific Medical Radiography & Radiology
Precision, Non-destructive Isotope Imaging
Isotope-Specific Tomography
Isotope-Specific Assay
Isotope Detection
Gamma optics R&D
Isotope Assay PoP
PoP Detection
GAMS6
LLNL CTD FY17
ϒ- Optics
LLNL FY14
T-REX
HIGS

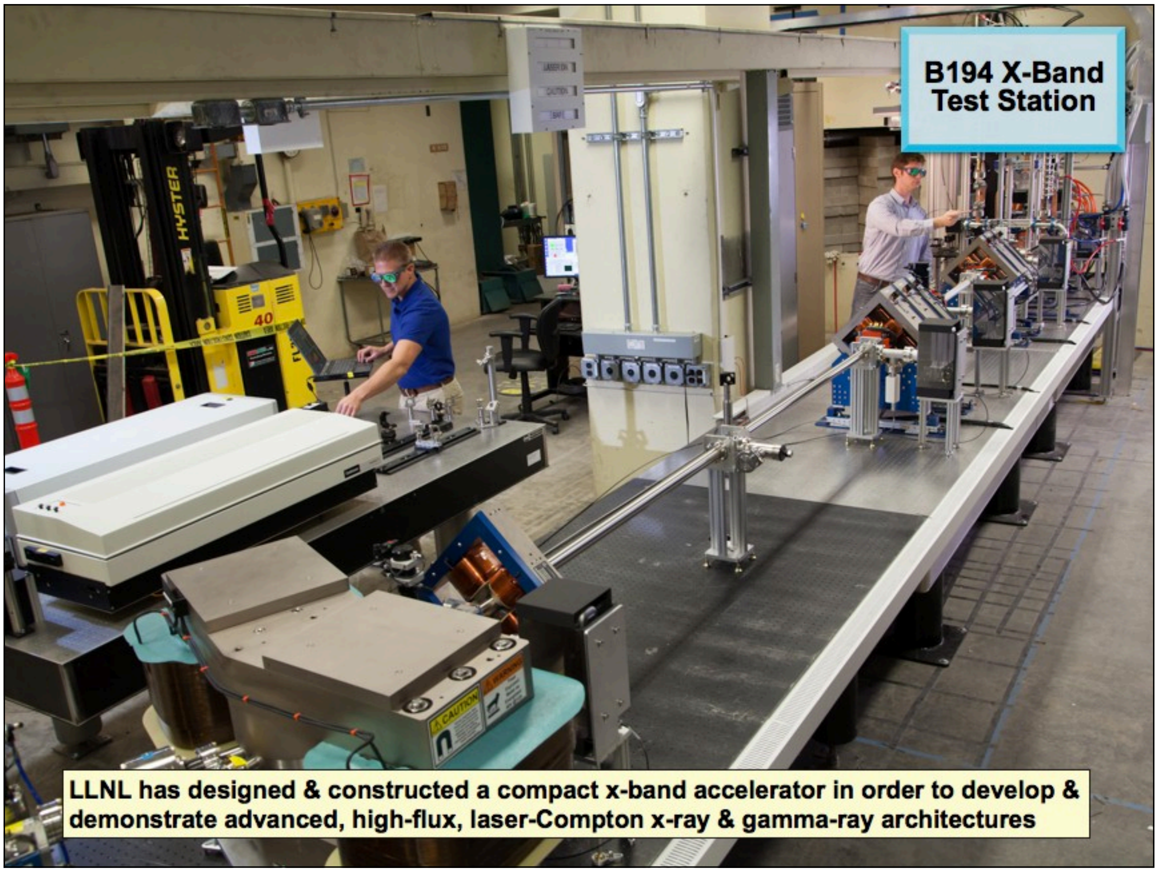
B194 X-Band Test Station
HYSTER
40
LLNL has designed & constructed a compact x-band accelerator in order to develop & demonstrate advanced, high-flux, laser-Compton x-ray & gamma-ray architectures

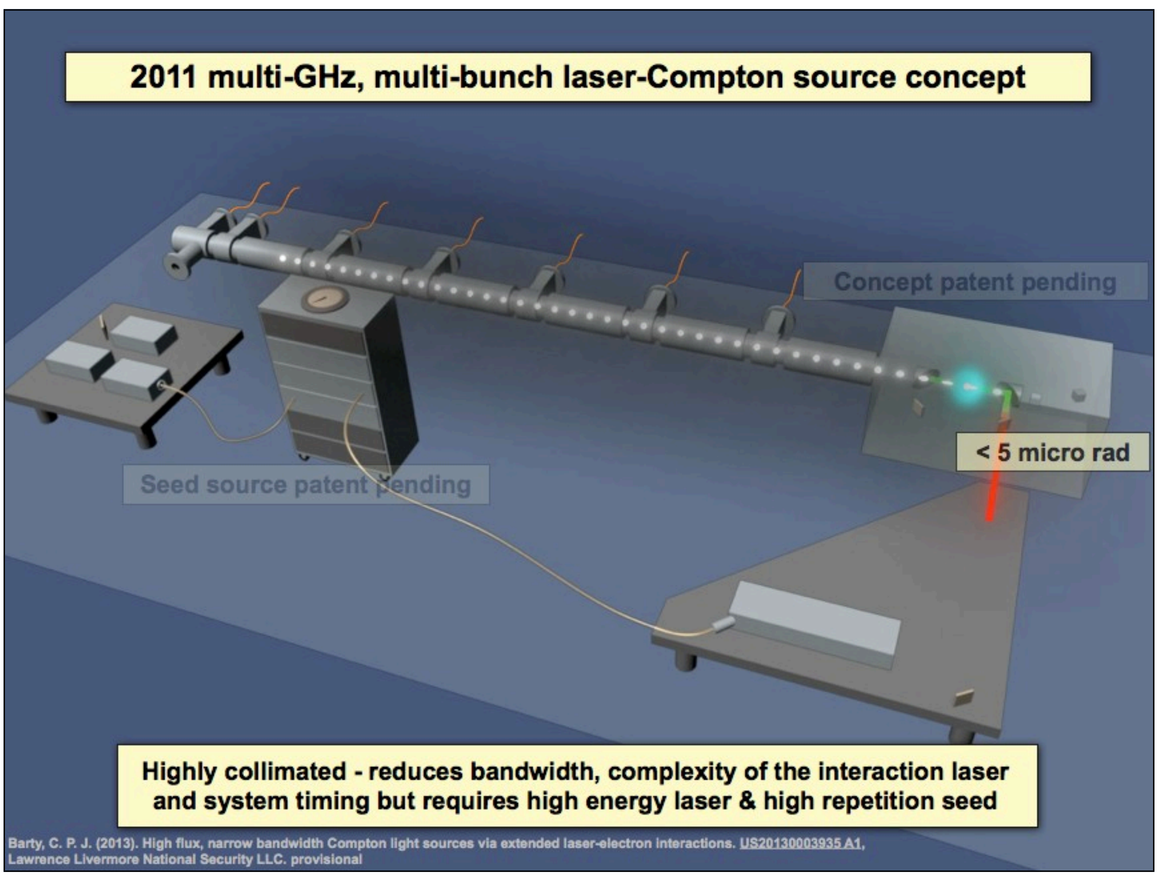
2011 multi-GHz, multi-bunch laser-Compton source concept
Concept patent pending
< 5 micro rad
Seed source patent pending
Highly collimated - reduces bandwidth, complexity of the interaction laser and system timing but requires high energy laser & high repetition seed
Barty, C. P. J. (2013). High flux, narrow bandwidth Compton light sources via extended laser-electron interactions. US20130003935 A1, Lawrence Livermore National Security LLC. provisional

“CW” method for generation of 11.424 GHz, synchronized train of picosecond IR seed pulses

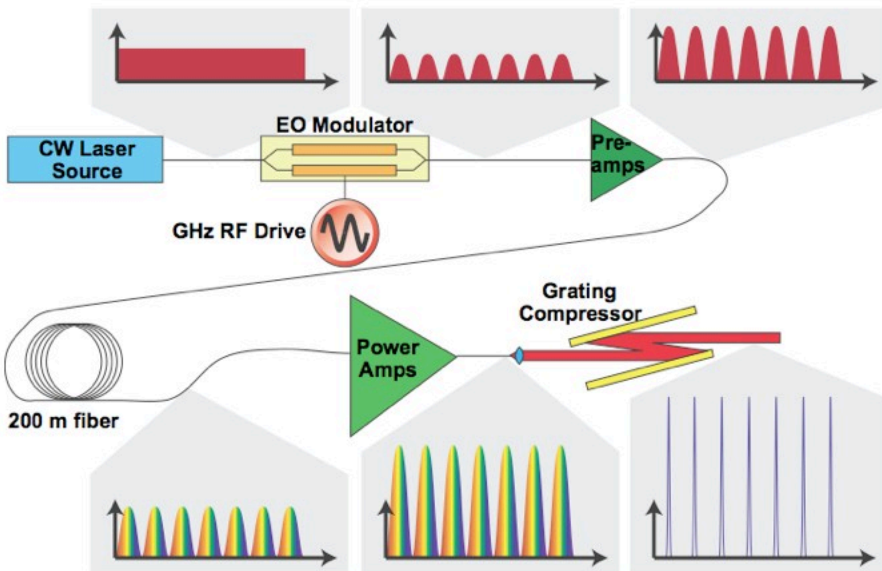

Barty, C. P. J., M. J. Messerly, J. W. Dawson, D. J. Gibson, M. A. Prantil, Eric Cormier (2012), Directly driven source of multi-gigahertz, sub-picosecond optical pulses. WO2013040041 A3, Lawrence Livermore National Security LLC. provisional

“CW” method for generation of 11.424 GHz, synchronized train of picosecond IR seed pulses

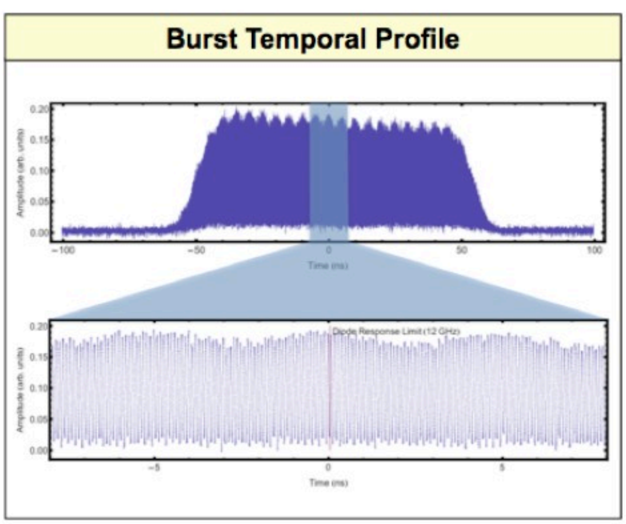

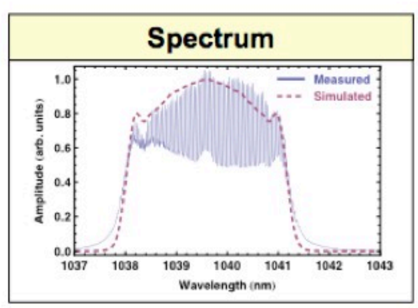

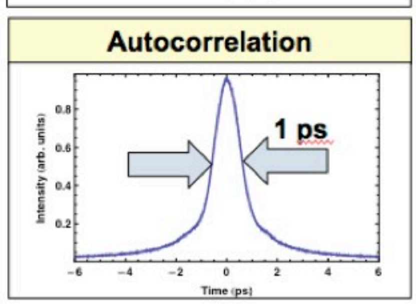

"CW" method for generation of 11.424 GHz, synchronized train of picosecond IR seed pulses

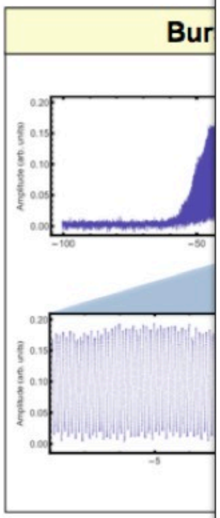

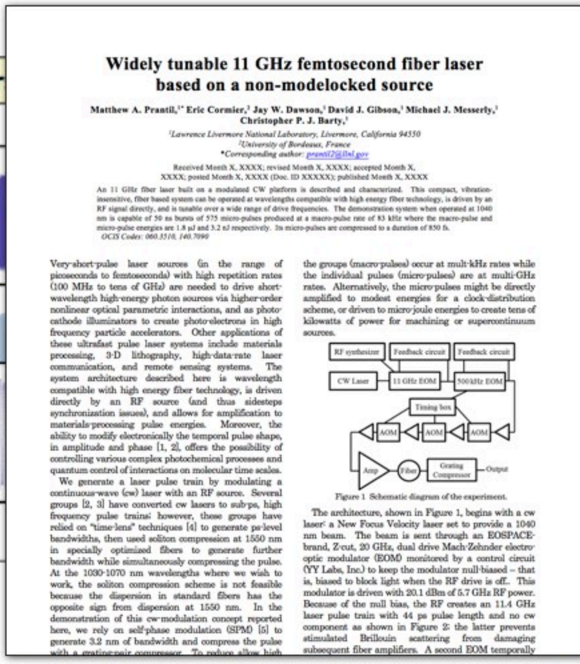

Widely tunable 11 GHz femtosecond fiber laser based on a non-modelocked source

Matthew A. Prantil,[1*] Eric Cormier,[2] Jay W. Dawson,[1] David J. Gibson,[1] Michael J. Messerly,[1] Christopher P. J. Barty,[1]

[1]Lawrence Livermore National Laboratory, Livermore, California 94550
[2]University of Bordeaux, France
*Corresponding author: prantil2@llnl.gov

Received Month X, XXXX; revised Month X, XXXX; accepted Month X, XXXX; posted Month X, XXXX (Doc. ID XXXXX); published Month X, XXXX

An 11 GHz fiber laser built on a modulated CW platform is described and characterized. This compact, vibration-insensitive, fiber based system can be operated at wavelengths compatible with high energy fiber technology, is driven by an RF signal directly, and is tunable over a wide range of drive frequencies. The demonstration system when operated at 1040 nm is capable of 50 ns bursts of 575 micro-pulses produced at a macro-pulse rate of 83 kHz where the macro-pulse and micro-pulse energies are 1.8 μJ and 3.2 nJ respectively. Its micro-pulses are compressed to a duration of 850 fs.

OCIS Codes: 060.3510, 140.7090

Very-short-pulse laser sources (in the range of picoseconds to femtoseconds) with high repetition rates (100 MHz to tens of GHz) are needed to drive short-wavelength high-energy photon sources via higher-order nonlinear optical parametric interactions, and as photo-cathode illuminators to create photo-electrons in high frequency particle accelerators. Other applications of these ultrafast pulse laser systems include materials processing, 3-D lithography, high-data-rate laser communication, and remote sensing systems. The system architecture described here is wavelength compatible with high energy fiber technology, is driven directly by an RF source (and thus sidesteps synchronization issues), and allows for amplification to materials-processing pulse energies. Moreover, the ability to modify electronically the temporal pulse shape, in amplitude and phase [1, 2], offers the possibility of controlling various complex photochemical processes and quantum control of interactions on molecular time scales.

We generate a laser pulse train by modulating a continuous-wave (cw) laser with an RF source. Several groups [2, 3] have converted cw lasers to sub-ps, high frequency pulse trains; however, these groups have relied on "time-lens" techniques [4] to generate ps-level bandwidths, then used soliton compression at 1550 nm in specially optimized fibers to generate further bandwidth while simultaneously compressing the pulse. At the 1030-1070 nm wavelengths where we wish to work, the soliton compression scheme is not feasible because the dispersion in standard fibers has the opposite sign from dispersion at 1550 nm. In the demonstration of this cw-modulation concept reported here, we rely on self-phase modulation (SPM) [5] to generate 3.2 nm of bandwidth and compress the pulse with a grating-pair compressor. To reduce allow high the groups (macro-pulses) occur at mult-kHz rates while the individual pulses (micro-pulses) are at multi-GHz rates. Alternatively, the micro-pulses might be directly amplified to modest energies for a clock-distribution scheme, or driven to micro-joule energies to create tens of kilowatts of power for machining or supercontinuum sources.

RF synthesizer | Feedback circuit | Feedback circuit
CW Laser | 11 GHz EOM | 500kHz EOM
Timing box
AOM | AOM | AOM
Amp | Fiber | Grating Compressor | Output

Figure 1 Schematic diagram of the experiment.

The architecture, shown in Figure 1, begins with a cw laser: a New Focus Velocity laser set to provide a 1040 nm beam. The beam is sent through an EOSPACE-brand, Z-cut, 20 GHz, dual drive Mach-Zehnder electro-optic modulator (EOM) monitored by a control circuit (YY Labs, Inc.) to keep the modulator null-biased – that is, biased to block light when the RF drive is off. This modulator is driven with 20.1 dBm of 5.7 GHz RF power. Because of the null bias, the RF creates an 11.4 GHz laser pulse train with 44 ps pulse length and no cw component as shown in Figure 2: the latter prevents stimulated Brillouin scattering from damaging subsequent fiber amplifiers. A second EOM temporally

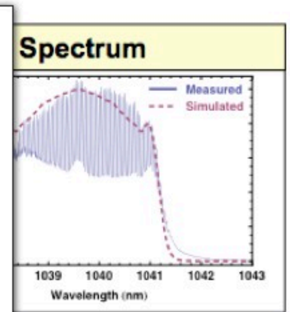

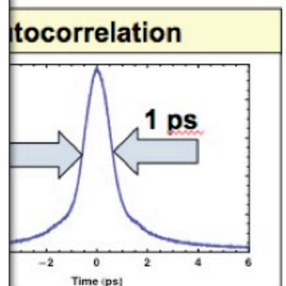

Prantil, M. A., E. Cormier, J. W. Dawson, D. J. Gibson, M. J. Messerly and C. P. J. Barty. "Widely tunable 11 GHz femtosecond fiber laser based on a nonmode-locked source." Optics Letters 38(17): 3216-3218 (2013)

A new custom, diode-pumped solid state laser architecture can generate > 1J per pulse @ 120 Hz

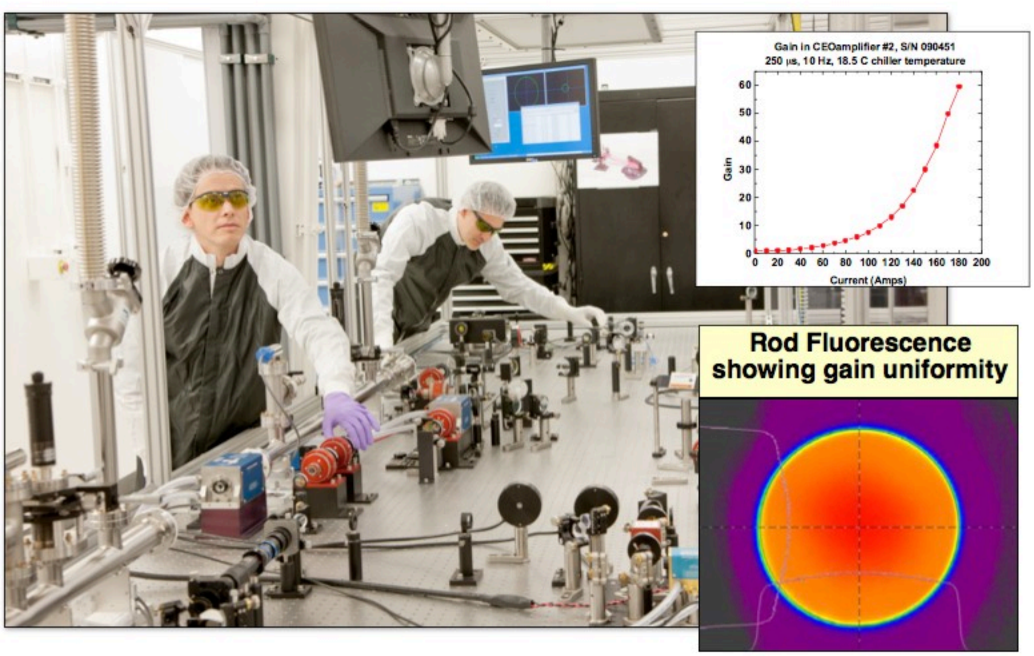

LLNL's "Picket Fence" multi-GHz, laser-Compton source concept

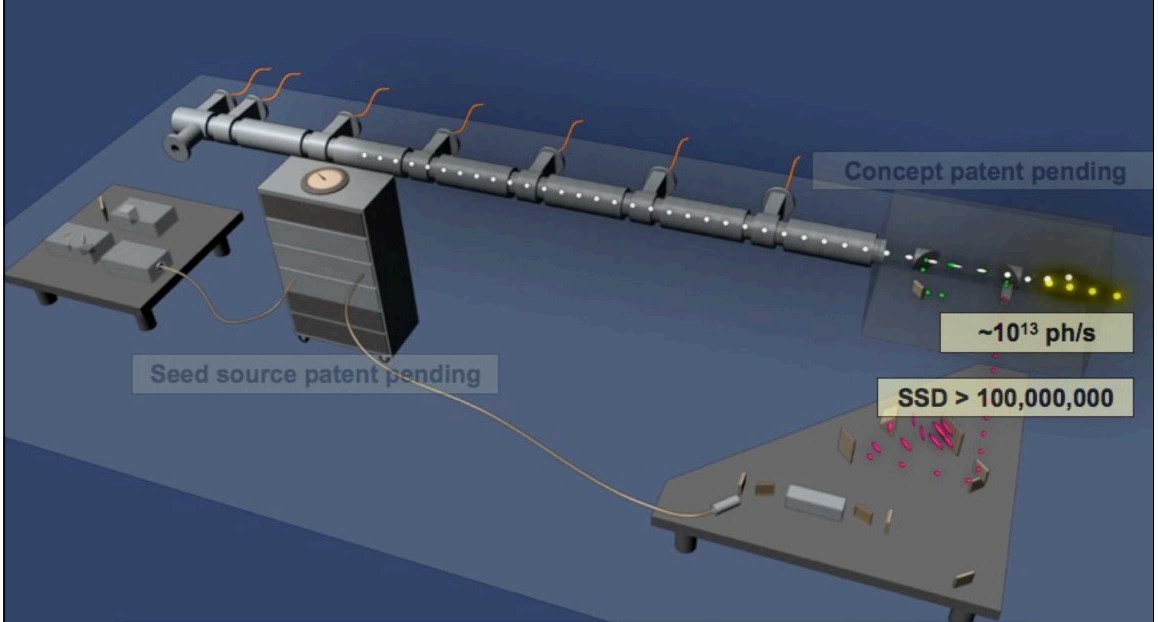

This configuration enables high efficiency, operates with high beam current, minimizes bandwidth and is intrinsically synchronized to RF clock

Barty, C. P. J., (2013), Modulated, Long-Pulse Method for Efficient, Narrow-bandwidth, Laser Compton X-ray and Gamma-ray Source. Lawrence Livermore National Security LLC. provisional

RF Power combines the best of SLAC klystron technology & commercial solid state modulators

State-of-the-art solid-state, 420 kV, 300 A Modulator and 50 MW Klystron

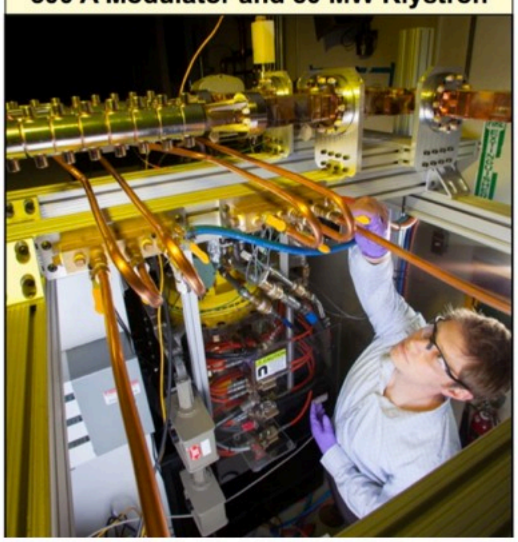

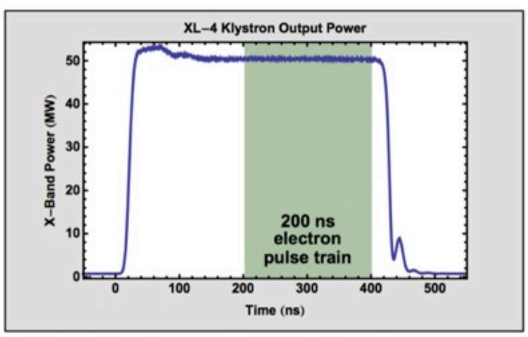

Performance of the XL4 klystron and ScandiNova modulator exceed all of our requirements

E-Beam Energy vs. RF Power

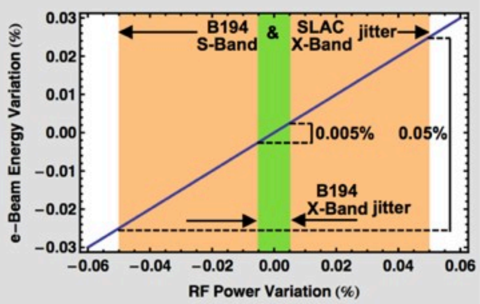

This system is 10x more stable in amplitude than existing SLAC and LLNL sources.

E-Beam Brightness vs. RF Phase

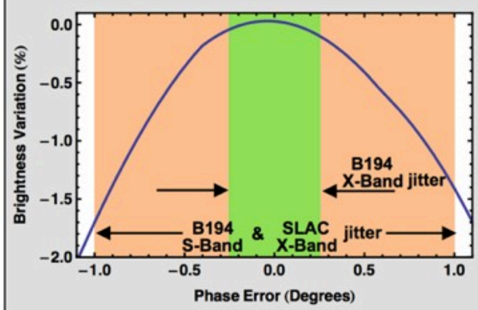

4x improvement in RF phase stability corresponds to 10x improvement in brightness stability.

Worldwide high power x-band sources

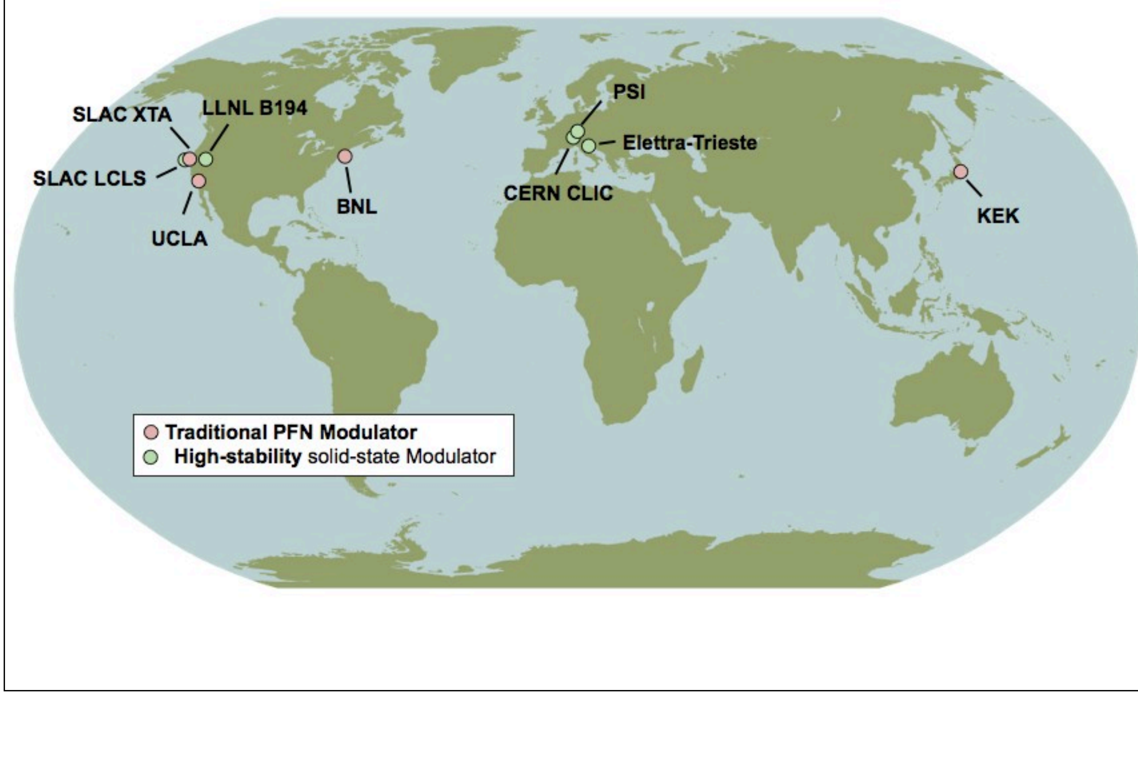

Worldwide high power x-band sources

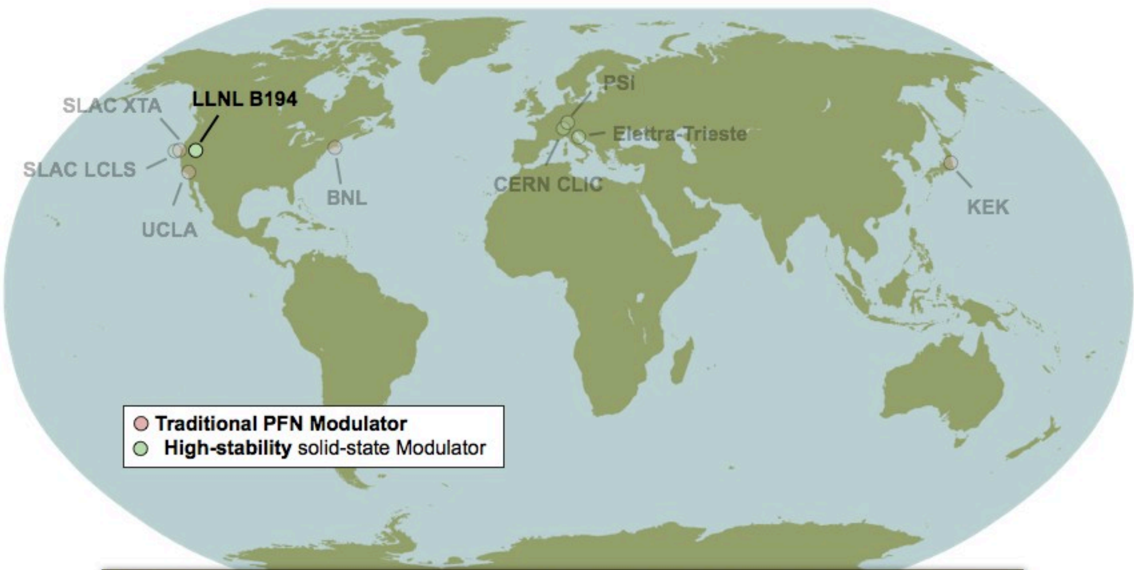

LLNL set up is currently the only facility where high quality x-band RF is coupled with state-of-the-art structures to produce beam

Photo-gun and first section

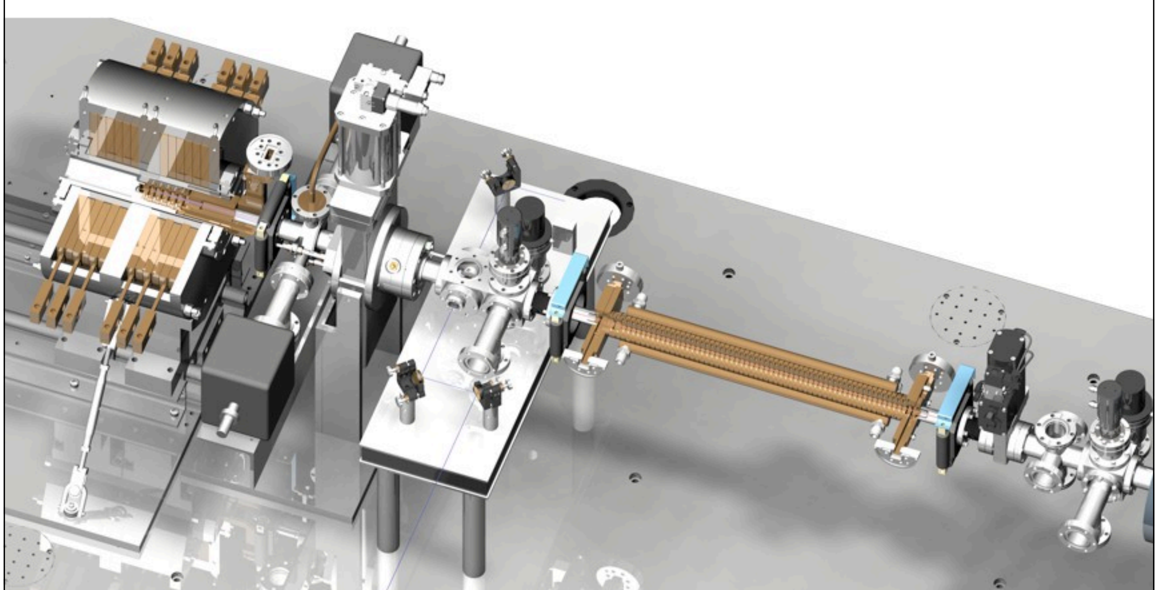

X-band photo-gun evolution

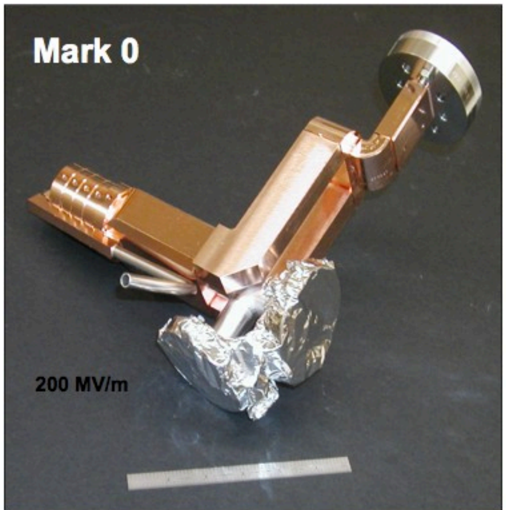

**SLAC 5.5 cell x-band gun
designed by Arnold Vlieks (SLAC)**

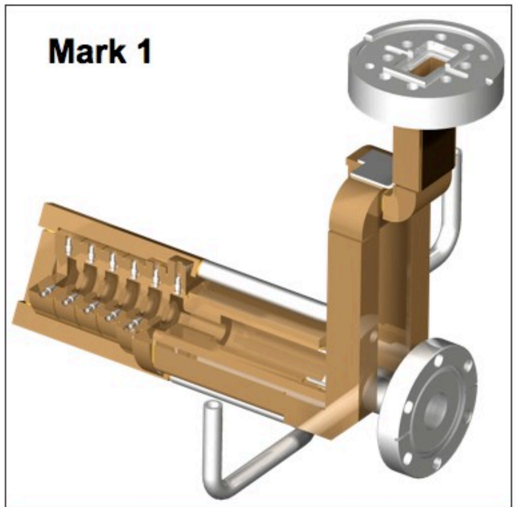

**LLNL/SLAC 5.59 cell x-band gun
design lead - Roark Marsh (LLNL)**

X-band photo-gun evolution

- Longer Half cell for lower final emittance
- Better mode separation for less mode beating on cathode surface
- Elliptical irises for lower peak surface electric field
- Dual feed racetrack coupler for minimized RF quadrupole kick
- Optimized beta for a balance of fast gun fill time and low pulsed heating

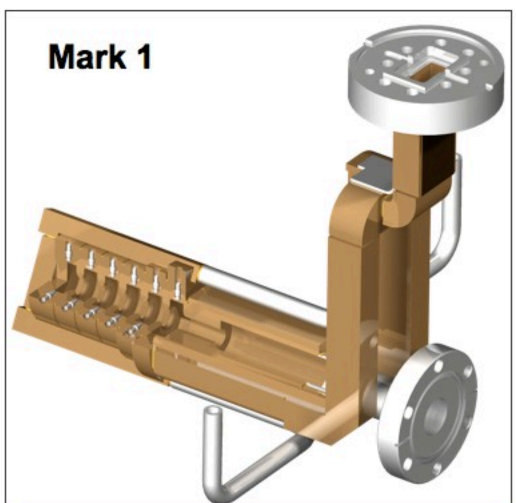

**LLNL/SLAC 5.59 cell x-band gun
design lead - Roark Marsh (LLNL)**

PARMELA results

Redesigned longer half cell optimizes the electron beam brightness and reduces Compton bandwidth

Optimized launch phase and solenoid strength
Beam parameters: Q = 250 pC, τφ = 10 deg.
200 MV/m cathode field

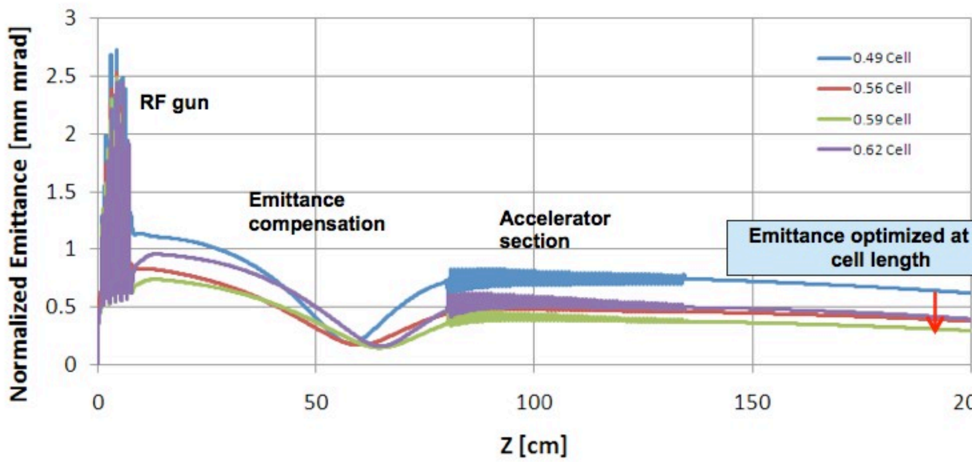

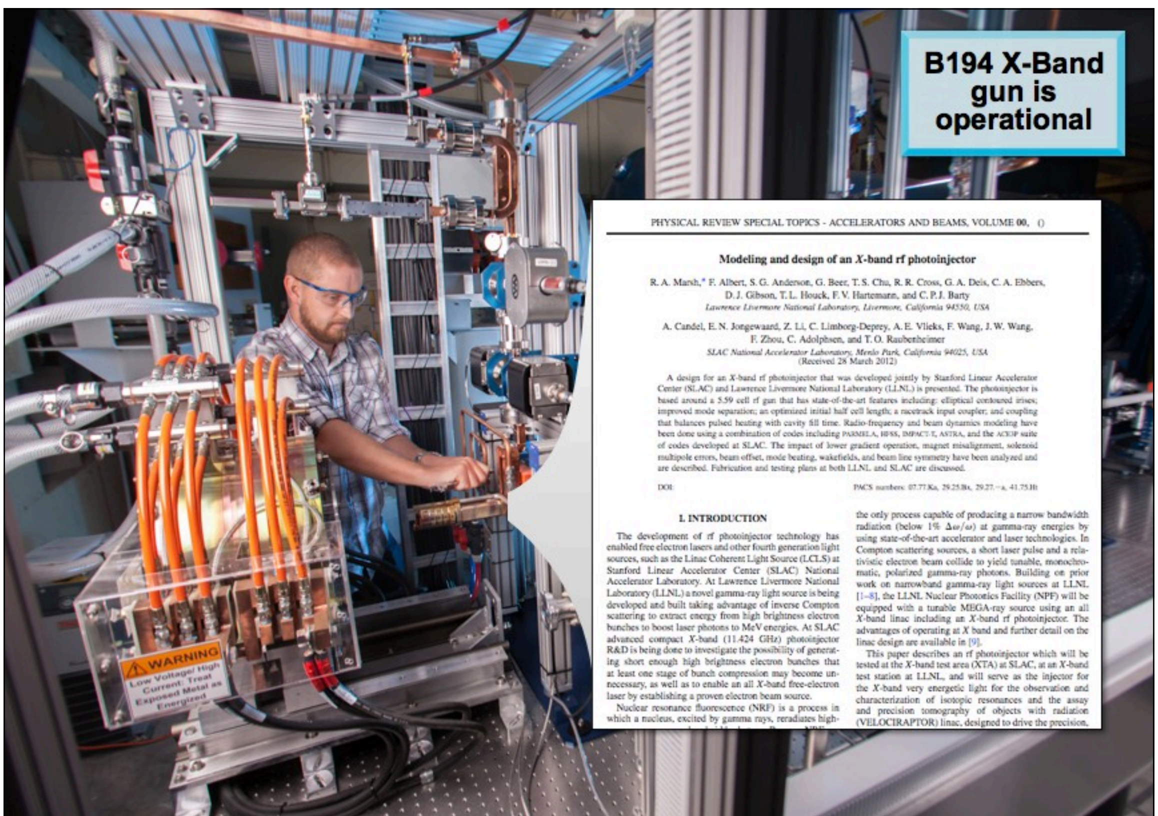

PHYSICAL REVIEW SPECIAL TOPICS - ACCELERATORS AND BEAMS, VOLUME 00, ()

Modeling and design of an X-band rf photoinjector

R. A. Marsh,* F. Albert, S. G. Anderson, G. Beer, T. S. Chu, R. R. Cross, G. A. Deis, C. A. Ebbers, D. J. Gibson, T. L. Houck, F. V. Hartemann, and C. P. J. Barty
Lawrence Livermore National Laboratory, Livermore, California 94550, USA

A. Candel, E. N. Jongewaard, Z. Li, C. Limborg-Deprey, A. E. Vlieks, F. Wang, J. W. Wang, F. Zhou, C. Adolphsen, and T. O. Raubenheimer
SLAC National Accelerator Laboratory, Menlo Park, California 94025, USA
(Received 28 March 2012)

A design for an X-band rf photoinjector that was developed jointly by Stanford Linear Accelerator Center (SLAC) and Lawrence Livermore National Laboratory (LLNL) is presented. The photoinjector is based around a 5.59 cell rf gun that has state-of-the-art features including: elliptical contoured irises; improved mode separation; an optimized initial half cell length; a racetrack input coupler; and coupling that balances pulsed heating with cavity fill time. Radio-frequency and beam dynamics modeling have been done using a combination of codes including PARMELA, HFSS, IMPACT-T, ASTRA, and the ACE3P suite of codes developed at SLAC. The impact of lower gradient operation, magnet misalignment, solenoid multipole errors, beam offset, mode beating, wakefields, and beam line symmetry have been analyzed and are described. Fabrication and testing plans at both LLNL and SLAC are discussed.

DOI: PACS numbers: 07.77.Ka, 29.25.Bx, 29.27.-a, 41.75.Ht

I. INTRODUCTION

The development of rf photoinjector technology has enabled free electron lasers and other fourth generation light sources, such as the Linac Coherent Light Source (LCLS) at Stanford Linear Accelerator Center (SLAC) National Accelerator Laboratory. At Lawrence Livermore National Laboratory (LLNL) a novel gamma-ray light source is being developed and built taking advantage of inverse Compton scattering to extract energy from high brightness electron bunches to boost laser photons to MeV energies. At SLAC advanced compact X-band (11.424 GHz) photoinjector R&D is being done to investigate the possibility of generating short enough high brightness electron bunches that at least one stage of bunch compression may become unnecessary, as well as to enable an all X-band free-electron laser by establishing a proven electron beam source.

Nuclear resonance fluorescence (NRF) is a process in which a nucleus, excited by gamma rays, reradiates high- ... the only process capable of producing a narrow bandwidth radiation (below 1% $\Delta\omega/\omega$) at gamma-ray energies by using state-of-the-art accelerator and laser technologies. In Compton scattering sources, a short laser pulse and a relativistic electron beam collide to yield tunable, monochromatic, polarized gamma-ray photons. Building on prior work on narrowband gamma-ray light sources at LLNL [1–8], the LLNL Nuclear Photonics Facility (NPF) will be equipped with a tunable MEGA-ray source using an all X-band linac including an X-band rf photoinjector. The advantages of operating at X band and further detail on the linac design are available in [9].

This paper describes an rf photoinjector which will be tested at the X-band test area (XTA) at SLAC, at an X-band test station at LLNL, and will serve as the injector for the X-band very energetic light for the observation and characterization of isotopic resonances and the assay and precision tomography of objects with radiation (VELOCIRAPTOR) linac, designed to drive the precision,

Marsh, R. A., F. Albert, S. G. Anderson, G. Beer, T. S. Chu, R. R. Cross, G. A. Deis, C. A. Ebbers, D. J. Gibson, T. L. Houck, F. V. Hartemann, C. P. J. Barty, et al. "Modeling and design of an X-band RF photoinjector." Physical Review Special Topics: Accelerators and Beams 15(10): 102001 (2012)

Other next generation laser-Compton gamma-ray projects are emerging to pursue isotope science

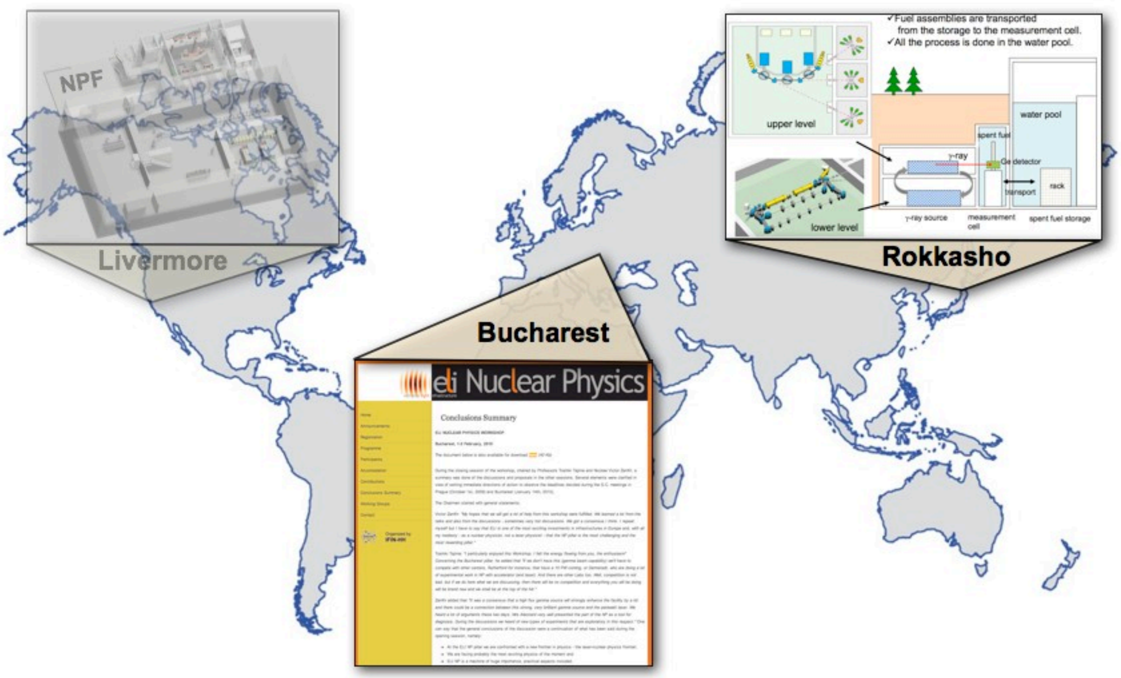

Other next generation laser-Compton gamma-ray projects are emerging to pursue isotope science

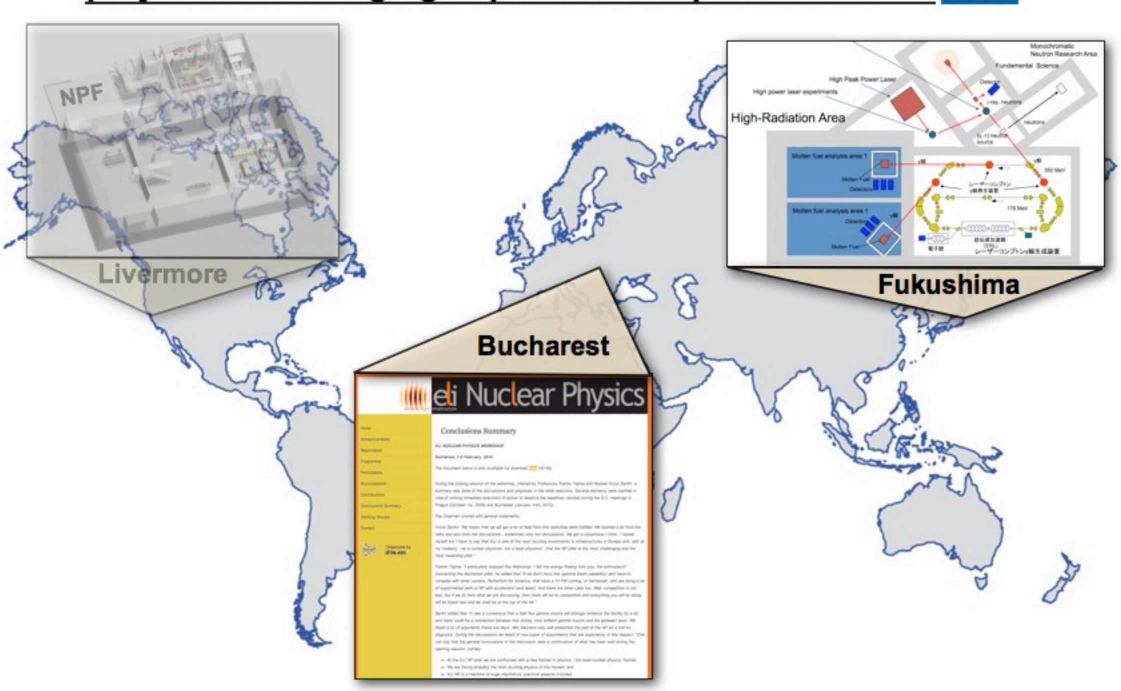


KEK/JAEA LCGS
PEARL

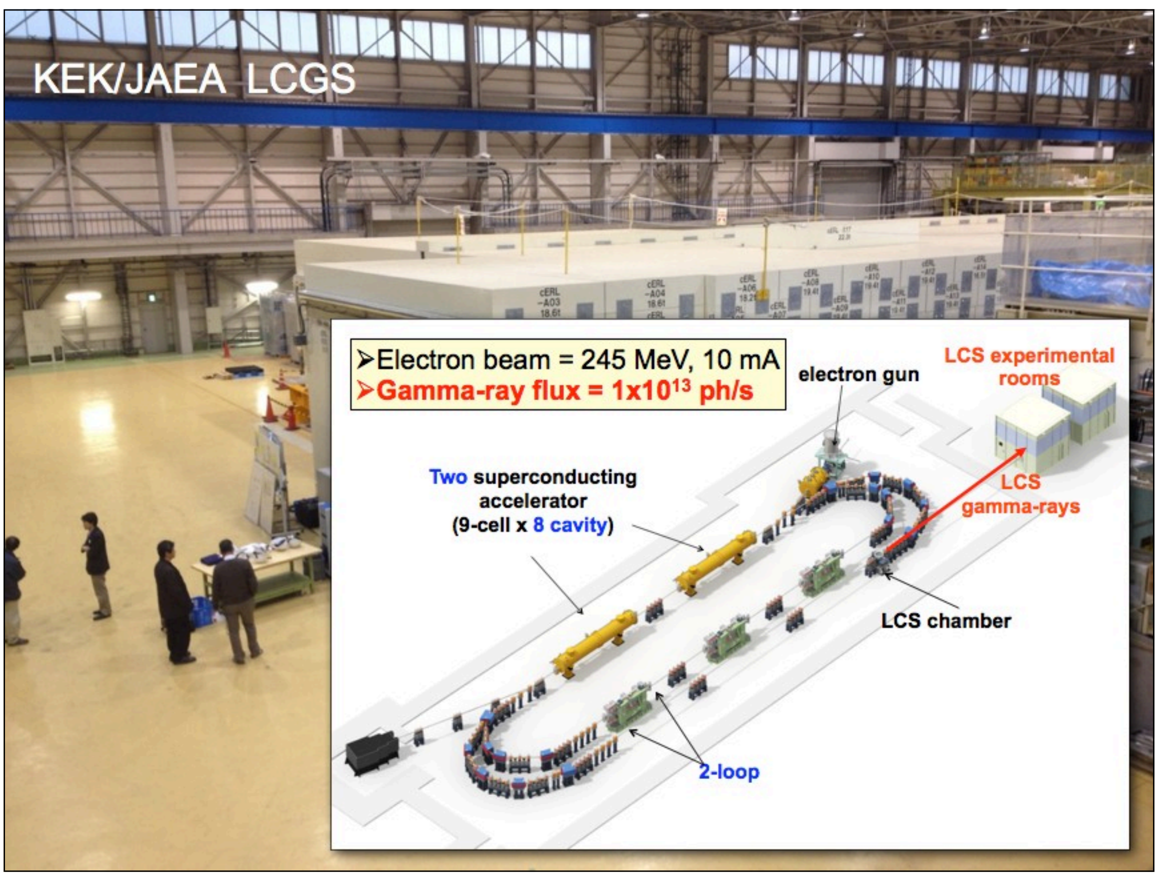
KEK/JAEA LCGS
➢Electron beam = 245 MeV, 10 mA
➢Gamma-ray flux = 1x10^13 ph/s
electron gun
LCS experimental rooms
Two superconducting accelerator (9-cell x 8 cavity)
LCS gamma-rays
LCS chamber
2-loop

ELI NP - ELI Nuclear Physics
Bucharest, Romania
293M euro project will include a 1MeV-20MeV MEGa-ray beam line

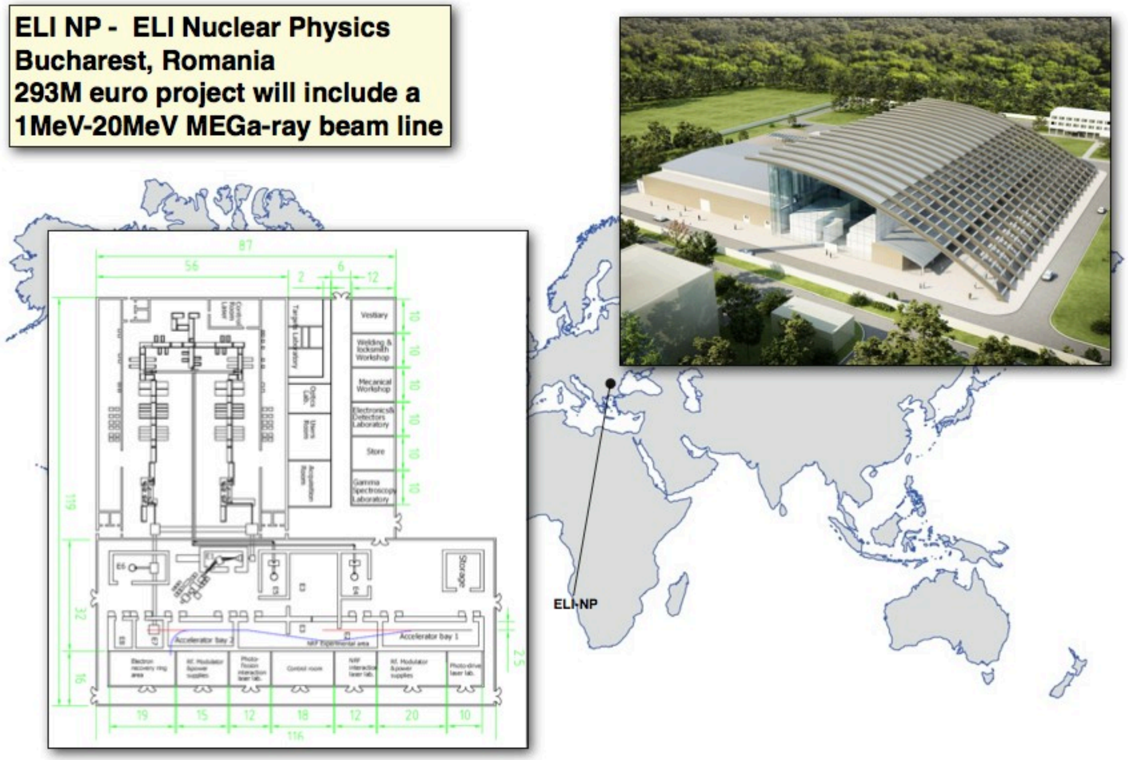

The White Book of ELI Nuclear Physics
Bucharest-Magurele, Romania

The ELI-Nuclear Physics working groups

The Scientific Case of ELI Nuclear Physic Pillar

The ELI-Nuclear Physics Experiment working group

Editors:
Dietrich Habs, Martin Groß, Nicolae Mărginean,
Florin Negoiţă, Peter G. Thirolf, Matthias Zepf

http://www.eli-np.ro/documents/ELI-NP-WhiteBook.pdf

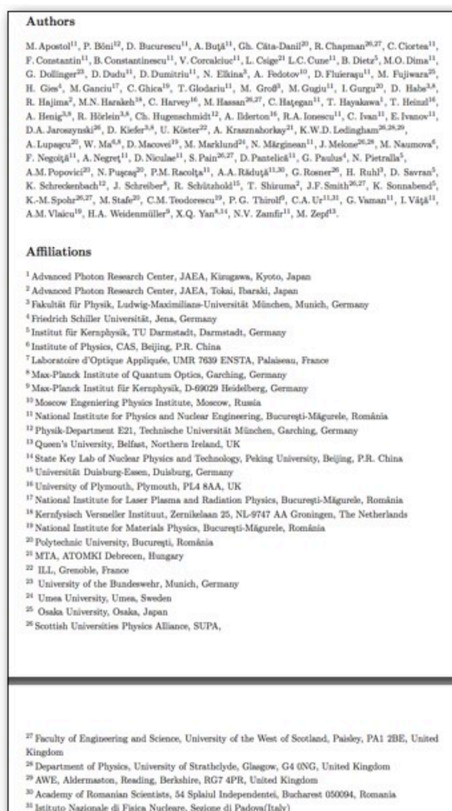

Authors

M. Apostol[11], P. Böni[12], D. Bucurescu[11], A. Buţă[11], Gh. Căta-Danil[20], R. Chapman[26,27], C. Ciortea[11], F. Constantin[11], B. Constantinescu[11], V. Corcalciuc[11], L. Csige[21] L.C. Cune[11], B. Dietz[5], M.O. Dima[11], G. Dollinger[23], D. Dudu[11], D. Dumitriu[11], N. Elkina[3], A. Fedotov[10], D. Fluieraşu[11], M. Fujiwara[25], H. Gies[4], M. Ganciu[17], C. Ghica[19], T. Glodariu[11], M. Groß[3], M. Gugiu[11], I. Gurgu[20], D. Habs[3,8], R. Hajima[2], M.N. Harakeh[18], C. Harvey[16], M. Hassan[26,27], C. Haţegan[11], T. Hayakawa[1], T. Heinzl[16], A. Henig[3,8], R. Hörlein[3,8], Ch. Hugenschmidt[12], A. Ilderton[16], R.A. Ionescu[11], C. Ivan[11], E. Ivanov[11], D.A. Jaroszynski[26], D. Kiefer[3,8], U. Köster[22], A. Krasznahorkay[21], K.W.D. Ledingham[26,28,29], A. Lupaşcu[20], W. Ma[6,8], D. Macovei[19], M. Marklund[24], N. Mărginean[11], J. Melone[26,28], M. Naumova[6], F. Negoiţă[11], A. Negreţ[11], D. Niculae[11], S. Pain[26,27], D. Pantelică[11], G. Paulus[4], N. Pietralla[5], A.M. Popovici[20], N. Puşcaş[20], P.M. Racolţa[11], A.A. Răduţă[11,30], G. Rosner[26], H. Ruhl[3], D. Savran[5], K. Schreckenbach[12], J. Schreiber[8], R. Schützhold[15], T. Shizuma[2], J.F. Smith[26,27], K. Sonnabend[5], K.-M. Spohr[26,27], M. Stafe[20], C.M. Teodorescu[19], P.G. Thirolf[3], C.A. Ur[11,31], G. Vaman[11], I. Văţă[11], A.M. Vlaicu[19], H.A. Weidenmüller[9], X.Q. Yan[8,14], N.V. Zamfir[11], M. Zepf[13].

Affiliations

[1] Advanced Photon Research Center, JAEA, Kizugawa, Kyoto, Japan
[2] Advanced Photon Research Center, JAEA, Tokai, Ibaraki, Japan
[3] Fakultät für Physik, Ludwig-Maximilians-Universität München, Munich, Germany
[4] Friedrich Schiller Universität, Jena, Germany
[5] Institut für Kernphysik, TU Darmstadt, Darmstadt, Germany
[6] Institute of Physics, CAS, Beijing, P.R. China
[7] Laboratoire d'Optique Appliquée, UMR 7639 ENSTA, Palaiseau, France
[8] Max-Planck Institute of Quantum Optics, Garching, Germany
[9] Max-Planck Institut für Kernphysik, D-69029 Heidelberg, Germany
[10] Moscow Engeniering Physics Institute, Moscow, Russia
[11] National Institute for Physics and Nuclear Engineering, Bucureşti-Măgurele, România
[12] Physik-Department E21, Technische Universität München, Garching, Germany
[13] Queen's University, Belfast, Northern Ireland, UK
[14] State Key Lab of Nuclear Physics and Technology, Peking University, Beijing, P.R. China
[15] Universität Duisburg-Essen, Duisburg, Germany
[16] University of Plymouth, Plymouth, PL4 8AA, UK
[17] National Institute for Laser Plasma and Radiation Physics, Bucureşti-Măgurele, România
[18] Kernfysisch Versneller Instituut, Zernikelaan 25, NL-9747 AA Groningen, The Netherlands
[19] National Institute for Materials Physics, Bucureşti-Măgurele, România
[20] Polytechnic University, Bucureşti, România
[21] MTA, ATOMKI Debrecen, Hungary
[22] ILL, Grenoble, France
[23] University of the Bundeswehr, Munich, Germany
[24] Umea University, Umea, Sweden
[25] Osaka University, Osaka, Japan
[26] Scottish Universities Physics Alliance, SUPA,

[27] Faculty of Engineering and Science, University of the West of Scotland, Paisley, PA1 2BE, United Kingdom
[28] Department of Physics, University of Strathclyde, Glasgow, G4 0NG, United Kingdom
[29] AWE, Aldermaston, Reading, Berkshire, RG7 4PR, United Kingdom
[30] Academy of Romanian Scientists, 54 Splaiul Independentei, Bucharest 050094, Romania
[31] Istituto Nazionale di Fisica Nucleare, Sezione di Padova(Italy)

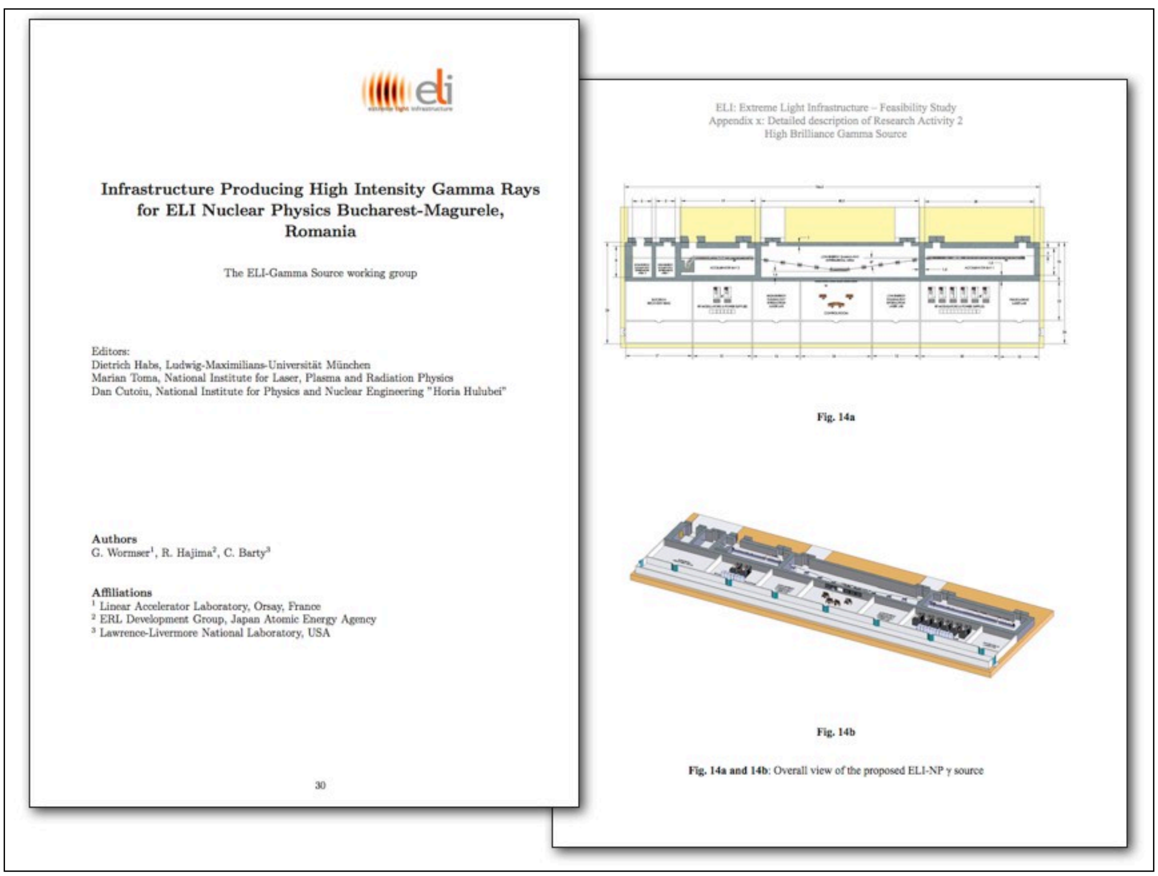

Infrastructure Producing High Intensity Gamma Rays for ELI Nuclear Physics Bucharest-Magurele, Romania

The ELI-Gamma Source working group

Editors:
Dietrich Habs, Ludwig-Maximilians-Universität München
Marian Toma, National Institute for Laser, Plasma and Radiation Physics
Dan Cutoiu, National Institute for Physics and Nuclear Engineering "Horia Hulubei"

Authors
G. Wormser[1], R. Hajima[2], C. Barty[3]

Affiliations
[1] Linear Accelerator Laboratory, Orsay, France
[2] ERL Development Group, Japan Atomic Energy Agency
[3] Lawrence-Livermore National Laboratory, USA

30

ELI: Extreme Light Infrastructure – Feasibility Study
Appendix x: Detailed description of Research Activity 2
High Brilliance Gamma Source

Fig. 14a

Fig. 14b

Fig. 14a and 14b: Overall view of the proposed ELI-NP γ source

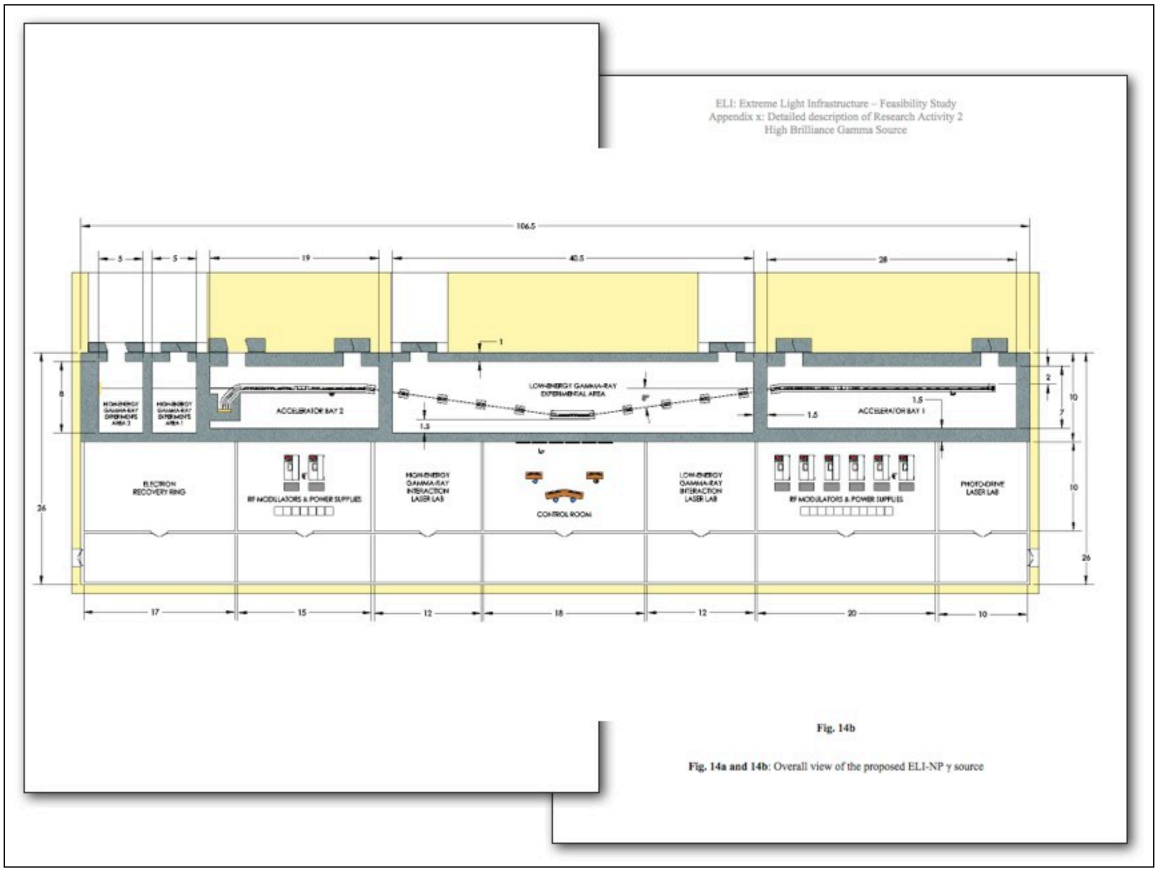
ELI: Extreme Light Infrastructure – Feasibility Study
Appendix x: Detailed description of Research Activity 2
High Brilliance Gamma Source
106.5
5
5
19
40.5
28
LOW-ENERGY GAMMA-RAY EXPERIMENTAL AREA
HIGH-ENERGY GAMMA-RAY EXPERIMENTS AREA 2
HIGH-ENERGY GAMMA-RAY EXPERIMENTS AREA 1
ACCELERATOR BAY 2
ACCELERATOR BAY 1
ELECTRON RECOVERY RING
RF MODULATORS & POWER SUPPLIES
HIGH-ENERGY GAMMA-RAY INTERACTION LASER LAB
CONTROL ROOM
LOW-ENERGY GAMMA-RAY INTERACTION LASER LAB
RF MODULATORS & POWER SUPPLIES
PHOTO-DRIVE LASER LAB
17
15
12
18
12
20
10
Fig. 14b
Fig. 14a and 14b: Overall view of the proposed ELI-NP γ source


02.02.2014

Other next generation MEGa-ray projects are now emerging to pursue isotope science & applications

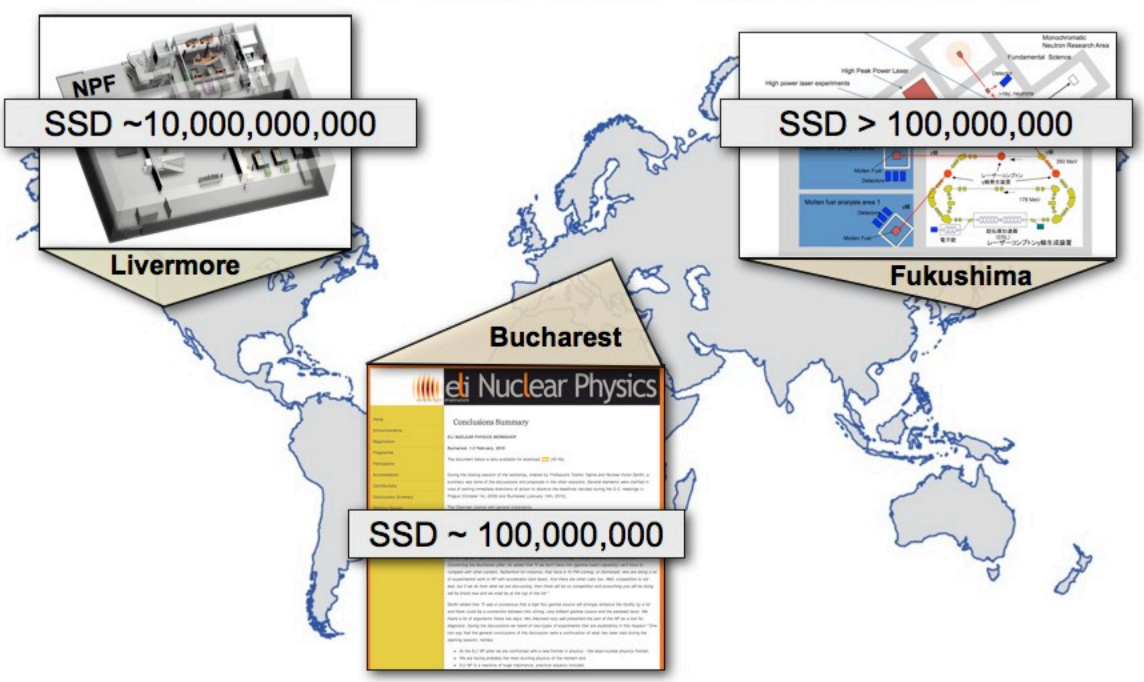

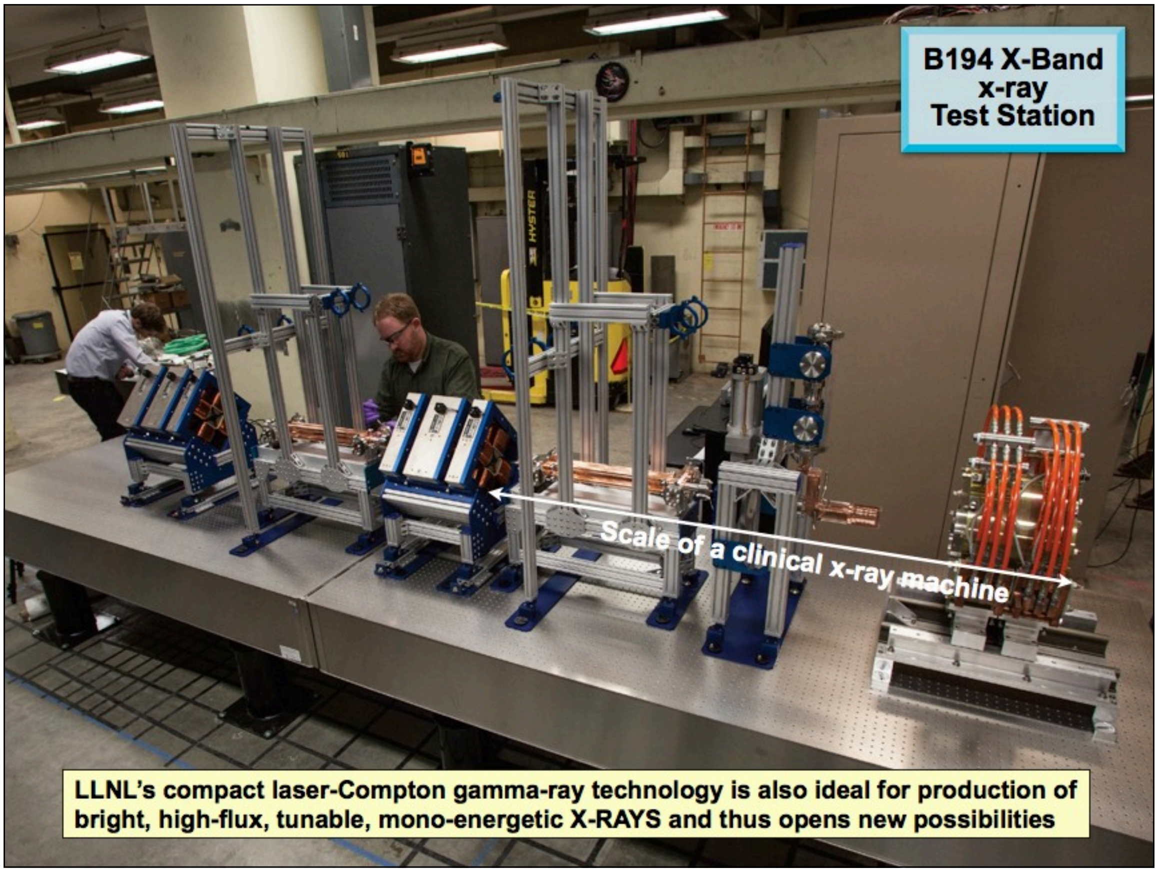

Optimized laser-Compton x-ray technology could revolutionize medical radiography & radiology

- Mono-energetic (reduces dose for all x-ray radiographic procedures)

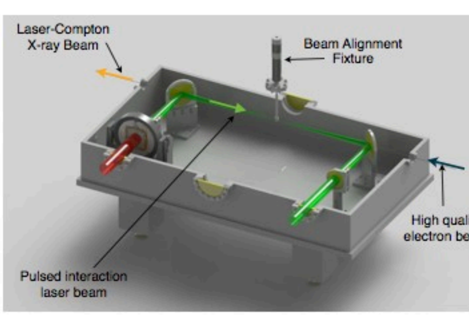

Laser-Compton X-ray Source

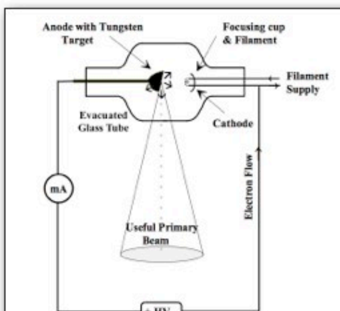

Rotating Anode X-Ray Source

The mono-energetic spectrum of laser-Compton source vs. rotating anode enables dose reduction

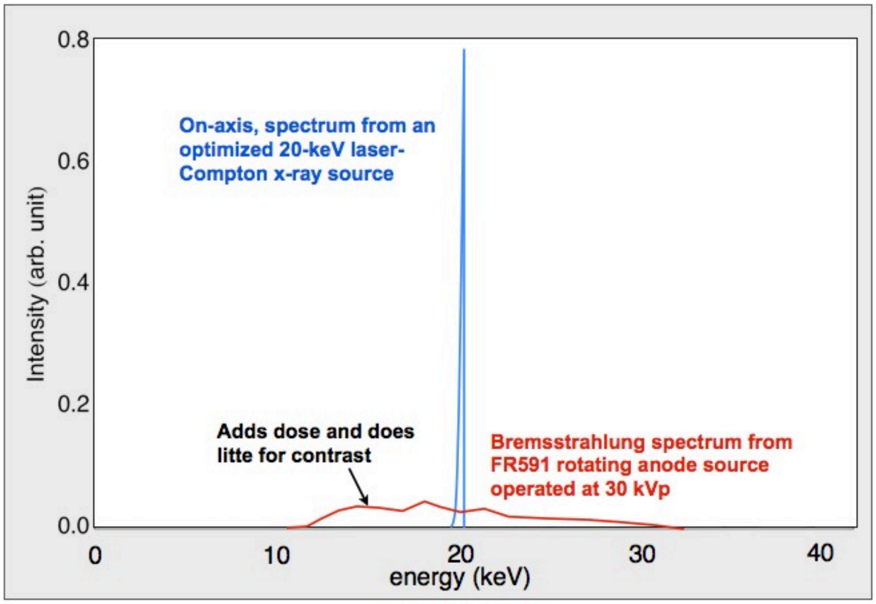

Optimized laser-Compton x-ray technology could revolutionize medical radiography & radiology

- Mono-energetic (reduces dose for all x-ray radiographic procedures)
- Highly collimated (enables multi-angle radiology & dose localization)
- Superior spatial resolution (enables small subject radiography)
- Instantaneously adjustable output (enables minimum dose radiography)
- High flux (enables fast imaging and treatment times)
- Easily tunable (enables k-edge imaging and Auger-cascade therapy)

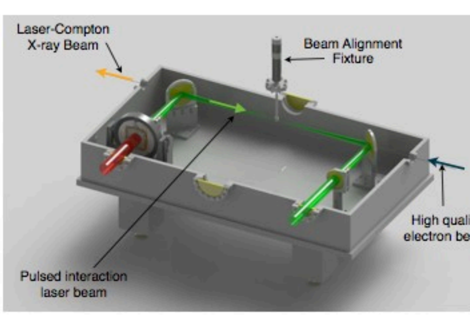

Laser-Compton X-ray Source

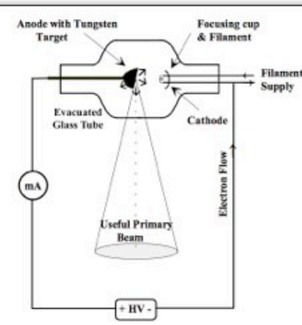

Rotating Anode X-Ray Source

Two color subtraction imaging has been studied for coronary angiography

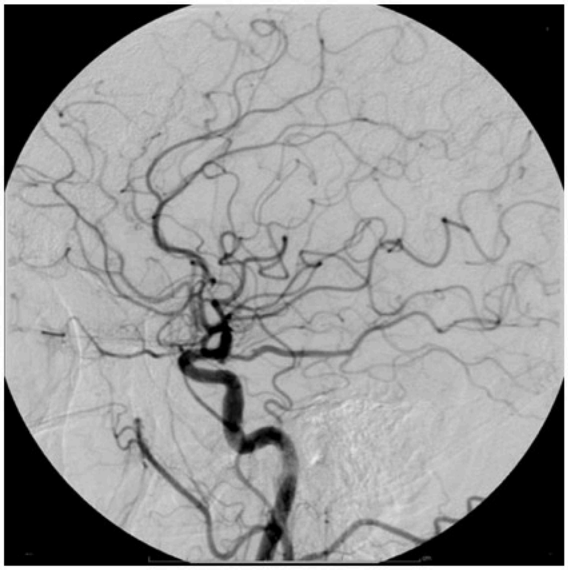

Mono-energetic imaging has been investigated using the output of synchrotron sources

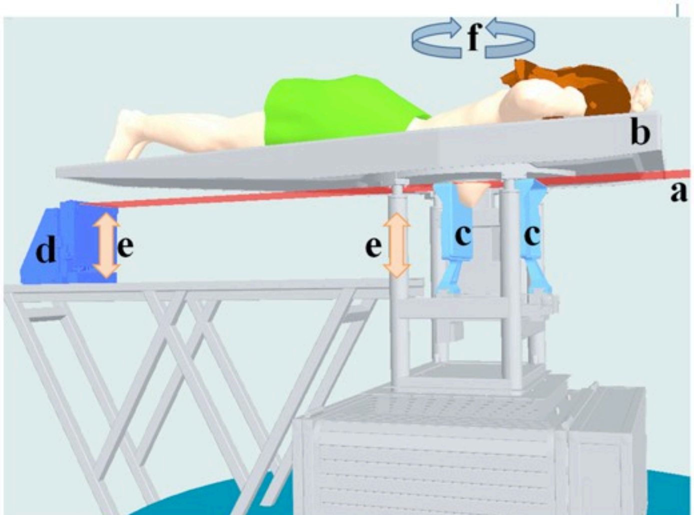

Figure E1: Imaging system for mammography with synchrotron radiation. (*a*) Stationary and laminar x-ray beam. (*b*) Movable patient support platform. (*c*) Compression system. (*d*) Holder for screen-film cassette. (*e*) Vertical movement of patient and screen-film system through the beam, which facilitates the acquisition of planar radiographic images. (*f*) Rotational movement of patient, which facilitates the acquisition of craniocaudal and mediolateral oblique views.

From Italian mammography study with synchrotron radiation. Note this geometry does not require breast compression

Conventional breast tissue imaging is a compromise between contrast and dose

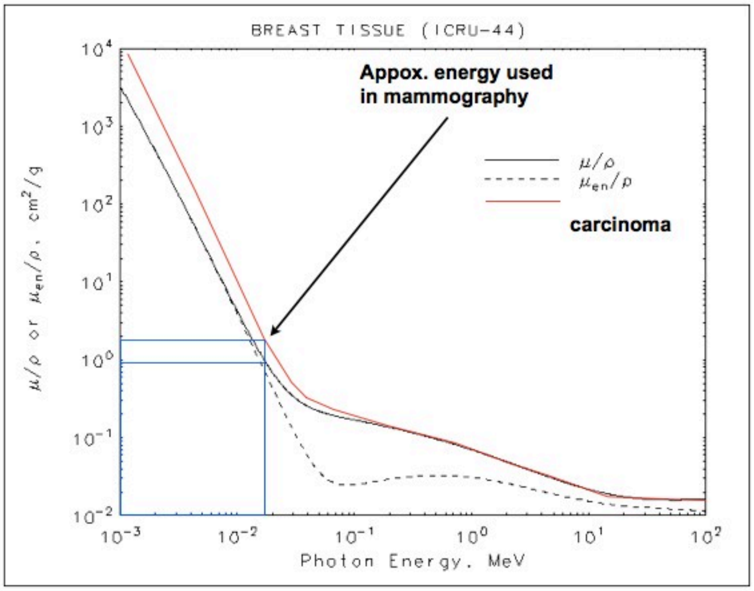

absorption coefficient at the energy of the Gd k-edge is 0.032 for breast vs 20 for Gd!

Conventional breast tissue imaging is a compromise between contrast and dose

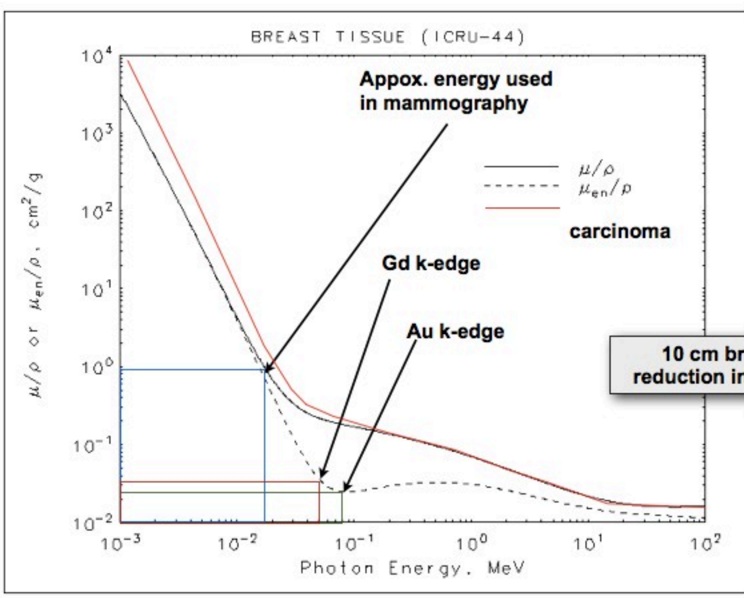

10 cm breast = ~20,000x reduction in deposited energy

absorption coefficient at the energy of the Gd k-edge is 0.032 for breast vs 20 for Gd!

Gd has excellent k-edge properties and is already an approved contrast agent for breast MRI

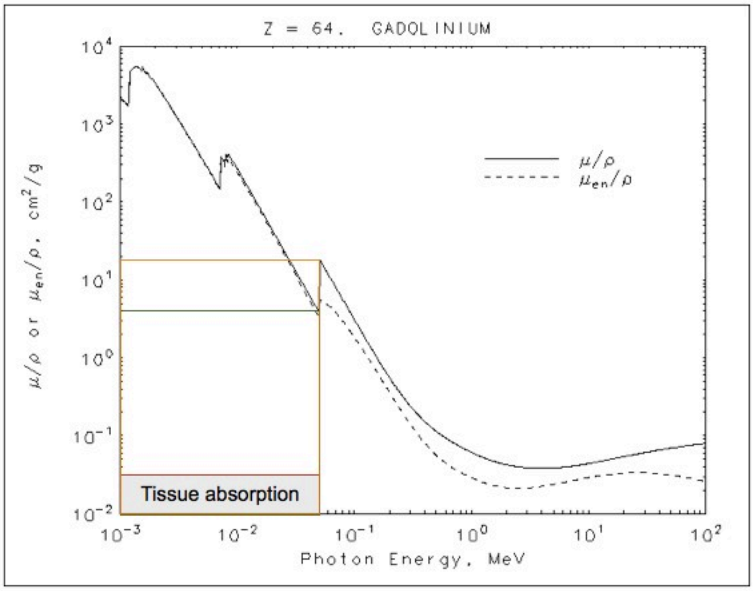

Optimized laser-Compton x-ray technology could revolutionize medical radiography & radiology

- **Mono-energetic (reduces dose for all x-ray radiographic procedures)**
- **Highly collimated (enables multi-angle radiology & dose localization)**
- **Superior spatial resolution (enables small subject radiography)**
- **Instantaneously adjustable output (enables minimum dose radiography)**
- **High flux (enables fast imaging and treatment times)**
- **Easily tunable (enables k-edge imaging and Auger-cascade therapy)**

Attribute	LLNL Picket Fence c-2013	LLNL RING c-2013	LLNL T-REX c-2009	MXIS/Vanderbilt c-2007	Rotating Anode	Units
bandwidth	~0.1%	<0.5%	8%	10%	100%	ΔE/E
collimation	~0.5	1	1	2	524	mrad
source size	5	15	30	35	150	microns
average brilliance	>1E+13*	>1E+13*	8.89E+10	3.60E+06	6.00E+07	ph/s/mm2/mrad2/0.1%BW
e-beam current	6.00E-03	6.00E-04	1.50E-06	2.08E-09	100	mA
laser power	1200	120	2.5	0.0036	n/a	W

- **These attributes are important to many other applications besides medicine**

* LLNL "picket fence" average brilliance is equivalent to the bending magnet output from a large-scale, modern synchrotron, e.g. SSRL at Stanford

Optimized laser-Compton sources will enable “lab-scale” synchrotron science & “nuclear” photonics

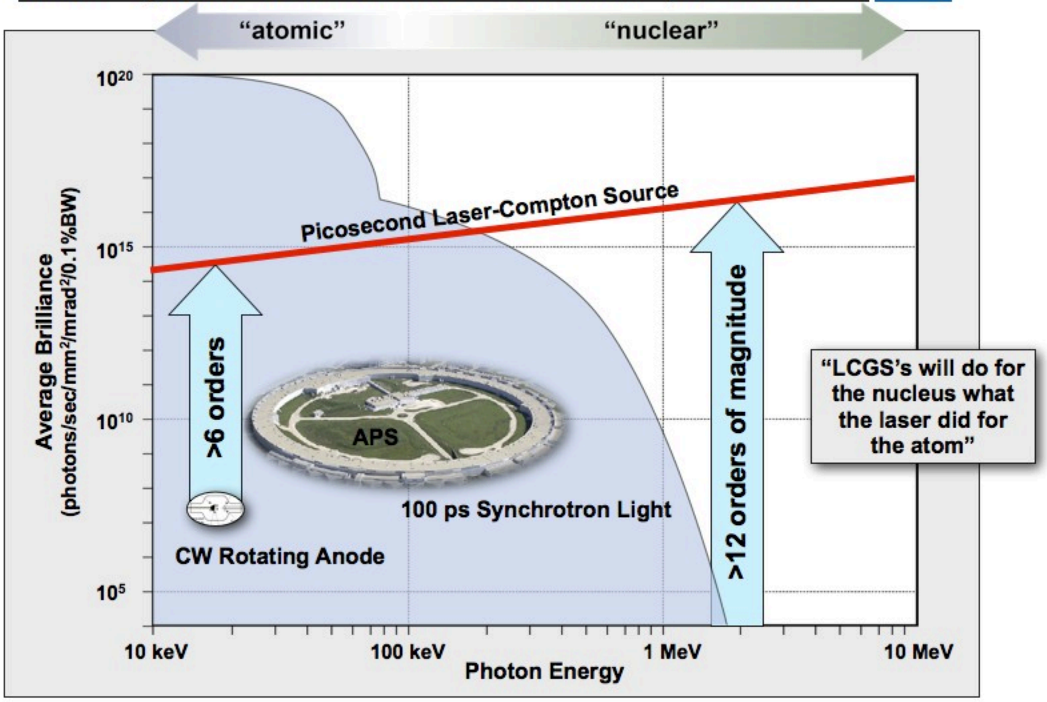

Optimized laser-Compton sources will enable “lab-scale” synchrotron science & “nuclear” photonics

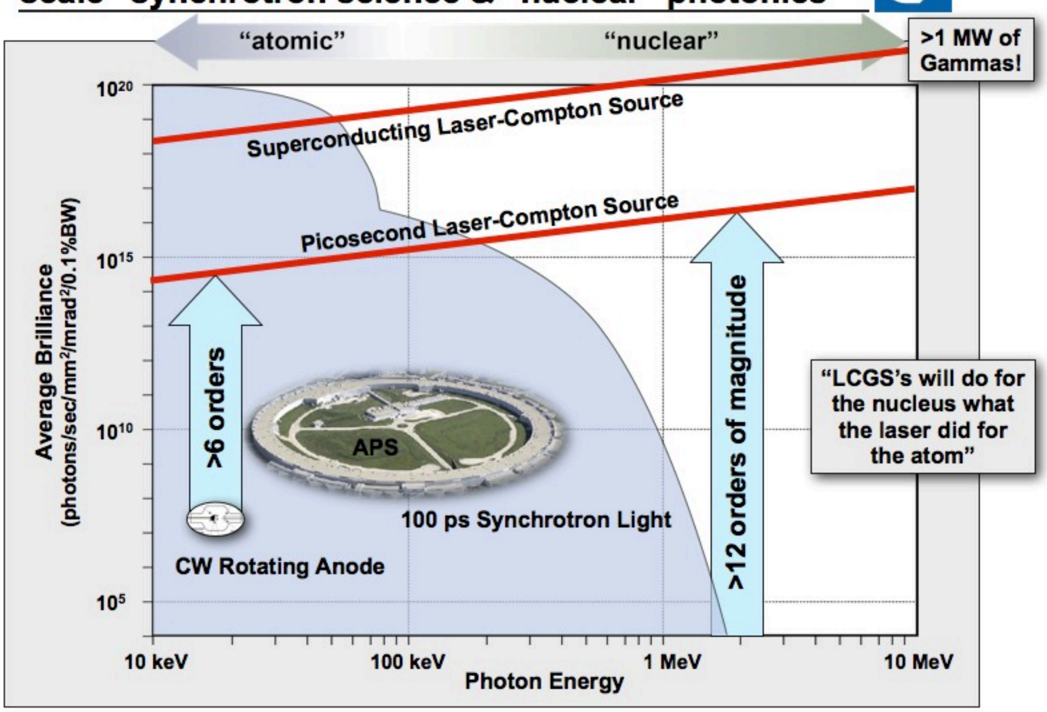

The Laser-Compton and Nuclear Photonics efforts described in this presentation represent contributions from ~~10~~ 12 institutions

Marvin	Adams	TAMU	Shawn	Densberger	LLNL	Ed	Morse	UCB
Chris	Adolphsen	SLAC	Valery	Dolgashev	SLAC	Kaila	O'Neil	LLNL
Felicie	Albert	LLNL	Chris	Ebbers	LLNL	Henry	Phan	LLNL
Gerry	Anderson	LLNL	Mike	Fazio	SLAC	Norbert	Pietralla	GSI
Scott	Anderson	LLNL	Diana	George	LLNL	John	Post	LLNL
Paul	Armstrong	LLNL	David	Gibson	LLNL	Matt	Prantil	LLNL
Chris	Barty	LLNL	Marc	Gunther	LMU	Cesar	Pruneda	LLNL
Andy	Bayramian	LLNL	Dietrich	Habs	LMU	Sofia	Quagllioni	LLNL
Bret	Beck	LLNL	Chris	Hagmann	LLNL	Tor	Raubenheimer	SLAC
Glenn	Beer	LLNL	Ryoichi	Hajima	JAEA	Vladimir	Semenov	LLNL
Shawn	Betts	LLNL	James	Hall	LLNL	Michio	Seya	JAEA
Dave	Boyle	TAMU	Fred	Hartemann	LLNL	Rich	Shuttlesworth	LLNL
Patrick	Brantley	LLNL	Corrine	Izak	CEA	David	Stevens	LLNL
Eugene	Brooks	LLNL	Michael	Jentschel	ILL	Sami	Tantawi	SLAC
Arno	Candel	SLAC	Micah	Johnson	LLNL	Peter	Thiorlf	LMU
Bill	Charlton	TAMU	Ed	Jones	LLNL	Arnold	Vlieks	SLAC
Sam	Chu	SLAC	Erik	Jongewaard	SLAC	Faya	Wang	SLAC
Eric	Cormier	UBordeaux	Zenghai	Li	SLAC	Juwen	Wang	SLAC
Rick	Cross	LLNL	Cecile	Limborg-Deprey	SLAC	Caroline	Winters	LLNL
Dan	Cutiou	ELI-NP	Roark	Marsh	LLNL	Sheldon	Wu	LLNL
Gary	Deis	LLNL	Scott	McKinley	LLNL	Victor	Zamfir	ELI-NP
Bob	Demaret	LLNL	Dennis	McNabb	LLNL	Feng	Zhou	SLAC
			Jim	Morel	TAMU			